Nanoscale Horizons

REVIEW

View Article Online
View Journal | View Issue



Cite this: *Nanoscale Horiz.*, 2024, **9**, 2198

# Pyrene-based covalent organic frameworks (PyCOFs): a review

Yao Yang,[a] Shiqiong Peng,[c] Songhua Chen,*[b] Fangyuan Kang,[d] Jun Fan,[a] Huan Zhang,[a] Xianglin Yu,[c] Junbo Li*[a] and Qichun Zhang*[d]

Received 4th July 2024,
Accepted 19th September 2024

DOI: 10.1039/d4nh00317a

rsc.li/nanoscale-horizons

Recently, pyrene-based covalent organic frameworks (PyCOFs) have aroused great interest because the large planar structure of the pyrene unit could effectively enhance the interlayer π–π interaction and promote the separation and migration of carriers, significantly improving the crystallinity and photoelectrical properties of PyCOFs. Since the first PyCOF-containing boroxate linkage was reported in 2008 by the Yaghi group, many PyCOFs with different kinds of linkages have been reported, exhibiting great potential applications in different fields such as adsorption/separation, chemical sensing, catalysis, energy storage, *etc.* However, as far as we know, the reviews related to PyCOFs are rare, although PyCOFs have been widely reported to show promising applications. Thus, it is right time and important for us to systematically summarize the research advance in PyCOFs, including the synthesis with different linkages and applications. Moreover, the prospects and obstacles facing the development of PyCOFs are discussed. We hope that this review will provide new insights into PyCOFs that can be explored for more attractive functions or applications.



## 1. Introduction

Covalent organic frameworks (COFs) are a class of crystalline polymeric materials made from small molecular building blocks connected through covalent bonds.[1] They have the advantages of high crystallinity, rich pore structure, high stability, high functionality, structural designability, *etc.*[2] Since the first COF was synthesized by the Yaghi group in 2005,[3] the advances in diverse building units and different synthetic methods have greatly promoted the development of COFs, leading to rich types and various applications.[4] Especially, topology-guided design of COFs can enable scientists to prepare targeted COFs with large specific surface area, tunable pore sizes, and functional pore environment.[5] These features have led to the excellent application of COFs in the fields of adsorption and separation,[6] catalysis,[7] photovoltaics,[8] sensing,[9] and biology.[10]

Pyrene is a highly symmetrical four-benzene-ring polycyclic aromatic hydrocarbon, which was discovered in the residue of the distillation of coal tar in 1837.[11] Among diverse building units, pyrene derivatives[12] have been widely employed as building units to construct framework materials due to their rich π-electrons,[13] planar structure, high stability, and tightly stacking patterns through strong intermolecular π–π interactions in aggregated states.[14] Besides, these factors are favorable for the preparation of porous framework materials.[15] The formed large π conjugated system based on pyrene derivatives can widen the range of light absorption, help electron migration, and reduce photogenerated electron–hole recombination.[16] Moreover, the conjugated nature of pyrene provides good chemical stability in energy storage and stimulation.[17] A series of novel pyrene-based porous materials, such as pyrene-based metal–organic frameworks (PyMOFs), pyrene-based covalent organic frameworks (PyCOFs), pyrene-based hydrogen-bonded organic frameworks (PyHOFs) and pyrene-based polyporous organic polymers (PyPOPs), have been developed and utilized in various applications. Among them, PyMOFs constructed from metal ions/clusters and organic linkers through coordination bonds have the characteristics of periodic and well-defined structures large specific surface area, structural diversity, and customizability. However, they usually have relatively low chemical stability and poor electrical conductivity, which hinders their practical applications.[18] PyHOFs are organic molecules with hydrogen bond interactions, well-defined structures and low density. However, their poor chemical stability limits

[a] *School of Chemistry and Environmental Engineering, Wuhan Institute of Technology, Wuhan 430074, China. E-mail: jbliwit@163.com*
[b] *College of Chemistry and Material, Longyan University, Longyan 364000, China. E-mail: songhua@iccas.ac.cn*
[c] *School of Chemical Engineering and Pharmacy, Wuhan Institute of Technology, Wuhan 430074, China*
[d] *Department of Materials Science and Engineering, Department of Chemistry, Center of Super-Diamond and Advanced Films (COSDAF) & Hong Kong Institute of Clean Energy, City University of Hong Kong, 999077 Hong Kong, China. E-mail: qiczhang@cityu.edu.hk*

their applications.[19] PyPOPs are highly stable porous materials composed of strong covalent bonds based on organic molecules. Unfortunately, due to their unclear structures and irregular pores, it is difficult to gain a deep understanding of their structure–activity relationship.[20] PyCOFs are a type of fully designed crystalline material made from organic building blocks polymerized through strong covalent bonds. Compared with PyMOFs, PyHOFs and PyPOPs, PyCOFs not only integrate their particular advantages but also remedy their drawbacks, and hence have attracted increasing interest in various applications.[21] Furthermore, PyCOFs containing pyrene moieties exhibit extended π-conjugation and robust electronic interactions, allowing exceptional electron delocalization and transport. This enhances the capture and conversion of light energy, making them ideal for composite photocatalytic systems.[22]

The recent progress in PyCOFs strongly inspires us to summarize the linkages and applications of PyCOFs, and discuss the effects of different substitutes in pyrene-based linkages on the applications of PyCOFs, including photocatalysis (including hydrogen evolution, hydrogen peroxide production, reduction of carbon dioxide and conversion of organic matter), fluorescence detection, battery materials, *etc.* Finally, we will provide the fundamental issues and the future directions in the exploration of PyCOF-based applications.

## 2. Synthetic strategies of PyCOFs

In recent years, the formation of PyCOFs through polycondensation reactions among different building blocks has been widely observed to study how covalent bonds confer structural scalability and specific functional capabilities of COFs, and affect their crystallinity and chemical stability. Clearly, the linkages are very important because they not only connect the functional building blocks together, but also can extend the π-conjugation and facilitate the light absorption and electron transfer processes. Besides, according to different topological structures and connection modes, COFs with one-dimensional (1D),[23] two-dimensional (2D) and three-dimensional (3D) structures are constructed. Because of their different structures, they can have different applications. In contrast to 1D and 2D COFs with π–π packing in the process of plane covalent bonding, 3D COFs are three-dimensional assembly through covalent bonding, and their synthesis mainly depends on the formation of covalent bonds. Because of the high bond energy of covalent bonds and the weak reversible bond assembly ability, it is difficult to accurately control the bonding process of three-dimensional frameworks at the atomic level, and crystallization is more difficult.[24] The following is the summary of PyCOFs with different kinds of linkages.

### 2.1 Boron–oxygen-linked PyCOFs

Boron–oxygen-linked PyCOFs can be constructed through the dehydration condensation of diboronic acid and *o*-diphenol or the dehydration self-condensation of diboronic acid to form boric anhydride (boroxane) (Fig. 1a). These materials have been extensively investigated and can be easily formed with high reversibility, high yield, and high crystallinity.

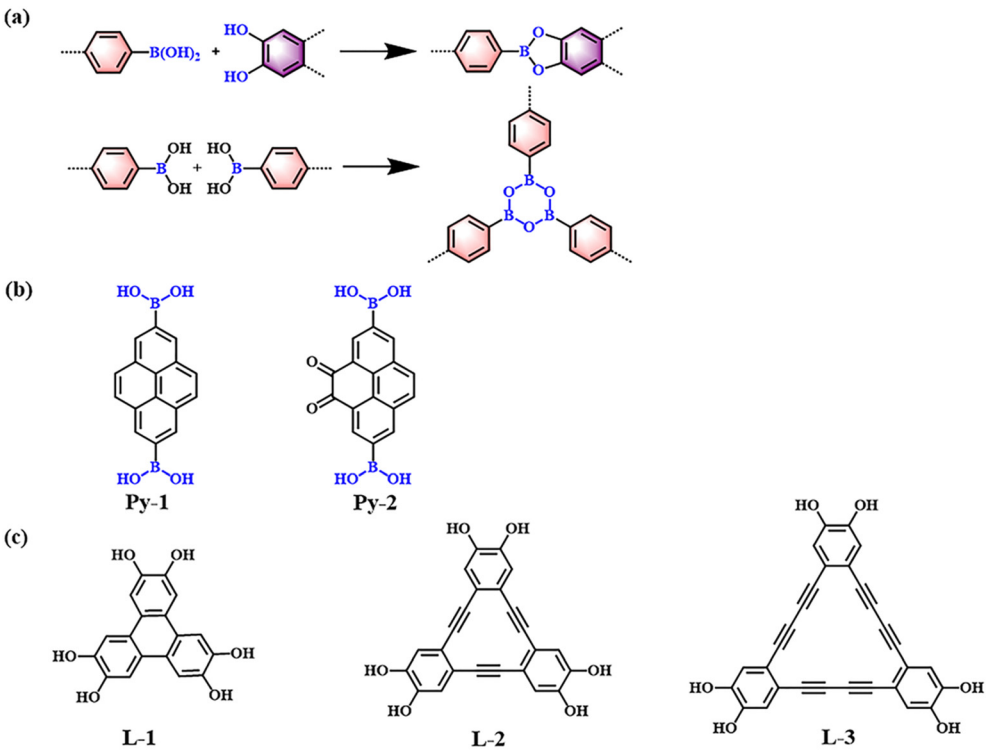


Fig. 1 (a) Schematic illustration of boron–oxygen-linked PyCOFs. (b) Frequently used monomers containing boron hydroxyl. (c) Phenolic hydroxyl monomers.

In 2008, Wan *et al.*[25] synthesized TP-COF through a condensation reaction between 2,3,6,7,10,11-hexahydroxytriphenylene (HHTP) and pyrene-2,7-diboronic acid (PDBA), which was the first example of PyCOFs containing boron–oxygen linkage. This TP-COF structure with hexagonal pores was designed to use $D_{3h}$ symmetric monomers as corners and $D_{2h}$ symmetric monomers as edges. Later on, Wan *et al.*[26] employed the self-condensation of pyrene-2,7-diboronic acid to prepare PPy-COF (Fig. 2) with an eclipsed alignment. The authors found that this structure could significantly facilitate exciton migration and carrier transport. Moreover, PyCOFs can capture visible light and generate large photocurrent. Besides these, they also have been demonstrated to show rapid response to optical radiation. All these factors have driven the quick research progress of PyCOFs in optoelectronic and photovoltaic applications.

Although the boron–oxygen-linked COFs could be prepared with high crystallinity using traditional solvothermal methods, their chemical stability is poor, and even they are unstable under weak acid, weak base, and relatively mild water vapor conditions. To enhance their stability, some of the boron–oxygen-linked PyCOFs were functionalized *via* post-modification. For example, in 2016, Salonen *et al.*[27] prepared a new pyrene-4,5-dione building block to react with 2,3,6,7,10,11-hexahydroxytriphenylene (HHTP), yielding a novel dione-COF (Fig. 3a). In 2022, the same group introduced *o*-phenylenediamine (Ph) and 2,3-diaminonaphthalene (Naph) into the pores of dione-COF, which could extend the π-system of the PyCOF backbone to produce pyrene-fused azaacene COFs, inhibiting the hydrolysis of COFs.[28] In 2023, Frey *et al.*[29] continued to graft (1*R*,2*R*)-(+)-1,2-diphenylethylenediamine onto dione-COF to obtain a shorter layer spacing while increasing the π-conjugated system, which could shift the absorption range to longer wavelengths (Fig. 3b).

It is possible to use the hybrid linker strategy for the creation of COFs with different pore channels or different degrees of conjugation. This factor is important to increase the structural diversity of COFs. For example, Zheng *et al.*[30] synthesized two boron–oxygen-linked COFs by a solvothermal method using CTC as the apex unit and PDBA or BPDA as the linkage. The introduction of the pyrene group makes CTC-COF-3 a potential semiconducting π-conjugated material. In the same year, Crowe *et al.*[31] reported three novel boron–oxygen-linked COFs (Fig. 4) (Py-DBA-COF 1, Py-DBA-COF 2, and Py-MV-DBA-COF) with π-conjugated DBA as the apex unit and PDBA as the connecting bridge. All three DBA-COFs are highly luminescent in the solid state, and the redshift in the emission wavelengths of Py-DBA-COF 1 and Py-MV-DBA-COF may be attributed to the symmetrically forbidden lowest energy jump in the ground state of the DBA[18] based materials compared to the DBA[12] based materials, facilitating the construction of materials with unique photovoltaics.

### 2.2 $sp^2$ carbon-linked PyCOFs

Knoevenagel condensation, a cascade nucleophilic addition-dehydration reaction between activated methylene groups and aldehydes or ketones, is one of the most common reactions to synthesize $sp^2$-COFs. Cyano-substitution is of great importance in the strategy of synthesis of $sp^2$c-COFs. As shown in Fig. 5a, $sp^2$c-COFs can be obtained through topologically oriented polymerization reactions between benzyl cyanide and aryl aldehyde monomers, where pyrene derivatives are used as vertex units (Fig. 5b) and a series of cyanide derivatives are used as linking units (Fig. 5c).

Xiao *et al.*[32] found that $sp^2$c-PyCOFs as the fully π-conjugated systems could provide better electrical and magnetic properties. In 2017, Jiang *et al.*[33] reported the synthesis of 2D crystalline COFs ($sp^2$c-PyCOF) *via* the Knoevenagel condensation reaction between 1,3,6,8-tetrakis(4-formylphenyl)pyrene (TFFPy) and 1,4-phenylenediacetonitrile (PDAN) (Fig. 6a). The as-prepared $sp^2$c-PyCOF has a surface area of 692 $m^2$ $g^{-1}$. The porous and ultrathin structure of $sp^2$c-PyCOF effectively shortened the transport distance of electrons, ions, and co-reactants

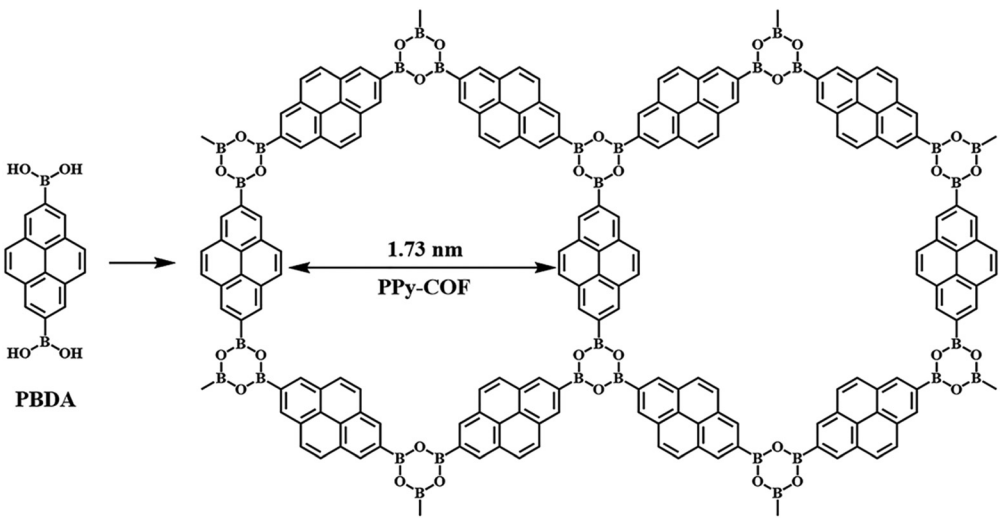


Fig. 2 Schematic representation of the synthesis of PPy-COF. Reproduced with permission.[26] Copyright 2009, Wiley-VCH GmbH.

 

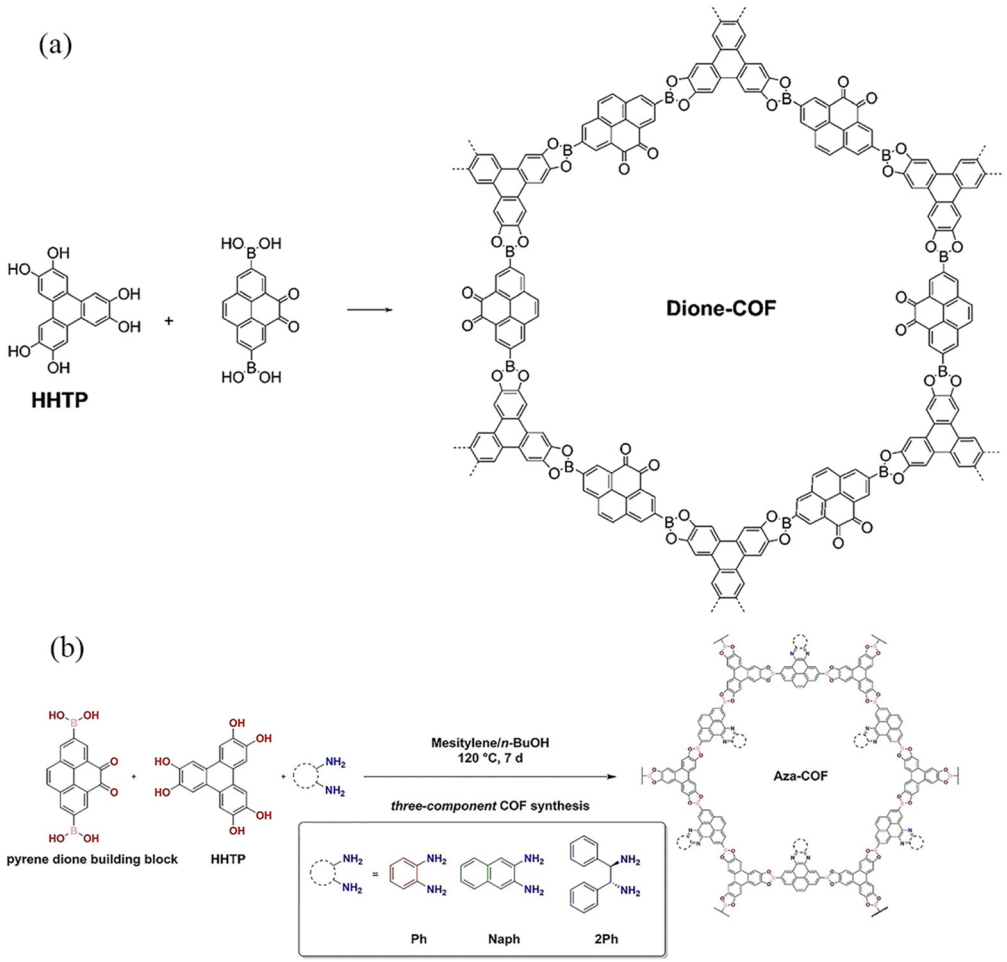


Fig. 3 (a) Synthesis of dione-COF. Reproduced with permission.[27] Copyright 2016, Royal Society of Chemistry. (b) Post-synthetic modification of dione-COF. Reproduced with permission.[29] Copyright 2023, Wiley-VCH GmbH.

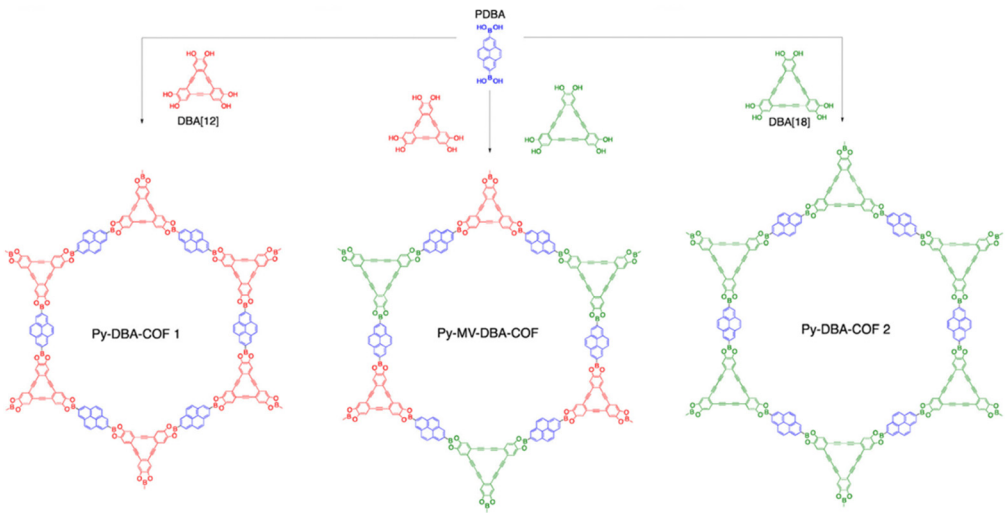


Fig. 4 Synthesis of DBA-COFs. Reproduced with permission.[31] Copyright 2016, American Chemical Society.

($S_2O_8^{2-}$), which enhanced the utilization of luminophores. In 2023, Jiang *et al.*[34] continued to study $sp^2$c-PyCOF and found that $sp^2$c-PyCOF could be used to degrade tetracycline hydrochloride in aqueous solution under visible light irradiation.

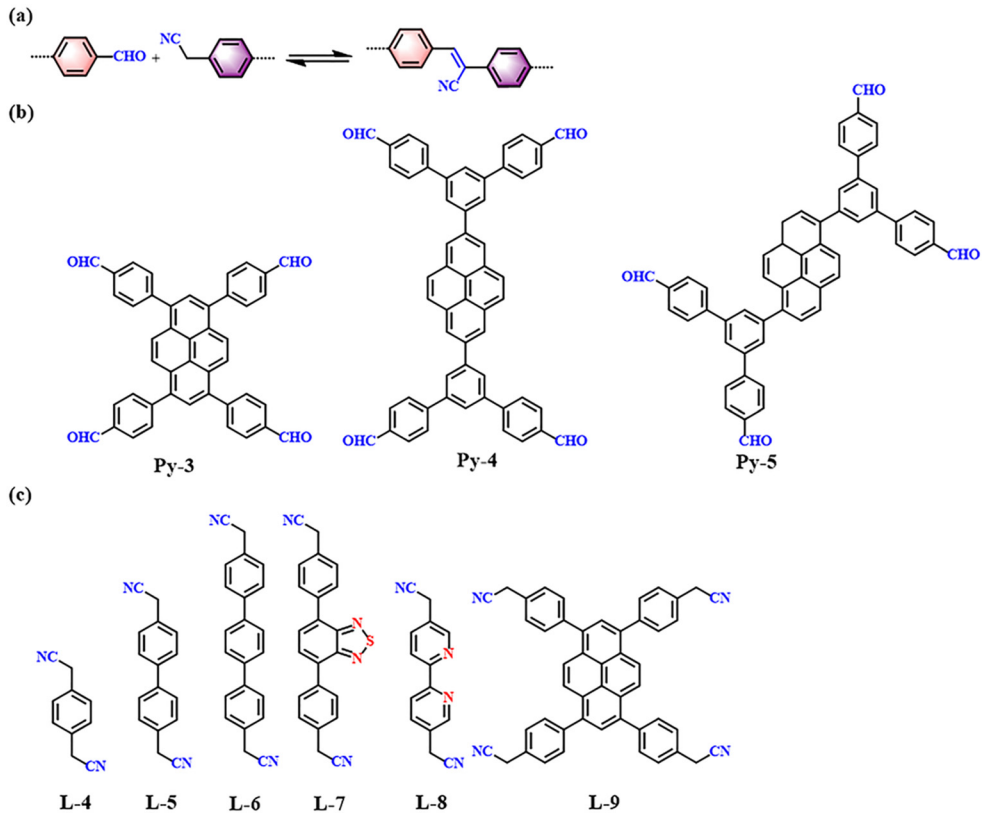


Fig. 5 (a) Schematic illustration of $sp^2$ carbon-conjugated-linked PyCOFs. (b) and (c) Frequently used monomers.

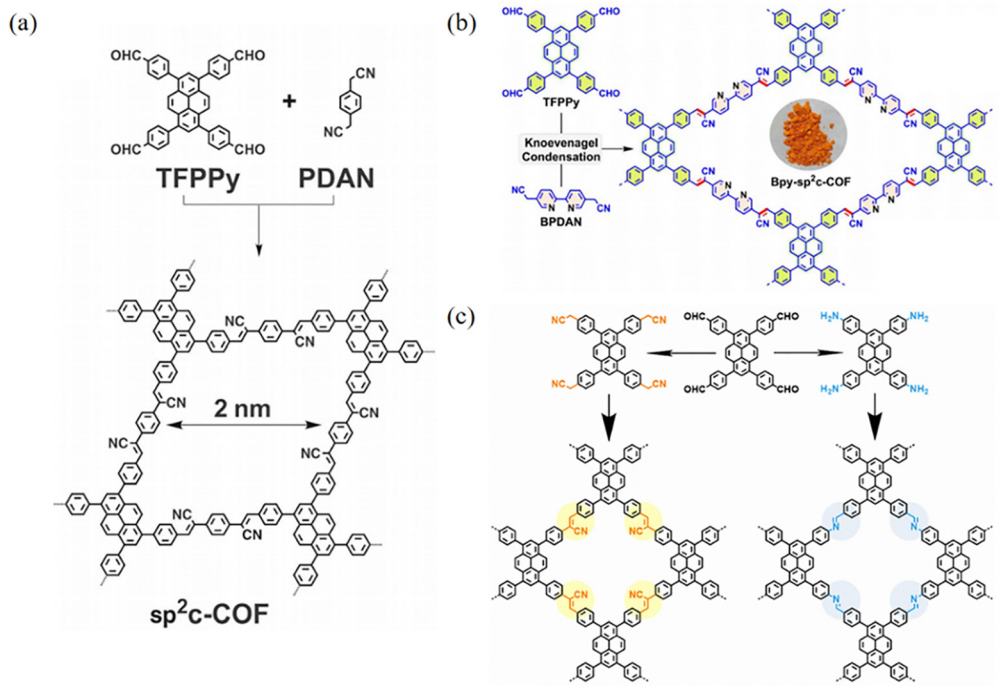


Fig. 6 (a) Synthesis of $sp^2$c-COF. Reproduced with permission.[35] Copyright 2017, The American Association for the Advancement of Science. (b) Synthesis of Bpy-$sp^2$c-COF. Reproduced with permission.[36] Copyright 2023, Royal Society of Chemistry. (c) Schematic representation of the syntheses of imCOF and viCOF. Reproduced with permission.[37] Copyright 2023, Wiley-VCH GmbH.

 

The most common method for designing and synthesizing new sp$^2$c-COFs is to increase the number of cyano-linked units and introduce heteroatoms. The introduction of heteroatoms modulates the pore size and electron cloud density of sp$^2$c-COFs and improves the chemical stability and photoelectronic properties of sp$^2$c-COFs through fully conjugated states. Nitrogen was introduced into the skeleton of the COF to form a pyrimidine structure, which significantly improved the electronic effect of sp$^2$c-PyCOF. Bpy-sp$^2$c-PyCOF was synthesized *via* the condensation reaction between TFPPy and 5,5′-diacetonitrile-2,2′-bipyridine (BPDAN) (Fig. 6b).[36,38] Bpy-sp$^2$c-PyCOF shortens the carrier transport distance, enhances electron–hole separation, and maintains high catalytic efficiency and reusability. In 2023, Lin *et al.*[38a] reported a sp$^2$c-PyCOF containing bipyridyl and its post-synthetic modification through the introduction of Ni. Under light irradiation, the enhanced energy transfer in this COF facilitated the excitation of Ni centers to catalyze borylation and trifluoromethylation reactions of aryl halides. Mi *et al.*[38b] found that Bpy-sp$^2$c-PyCOF showed excellent photocatalytic activity in aerobic hydroxylation and thiocyanation transformation in the visible range.

The photophysical properties of COFs are mainly affected by the structural features such as the conjugation degree, charge delocalization ability and exciton dynamics. In 2022, Jiang and co-workers[39] developed a module-patterned polycondensation strategy for the efficient synthesis of crystalline porous COFs. They prepared a series of sp$^2$c-COFs through polycondensation of two pyrene units with different substitution positions and three linkers (Fig. 7). Moreover, the $C_2$-symmetric knot module can be generalized to possess different π backbones and enables polymerization with diverse linker units, producing a library of unprecedented 2D sp$^2$-carbon polymers and open frameworks. In 2023, Han *et al.*[37] reported that two PyCOFs with imine and vinylene linkages, named imCOF and viCOF (Fig. 6c). It was found that viCOF has a longer fluorescence lifetime and more prominent solid-state photoluminescence quantum yield, and is the preferred charge transfer pathway in the intralaminar mode due to the D–A structure, which increases the charge separation ability. sp$^2$c-PyCOFs are not only of interest in the design of new 2D semiconducting frameworks but also provide insights into the development of π electronic functions.

### 2.3 Imine-linked COFs

As shown in Fig. 8a, imine-linked COFs are constructed by the acid-catalyzed co-condensation of amine and aldehyde derivatives based on a Schiff base reaction. Imine-linked COFs are abundant and readily available. Imine-linked PyCOFs are usually synthesized by substitution reactions at the 1, 3, 6, and 8 positions of pyrene units, increasing the types of vertex units (Fig. 8b), where [1+1] condensation reactions occur with different kinds of linkages (Fig. 8c), leading to the rapid development of imine-linked COFs.[40] The crystallinity and specific surface area of imine-linked COFs are lower than those of boron–oxygen-linked COFs with similar structures; however, their stability is significantly improved compared to boron–oxygen-linked COFs.

In 2019, Chen *et al.*[41] synthesized a bifunctional building block, 1,6-bis(4-formylphenyl)-3,8-bis(4-aminophenyl)pyrene (BFBAPy), to construct highly crystalline and porous Py-COFs through self-condensation in different solvents such as $CH_2Cl_2$, $CHCl_3$, tetrahydrofuran, methanol, ethanol, acetonitrile, and dimethylacetamide. This provides a 'two-in-one' molecular design strategy for readily preparing high-quality COFs. Self-condensation ensures that the optimal stoichiometric ratio during the polycondensation process to obtain COFs with good reproducibility and high crystallinity. In 2020, Py-COF films were used as stable acidic color change sensors with fast response times, low detection limits, and good reproducibility (Fig. 9a).[42] In 2022, Gan *et al.*[43] synthesized Py-COF *via* a one-pot polycondensation reaction using BFBAPy as a precursor to prepare amino-functionalized magnetic $Fe_3O_4$–$NH_2$ nanoparticles and synthesized a magnetic self-assembled COF adsorbent (Fig. 9b).

Currently, the mainstream of COF synthesis involves developing diverse strategies to construct different COFs through changing the length of the linkers, where the [1+1] strategy can also be used in two combinations of $C_4 + C_2$ and $C_4 + C_4$ so that 2D COFs with tetragonal apertures can be generated. By employing 1,3,6,8-tetrakis(4-aminophenyl)pyrene (PyTTA) as the building block to react with different linking units, a series of imine-linked COFs could be synthesized. Due to the high electron cloud density of pyrene units, the as-obtained imine-linked COFs are beneficial for charge separation and transfer, thus effectively improving the photoelectron absorption capacity of imine PyCOFs. In 2012, Nagao *et al.*[44] reported that PyTTA-DHTA-COF was synthesized through the condensation reaction between PyTTA and 2,5-dihydroxyterephthalaldehyde under solvothermal conditions. PyTTA-DHTA-COF contains two hydroxyl groups, and the extension of the hydrogen bonding framework with the water molecule provides the mode of transport of protons and the efficiency of proton transfer.

The introduction of electron-absorbing groups and electron-donating groups on the pore wall surfaces of the linkers, respectively, resulted in COFs with significantly different photoelectronic properties and photocatalytic activities.[45] In particular, this is solely due to the electron-donating conjugation effect of the electron-donor groups, which gives the COFs more charge separation and transport capabilities.[46] In 2023, Ma *et al.*[45b,47] prepared two new conjugated PyCOFs (PyDF-COF and PyBMT-COF) (Fig. 10a). The strong electron-donor conjugation effect of the thiomethyl group gives the PyBMT-COF wider visible absorption, narrower band gap, more negative reduction potential, and higher photocurrent response. Lin and co-workers[48] reported the synthesis of the Py-TT COF with Py as the donor and TT as the acceptor. The as-obtained donor–acceptor Py-TT COF displayed a narrow bandgap and high efficiency of charge separation and transfer, which could greatly improve the photocatalytic activity (Fig. 10b). Chen *et al.*[49] reported thickness tunable thienothiophene-pyrene COFs comprised of a carbon nanotube (CNT) core. The charge

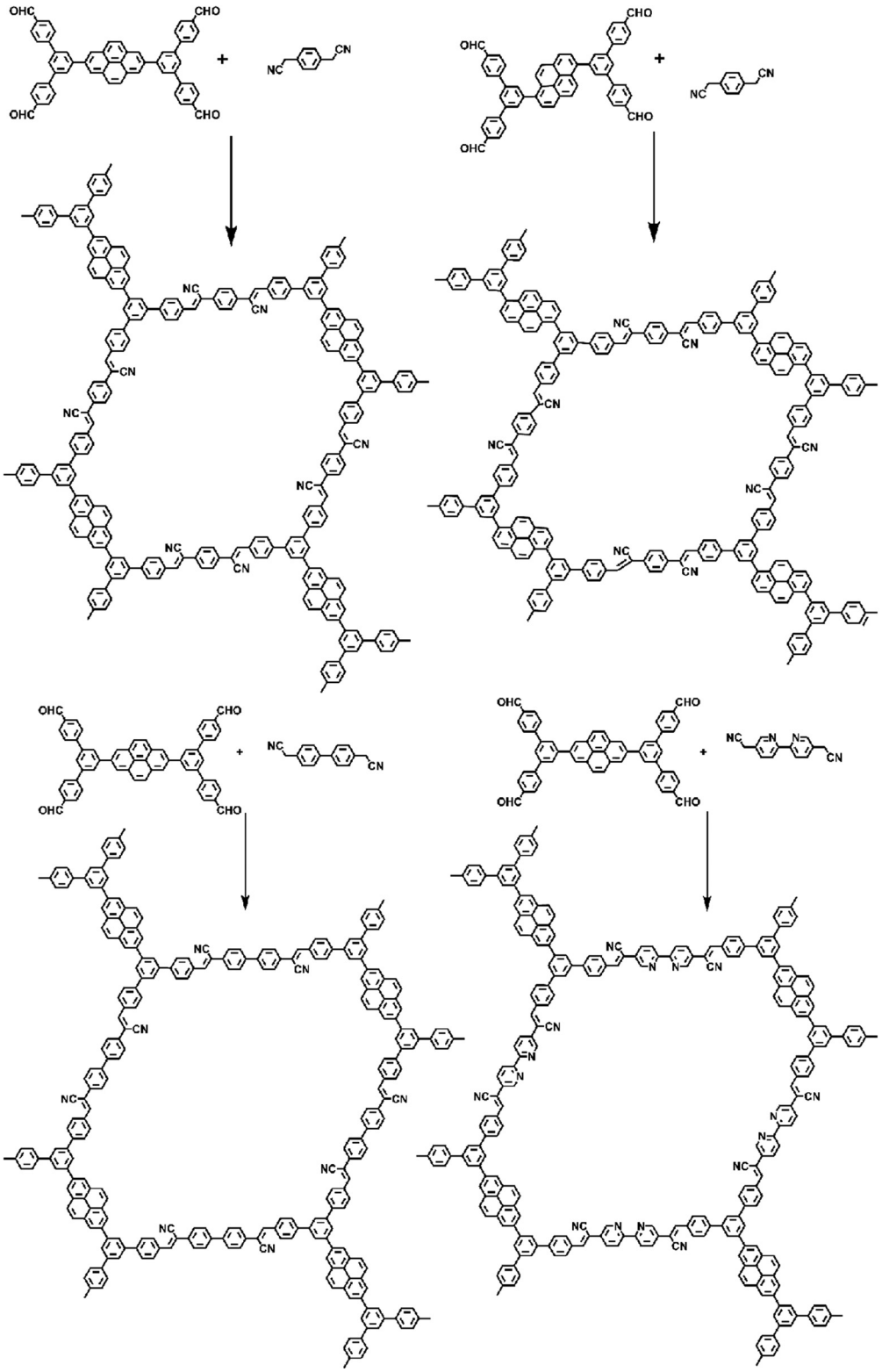

Fig. 7 Synthesis of $sp^2c$-PyCOFs. Reproduced with permission.[39] Copyright 2022, Wiley-VCH GmbH.

transfer potential barrier between the active catalytic site and the adsorbed oxygen intermediate was lowered, resulting in a significant increase in catalytic activity.

With the continuous advances in organic chemistry, the synthetic methods to prepare COFs are constantly innovated, and the degree of conjugation between the building blocks and

 

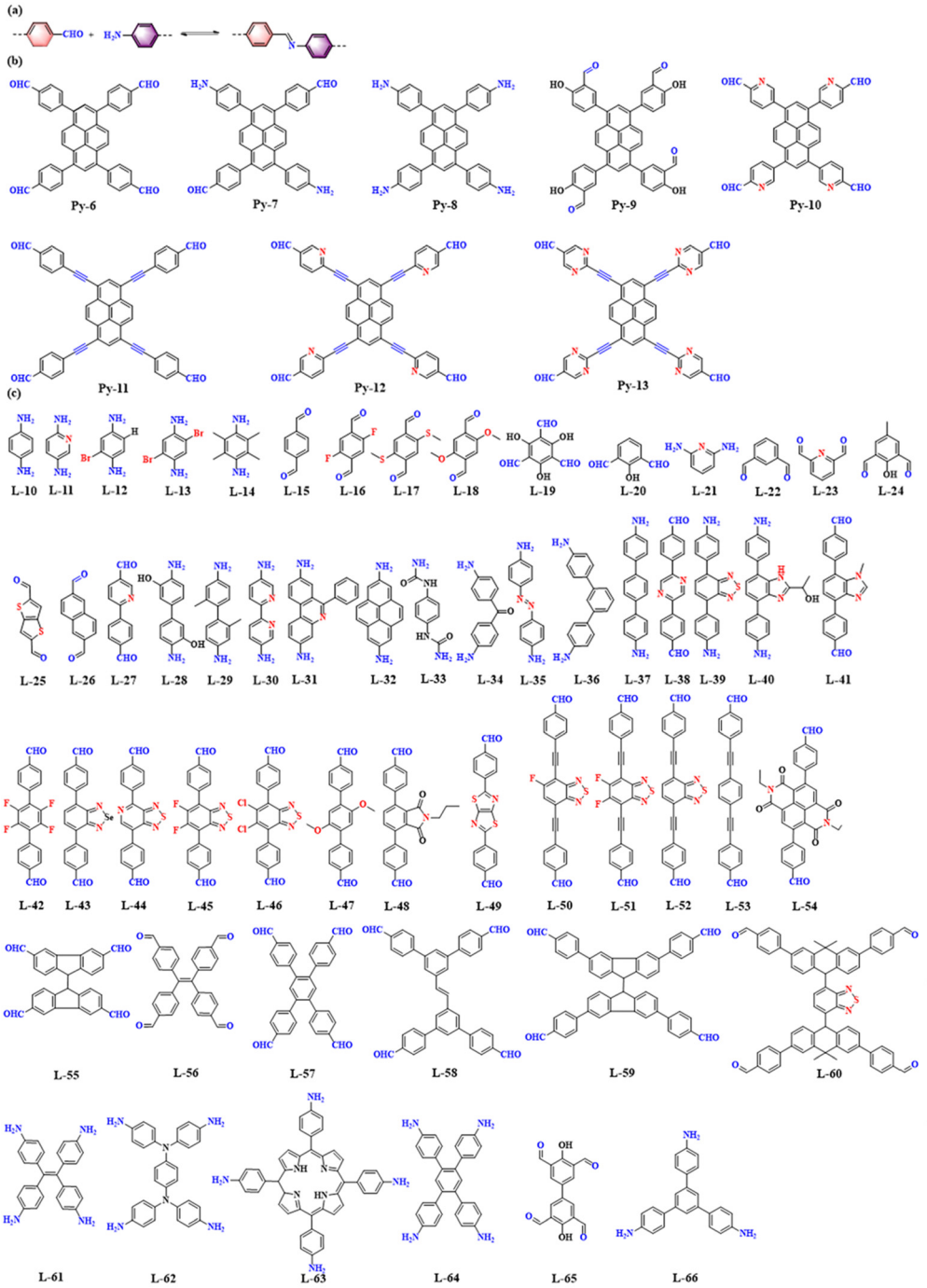


Fig. 8 (a) Schematic illustration of imine-linked PyCOFs. (b) Frequently used pyrene-based building blocks. (c) Frequently used monomers.

the connecting units can be changed from non-conjugated to partially conjugated or even to fully conjugated. In addition, the linkers of PyCOFs are development, leading to the large pores and surface area of COFs.[54] In 2013, Liu *et al.*[52] obtained an IM4F-Py-COF through the Schiff-base condensation reaction under solvothermal conditions (Fig. 10d), while in 2021, Wen *et al.*[53] synthesized donor–acceptor-type COF-JLU25 through the reaction between (4-aminophenyl)pyrene (PyTA) and 4-[4-(4-formylmethyl)-2,5-dimethoxyphenyl] benzaldehyde (TpDA) (Fig. 10e). The as-obtained COF-JLU25 exhibits excellent photocatalytic activity with high efficiency, robust reusability, and low catalyst loading, demonstrating the previously underexploited potential for application of COF-based photocatalysts consisting of only electron-rich units. In 2022, Gao *et al.*[55] prepared a new ETTA-PyTTA-COF, constructed through the condensation reaction between 4,4′,4″,4‴-(ethane-1,1,2,2-tetrayl)-tetrabenzaldehyde (ETTA) and PyTTA. Furthermore, some COFs with regular pore structures have been

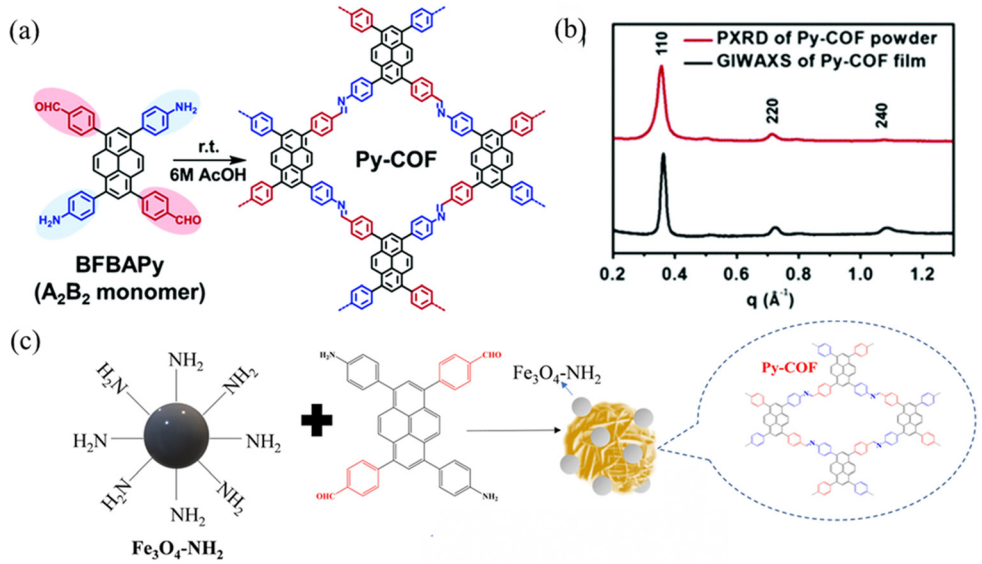


Fig. 9 (a) Synthesis of Py-COF. Reproduced with permission.[42] Copyright 2020, Royal Society of Chemistry. (b) Projection of in-plane GIWAXS data of the Py-COF film (black) and PXRD data of the Py-COF powder (red). (c) Synthesis of $Fe_3O_4$@Py-COF. Reproduced with permission.[43] Copyright 2022, Elsevier.

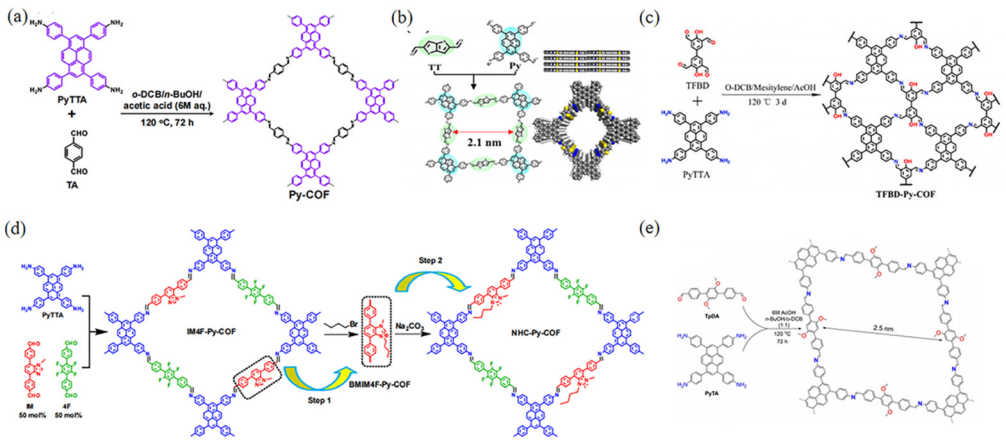


Fig. 10 (a) Schematic illustration of the synthesis of Py-COF. Reproduced with permission.[50] Copyright 2018, Royal Society of Chemistry. (b) Schematic of the synthesis of the Py-TT COF. Reproduced with permission.[48] Copyright 2021, American Chemical Society. (c) Illustration of the synthesis and structure of TFBD-Py-COF. Reproduced with permission.[51] Copyright 2022, Elsevier. (d) Synthesis of NHC-Py-COF. Reproduced with permission.[52] Copyright 2021, MDPI. (e) Synthesis of COF-JLU25. Reproduced with permission.[53] Copyright 2021, Wiley-VCH GmbH.

demonstrated to show large π-conjugated structures with interesting photovoltaic properties (Fig. 8c).[51]

As to imine-linked PyCOFs, they have been synthesized with different linkers using TFPPy as a $C_4$ node.[56] In 2013, Kaderi and co-workers[57] reported the synthesis of highly crystalline mesoporous TFPPy-PPD-COF through the condensation reaction between TFPPy and p-phenylenediamine, where strong π–π stacking interactions between the pyrene moieties could enhance the porosity and adsorption properties of COFs. In 2017, Wang *et al.*[58] integrated TFPPy-PPD-COF with single-layered graphene (SLG) for application in the field of organic electronics and optoelectronics (Fig. 11a). In 2023, Hu and collages[56e] synthesized TFPPy-TMPD-COF through methyl substitution of TFPPy-PPD-COF, where they found that Me-substitution endowed the as-modified COFs with stronger charge transfer ability to increase the electron density of the backbone, enhancing the ability to interact with anions. Grafting methyl groups onto COFs changed the pore environment, promoted the formation of iodine anions, enhanced framework–iodine interactions, and facilitated the iodine trapping ability of TFPPy-TMPD-COF. In 2021, Yang *et al.*[59] synthesized the DP-Py COF using TFPPy and 2,6-methyldiamino-pyridine (DP) as building blocks. The obtained DP-Py COF was employed to fabricate a novel electrochemical sensing platform for sensitively and selectively detecting theophylline (TP) and caffeine (CAF) simultaneously through compounding with AuNPs.

 

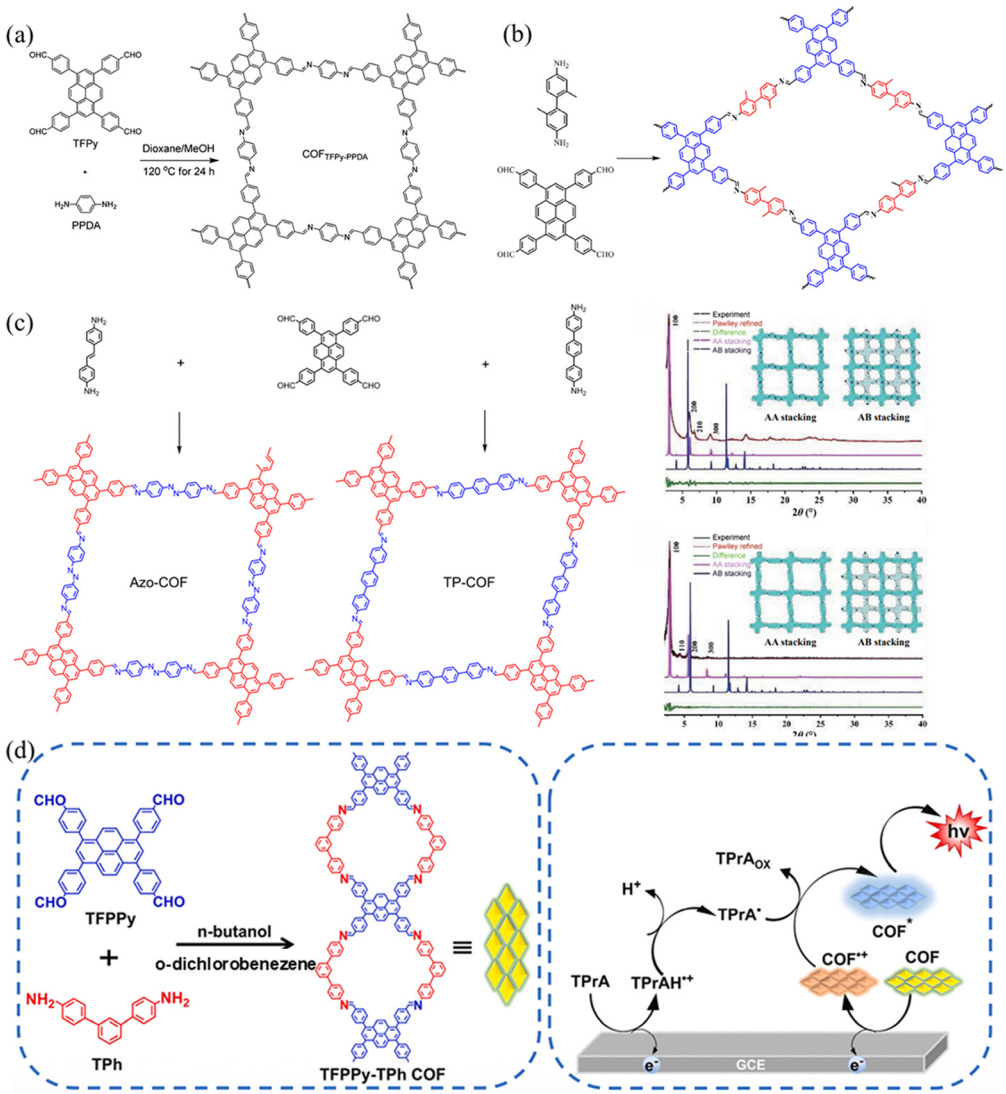


Fig. 11 (a) The synthesis of COF TFPPy-PPDA. Reproduced with permission.[58] Copyright 2017, American Chemical Society. (b) Schematic representation of the transformation of imine COFs into amide COF TFPPy-DP *via* oxidation by oxone. Reproduced with permission.[56c] Copyright 2022, Elsevier. (c) The synthesis of Azo-COF and Tp-COF. Reproduced with permission.[60] Copyright 2022, Springer Nature. (d) Schematic diagram of TFPPy-TPh-COF. Reproduced with permission.[61] Copyright 2024, Elsevier.

COFs can allow atomically precise design and integration of nodes and linkers into ordered networks with permanent porosity through linkages.[62] Developing novel linkers enables the design and synthesis of new COFs.[3,63] In 2020, Guo and co-workers[56d] synthesized COF-TP based on TFPPy and 4,4′-diaminobenzophenone (DABP), exhibiting a rare 1D structure. The obtained COF-TP possessed a comparatively high BET surface area and relatively high chemical stability. The Liang group and Hou group used 4,4′-diamino-[1,1′-biphenyl]-3,3′-diol and 2,2′-dimethylbenzidine to synthesize two kinds of two-CoFs (TFPPy-BDOH and TFPPY-DM COF) with TFPPy, and the resulting COFs showed different properties (Fig. 11b).[56c,64] TFPPy-BDOH has good selectivity for uranium due to the synergistic interaction between the nitrogen atom in the imine bond and the hydroxyl group in the conjugated framework, while the TF-DM COF is a metal-free catalyst for the hydroxylation of aryl boronic acids. In 2022, Yang *et al.*[60] synthesized two COFs (Azo-COF and Tp-COF) using TFPPy as a building node and p-AA or DATP as the linear linkage through the Schiff base reaction (Fig. 11c). The two as-synthesized mesoporous COFs (Azo-COF and Ip-COF) adopt the AA stacking mode and have highly crystalline and stable frames. Because the lengths of the two chains did not show too much difference, the pore size of PyCOFs are slightly adjusted with high specificity for protein selection.

### 2.4 Hydrazone-linked PyCOFs

Hydrazones are a class of compounds containing the C═NNHCOR group, formed through the reaction between hydrazines or substituted hydrazines (such as phenylhydrazine) and carbonyl compounds (such as aldehydes or ketones) (Fig. 12). Due to the long non-aromatic portion of the

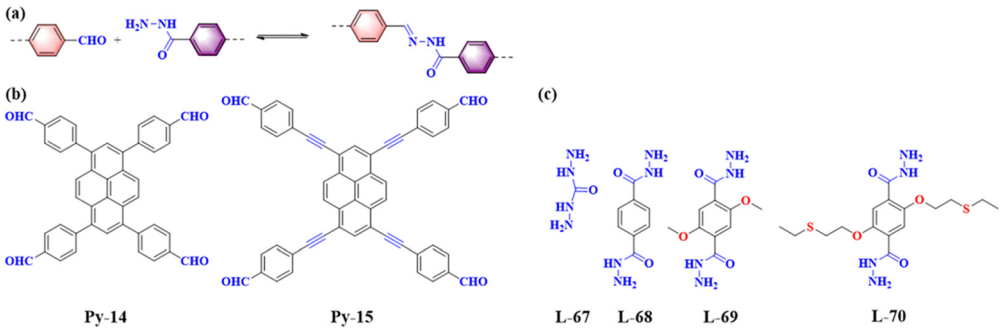


Fig. 12 (a) Schematic illustration of hydrazone-linked PyCOFs. (b) Frequently used pyrene-based building blocks. (c) Frequently used monomers.

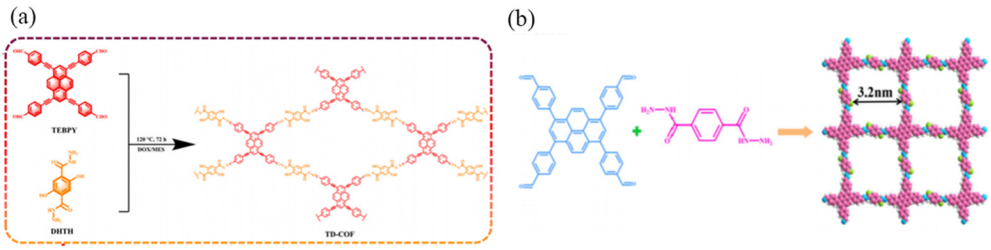


Fig. 13 (a) Schematic representation of the synthesis of TD-COF. Reproduced with permission.[65b] Copyright 2023, Elsevier. (b) Synthetic diagram of DTF-ANDI-COF. Reproduced with permission.[67] Copyright 2023, Elsevier.



hydrazone-linked COFs, such materials require the integration of ethoxy groups into the neighbour of the linear linker, to maintain the 2D conformation of the materials as well as facilitate the crystallizationprocess.[65]

Xu *et al.*[66] constructed a hydrazone-linked Pythz-COF and a urea-linked Pyurea-COF based on TFPPy as the building block. Pythz-COF has a high specific surface area, with the pore size mainly concentrated at 2.34 nm and a small amount of pore size distributed around 1.36 nm, with good reusability. In 2012, Zhang *et al.*[65c] synthesized TFPPy-DMeTHz-COF with hydrazone bonds as the linkage and 2,5-dimethoxyterephthalohydrazide (DMeTHz) and TFPPy as the monomers. The π-conjugated skeleton formed in TFPPy-DMeTHz-COF results in a low bandgap. The COF showed stable photocurrent response and excellent photoelectronic behavior. In the same year, Liu and co-workers[65b] selected TEBPY with a complete planar structure and DHTH with the functional group (–OH) as the building blocks to prepare another COF (TD-COF) (Fig. 13a), where –OH is distributed throughout the molecular backbone, leading to dramatic changes in the orbital distribution and energy gap of TD-COF. In 2022, Qiu *et al.*[67] discovered synergism between Pythz-COF neutral amide functional groups and Au(III) and hydrogen bonding between protonated amides and $AuCl_4^-$ for fluorescence detection of Au(III) (Fig. 13b).

### 2.5 Heterocycle-linked PyCOFs

Heterocycle-linked COFs generally possess imine structures, which can be post-modified to produce cyclic compounds such as pyrazines, pyridines, pyrimidines, thiazoles, or oxazoles through redox reactions. Heterocyclic COFs have the advantages of structural stability and irreversibility and are commonly used in catalysis and energy storage (Fig. 14).

Pyrazine-linked COFs are one of the common heterocycle-linked COFs, which are usually constructed through the reaction between 1,2-diketone and 1,2-diamine moieties. This makes pyrazine-connected COFs a promising material for optoelectronic applications. In 2018, Hoberg *et al.*[68] reported a series of pyrazine-based PyCOFs with highly stable aromatic backbones and intrinsically ordered nanoscale pores (Fig. 15a). The nanoscale pores are modified to incorporate various desired functional groups. This new bottom-up approach provides an idiomatic way to achieve highly ordered and modifiable materials for design and synthesis. Jiang *et al.*[69] reported a chemically stable, electronically conjugated 2D COF with topologically designed wire frameworks and open nanochannels (Fig. 15b). The conjugated COF permits inherent periodic ordering of conjugated chains in all three dimensions and displays a striking combination of physical properties: chemical stability, extended π-conjugation, and high carrier mobility. Fully π-conjugated COFs are useful for high on–off ratio photoswitches and photovoltaic cells.

Porphyrin, possessing a highly conjugated core ring structure similar to chlorophyll and with flexible physical and chemical properties, has become one of the most investigated photosensitizers.[71] Fully conjugated COFs were synthesized from porphyrin derivatives and pyrene-4,5,9,10-tetraketone, which can be complexed with metal ions to increase photocatalytic performance. In addition, tetragonal topology can be

 

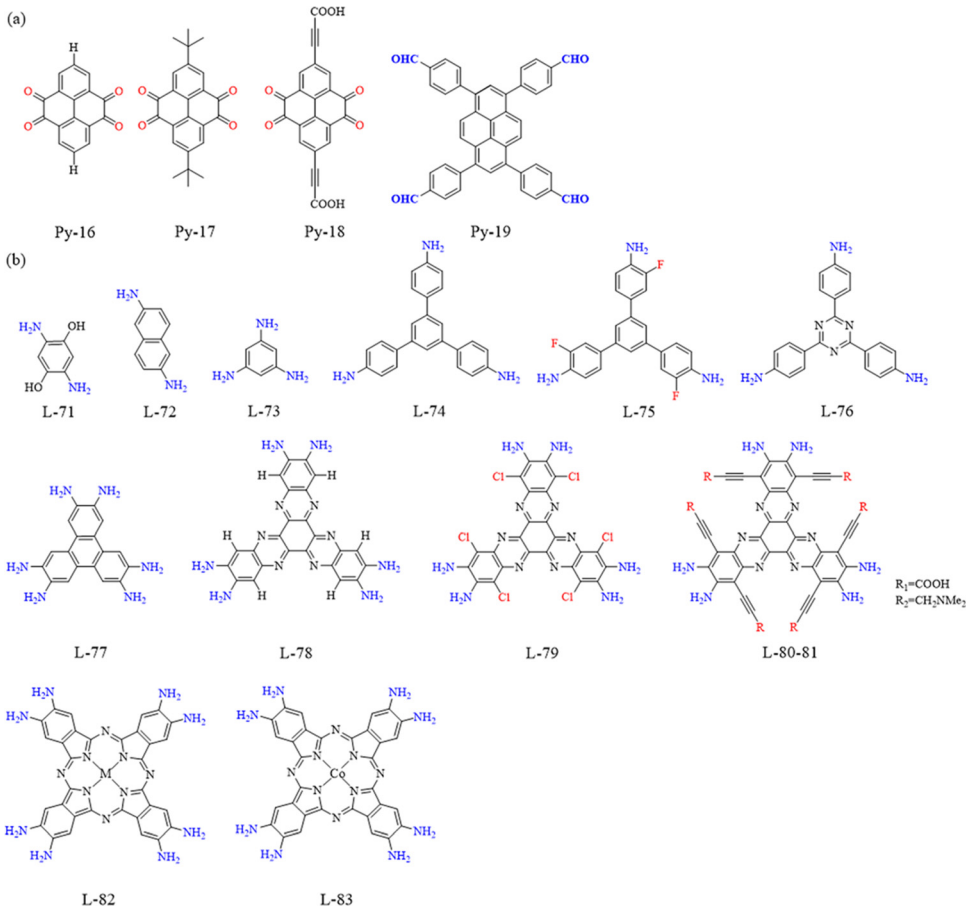


Fig. 14 (a) Frequently used pyrene-based building blocks. (b) Frequently used monomers.

used to increase conjugated bonds for connecting catalytic sites.[70] In 2020, Jiang and co-workers[70,a] integrated cobalt(II) phthalocyanine into 2D COFs *via* a robust phenazine bond, where the COFs displayed excellent stability, even under boiling water, acid, or base conditions (Fig. 15d). The MPc-pz COF can be used as an electrocatalyst due to its unique ability. By integrating the all-π conjugated stable backbone and catalytic sites into one single lattice, the MPc-pz COF exhibits excellent stability, high conductivity, and good catalytic activity in the reduction of $CO_2$ to CO in water. Feng and co-workers[70,b] reported a series of pyrazine-connected metal-phthalocyanine-based conjugated 2D M-COFs (M = Zn, Cu, Ni) (Fig. 15c), which can provide a reliable way to design and develop semiconductor COF materials with enhanced charge transport properties.

Multicomponent reactions (MCRs) are widely used in organic synthesis to improve synthetic efficiency and versatility, especially for constructing ring structures. The classical synthesis of imidazole rings can be easily realized through the three-component Debus–Radziszewski reaction. In 2019, Wang *et al.*[72] used this MCR strategy to construct a series of imidazolium-conjugated stable COFs (Fig. 16). A new approach to establish the precise composition of crystalline COFs is provided by the *in situ* formation of five covalent bonds in each cyclic imidazole ring. The synthesized pairs of imidazole-linked COFs are highly stable and also provide an additional driving force for crystallization.

A simple solution to improve the stability of COFs is to make covalent joints stable. Benzoxazole and benzothiazole structures are common solutions to achieve high stability. The classical synthesis of benzoxazole/benzothiazole structures is realized through a cascade reaction involving reversible imine bond formation followed by irreversible oxazole/thiazole ring formation. This reversible/irreversible sequence may be ideal for building robust COF structures. In 2018, Wang *et al.*[73] synthesized highly crystalline benzobisoxazole-conjugated COFs using *N*-methyl-2-pyrrolidone/resorcinol as a solvent mixture and benzoxazole as an additive. It has been found that this COF is highly chemically stable. In addition, the binding of the benzothiazole portion in the π-conjugated COF backbone reduced the optical band gap and enhanced visible light absorption. Cooper and co-workers[74] reported a simple and efficient three-component assembly reaction between readily available aldehydes, amines, and elemental sulfur *via* CH-functionalisation and oxidative cyclisation (Fig. 17a). Highly stable thiazole-conjugated COFs were successfully prepared through a one-pot method with a series of functionalized aldehydes and amines.

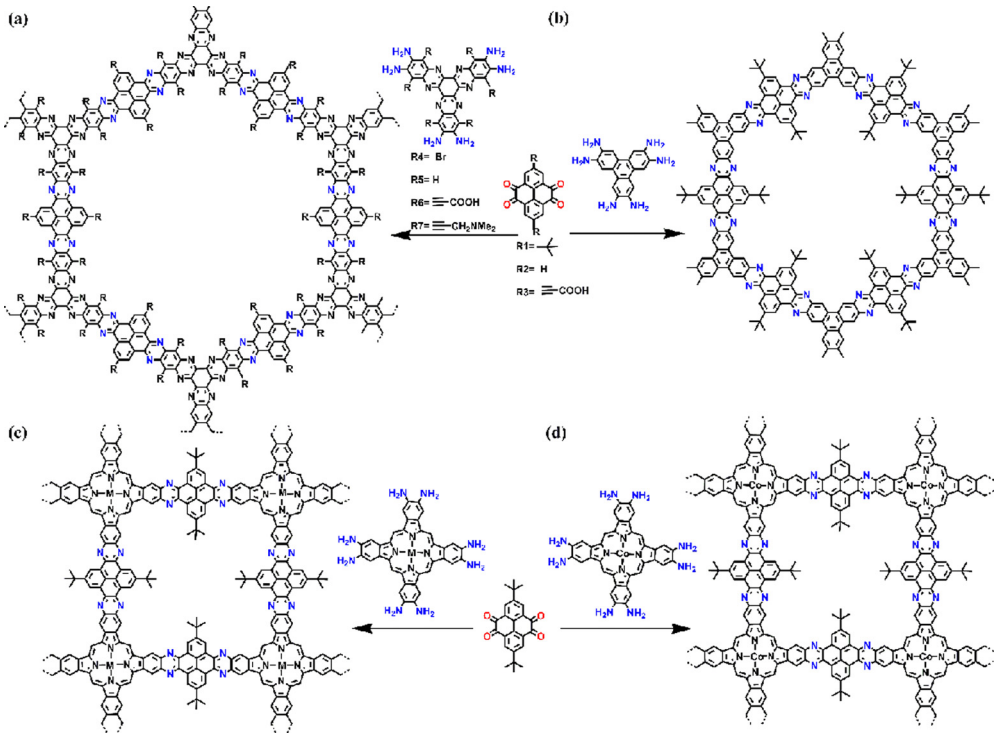


Fig. 15 (a) Schematic representation of the synthesis of PyCOFs. Reproduced with permission.[68] Copyright 2018, American Chemical Society. (b) Schematic representation of the synthesis of CS-COF. Reproduced with permission.[69] Copyright 2013, Springer Nature. (c) Design and synthesis of the MPc-pz COF. Reproduced with permission.[70,b] Copyright 2019, American Chemical Society. (d) Design and synthesis of the CoPc-pz COF. Reproduced with permission.[70,a] Copyright 2020, Wiley-VCH GmbH.

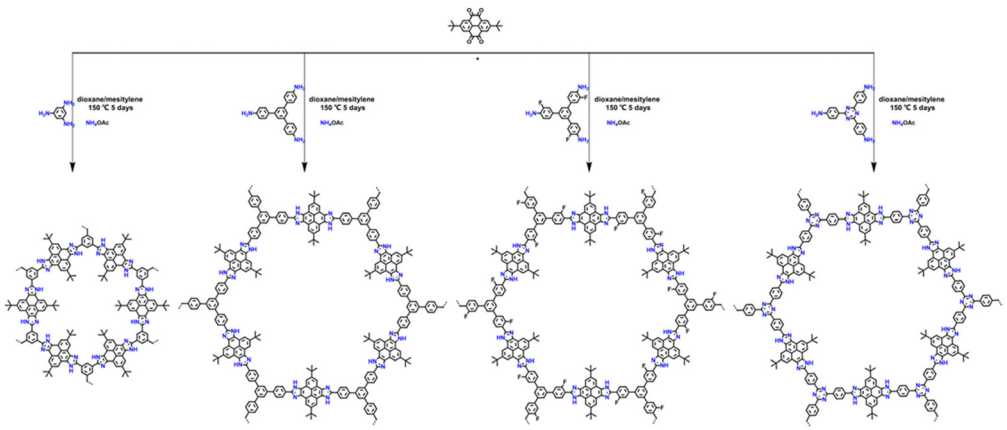


Fig. 16 One-pot construction of imidazole-linked COFs by *in situ* formation of five-membered cyclic linkages. Reproduced with permission.[72] Copyright 2019, American Chemical Society.

Furthermore, fully conjugated COFs with enhanced chemical stability and optoelectronic properties can be achieved through post-synthetic modification. Imine-linked COFs can be post-oxidized to convert the imine bonds into heterocyclic linkages from cyclic units such as oxazole and thiazole linkages. In 2018, Yaghi *et al.*[75] showed that imine-linked COFs could be transformed into two different heterogeneous COFs containing thiazole and oxazole bonds, respectively (Fig. 18). This conversion was achieved by successive substitution and oxidative cyclization procedures, and these materials exhibited higher chemical stability compared to the amine-substituted starting materials.

### 2.6 Other linked COFs

These COFs, formed through the reaction of amine derivatives with anhydrides, are linked by an imide bond, where higher reaction temperatures and longer polymerization times are

 

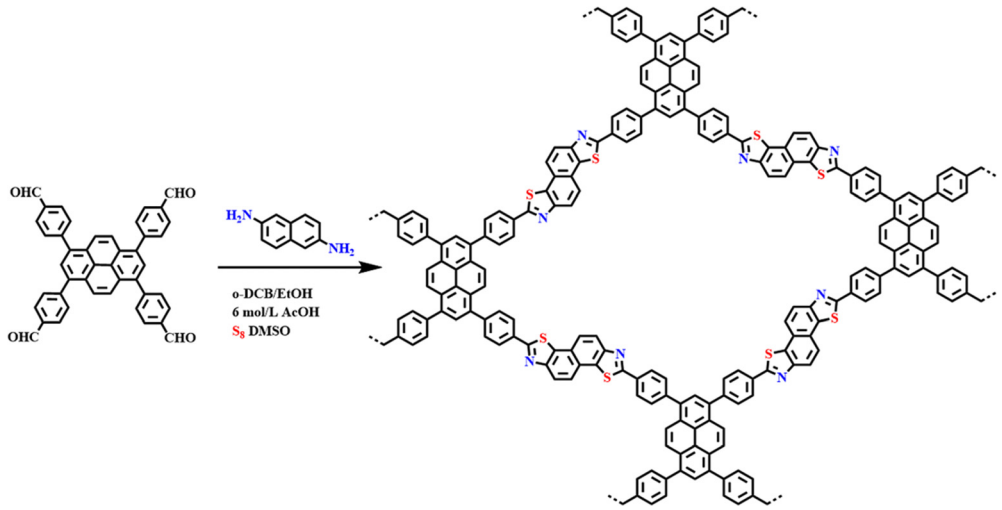


Fig. 17 One-pot construction of benzoxazole-linked COFs *via* the cascade reactions. Reproduced with permission.[74] Copyright 2018, American Chemical Society.

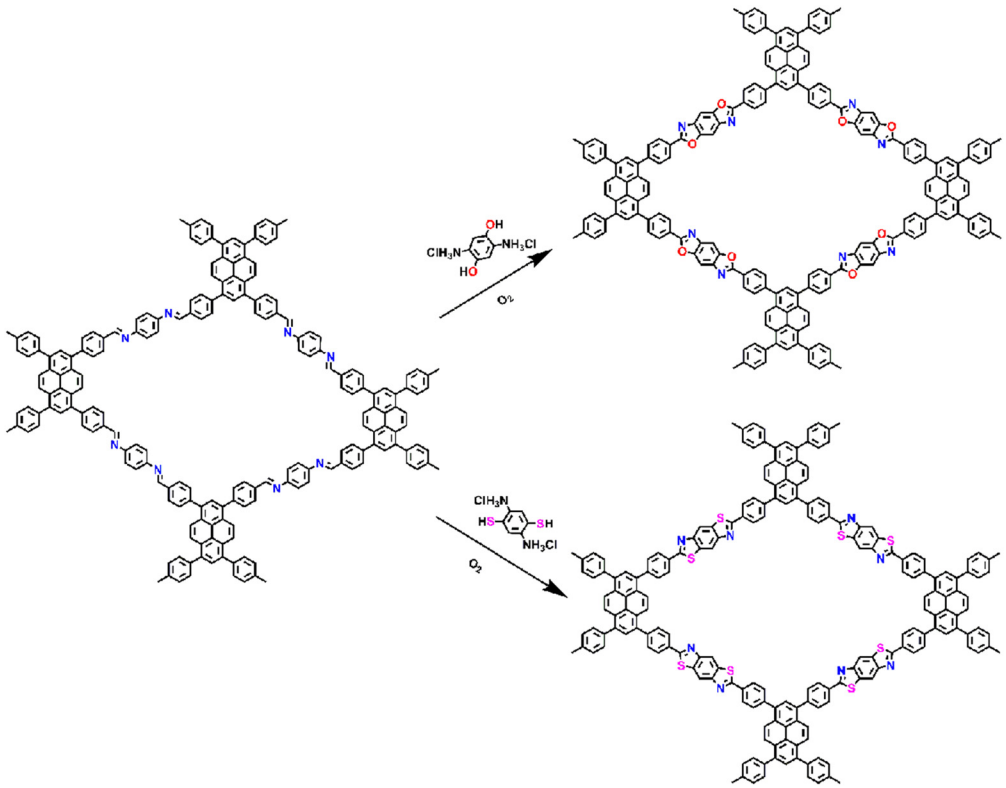


Fig. 18 The synthesis and structures of heterocyclic linked PyCOFs through post-synthetic modification.[73] Copyright 2020, American Chemical Society.

mostly required for such synthesis due to the lower degree of reversibility of the reaction when forming the imide bond. However, the introduction of the imide bond can increase the forces with some guest molecules resulting in unique properties (Fig. 19).

In 2023, Cao and co-workers[76] reported a stabilization strategy of D–A PyCOFs by intramolecular hydrogen (H)-bonds and a membrane-based mass transfer strategy for photocatalytic modulation (Fig. 20a). The high stability of these COFs comes from the strong π–π interactions and the H-bonds of adjacent PyTTA and naphthalene diimide units as well as the D–A charge transfer. Abbaspourrad and co-workers[77] reported a new PEPy-COF, where the pyrene monomers with $D_{4h}$ symmetry were in the corners geometrically, and the $D_{2h}$ symmetric

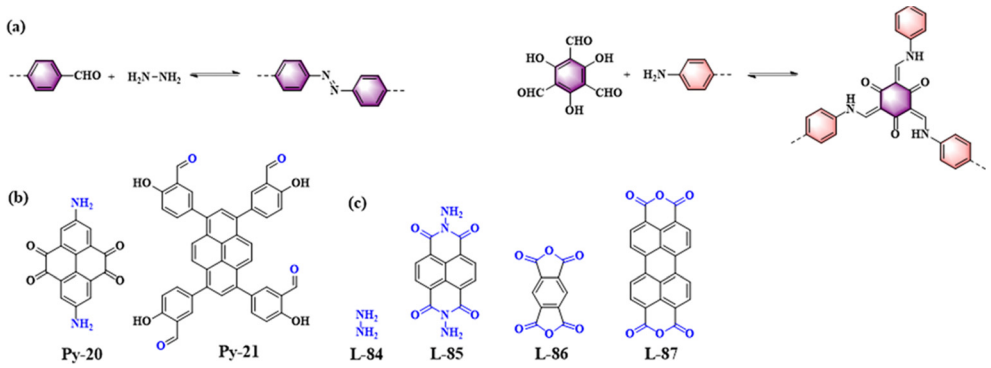


Fig. 19 Monomers used in the synthesis of PyCOFs.

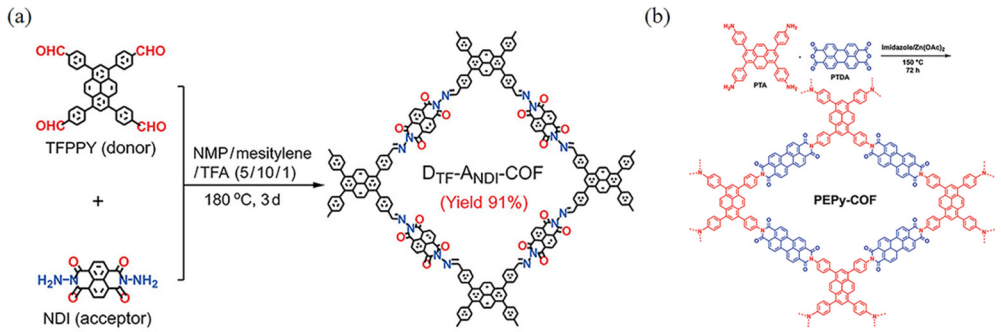


Fig. 20 (a) Synthesis of $D_{TF}$–$A_{NDI}$-COF. Reproduced with permission.[76] Copyright 2023, Wiley-VCH GmbH. (b) Synthesis of PEPy-COF. Reproduced with permission.[77] Copyright 2023, Wiley-VCH GmbH.



perylene units were located at the edges of the mesoporous tetragons (Fig. 20b).

# 3. Application of PyCOFs

## 3.1 Photocatalytic applications of PyCOFs

**3.1.1 Photocatalytic hydrogen evolution.** The energy conversion system for water decomposition must meet the following thermodynamic requirements:[78] (1) the photon energy must be equal to or greater than the energy required to transfer one electron from a water molecule, which is 1.23 eV; (2) the catalyst must fulfill both the half-reaction potential for the oxidation of water, $E_{ox} > 1.23$ V (pH = 0, NHE), and the half-reaction potential for the reduction of water, $E_{red} < 0$ V (pH = 0, NHE).[79] The photocatalytic system consists of three main aspects: (1) semiconducting photocatalysts with conduction band and valence band potentials spanning the $H^+/H_2$ and $O_2/H_2O$ levels, respectively, absorbing light to generate electron–hole pairs; (2) separation and migration of photogenerated electron–hole pairs; and (3) redox reaction of water molecules on the catalyst surface. By broadening the light absorption range of the semiconductor photoresponse, improving the separation efficiency of the photogenerated carriers, and accelerating the kinetics of the surface catalytic reaction, these three processes cooperate to efficiently carry out the corresponding redox reactions.[80] This cooperation is crucial for the design and synthesis of efficient photocatalysts.[81]

*3.1.1.1 Single-phase photocatalysis based on PyCOFs.* In the development of photocatalytic catalysts, it has been observed that the structural adaptability of inorganic photocatalysts is limited.[82] This limitation further impacts the bandgap, molecular orbital energy level, and photocatalytic activity. On the other hand, organic photocatalysts address these shortcomings and exhibit strong visible light absorption characteristics.[83] COF materials are becoming ideal materials for photocatalytic hydrogen evolution.[4,83c,84] The PyCOFs with a large conjugation degree provide a high density of surface active sites for mass transport, thus shortening the distance from the photogenerated carriers to the reaction center. Besides, PyCOFs exhibit large conjugated skeletons. Their band gaps could be finely tuned by changing the linkers. Actually, different linkers exhibit different conjugation and electronic properties, which affect the energy levels of the COFs.

Jiang and co-workers synthesized $sp^2$c-COF and $sp^2$c-$COF_{ERDN}$, which are entirely based on π-conjugation (Fig. 21a).[85] 3-Ethylrhodanine (ERDN) is electron-deficient unit, the push–pull effect of a 2D π-conjugated structure can enhance light trapping and narrow the band gap (Fig. 21b). The higher HOMO level of $sp^2$c-$COF_{ERDN}$ results in a narrower band gap, facilitating the excitation of electrons to the LUMO

 

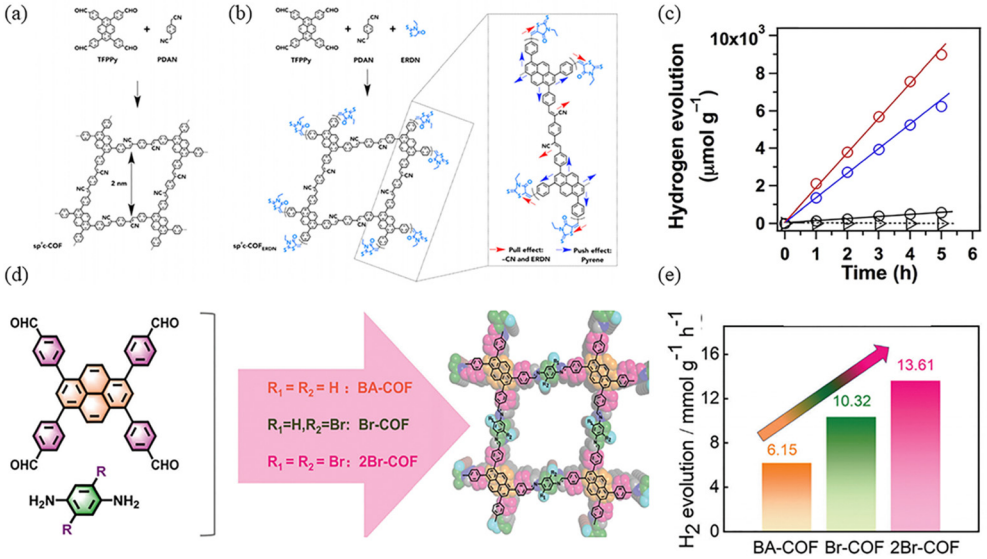


Fig. 21 (a) Synthesis of the tetragonal sp$^2$c-COF. (b) Synthesis of sp$^2$c-COF$_{ERDN}$. (c) Hydrogen production monitored over 5 h with sp$^2$c-COF (blue circles), sp$^2$c-COFERDN (red circles), sp$^2$c-CMP (black circles), and imine-linked pyrene COF (triangles) as photocatalysts under irradiation with wavelengths $\geq$420 nm. Reproduced with permission.[85] Copyright 2019, Elsevier. (d) Schematic diagram of BA-COF. (e) Photocatalytic $H_2$ evolution performance of as-prepared COFs. Reproduced with permission.[86] Copyright 2024, Wiley-VCH GmbH.

level, further enhancing the photocatalytic water decomposition capability. Using Pt as a co-catalyst to catalyze hydrogen production from water by shortening the electron transport distance and the photochemical processes of light harvesting, exciton migration and exciton splitting as well as electron transfer and harvesting were seamlessly integrated. In contrast, the photocatalytic hydrogen evolution performance of sp$^2$c-COF$_{ERDN}$ is better than that of sp$^2$c-COF, with 2120 and 1360 μmol h$^{-1}$ g$^{-1}$, respectively (Fig. 21c).

Sp$^2$c-conjugated-linked COFs are highly rigid and well conjugated, but the sp$^2$c-conjugated linkage is irreversible, leading to possible poor structural stability under photoexcitation. In order to improve the reversibility of COFs, Deng *et al.* introduced imide structure in PyCOFs for photocatalytic hydrogen evolution, and modified the linked unit with different contents of bromine atoms. It was found that the introduction of bromine atoms was helpful in the electron transfer process and increased the hydrogen production rate; the hydrogen production rate of 2Br-COF was also the highest at 13.61 mmol g$^{-1}$ h$^{-1}$ (Fig. 21e).

Symmetrical imine-linked PyCOFs have been reported. Compared to 2D COFs, 1D COFs can be constructed using V-shaped $C_2$ connectors and planar $C_4$ connectors to form a ribbon structure, where V-shaped $C_2$ connectors promote the creation of ultra-small holes, enhancing the filling of micropores in the atmospheric water harvesting (AWH) and facilitating the cleavage of the optical water splitting. Gu *et al.*[87] synthesized one-dimensional PyCOFs using asymmetric units, which have adsorption capacity for water to produce hydrogen. The exciton binding energy and band gap of Py-HMPA were found to be much lower than those of Py-MPA and Py-PDCA (Fig. 22a), respectively. The results suggest that the introduction of pyridine and –OH groups may facilitate the separation of electrons and holes. Appropriate hydrophilic groups such as –OH not only promoted the rapid nucleation of water molecules, but also enhanced the separation of photogenerated charges and improved the photocatalytic performance of COF The photocatalytic hydrogen evolution rate (HER) of Py-HMPA reached a value of 37.925 mmol g$^{-1}$ h$^{-1}$ at 7 wt% Pt, and its photocatalytic hydrogen evolution ability was much higher than that of Py-MPA and Py-PDCA (Fig. 22b–d).

Elemental doping is an effective strategy to modulate the physicochemical properties of photocatalysts, which can broaden the light absorption range of photocatalysts and enhance the efficiency of photocatalytic energy conversion. The integration of benzidine and 4,4′-diaminoazobenzene together as connecting wires can produce two new COFs: Benzd-COF and Azod-COF (Fig. 23a).[88] Using 4′-(pyrazine-2,5-diyl)dibenzaldehyde as the acceptor, Yan *et al.*[89] synthesized imine-linked PyPz-COF with adjustable photocatalytic activity (Fig. 23b). The introduction of the pyrazine ring endows PyPz-COF with distinct optical, electrochemical and charge transfer properties. It also introduces abundant C=N groups, which could enhance proton transfer through hydrogen bonding. The bandgap of PyPz-COF is slightly smaller than that of PyTp-COF, which may be due to the introduction of the electron-deficient pyrazine ring that gives PyPz-COF the potential for photocatalytic cleavage of water to hydrogen (Fig. 23c). PyPz-COF demonstrates a significantly enhanced photocatalytic hydrogen generation rate of up to 7542 μmol g$^{-1}$ h$^{-1}$ with Pt as a cocatalyst, which is in stark contrast to that of PyTp-COF without pyrazine introduction (1714 μmol g$^{-1}$ h$^{-1}$) (Fig. 23d). The introduction of nitrogen effectively reduces the band gap

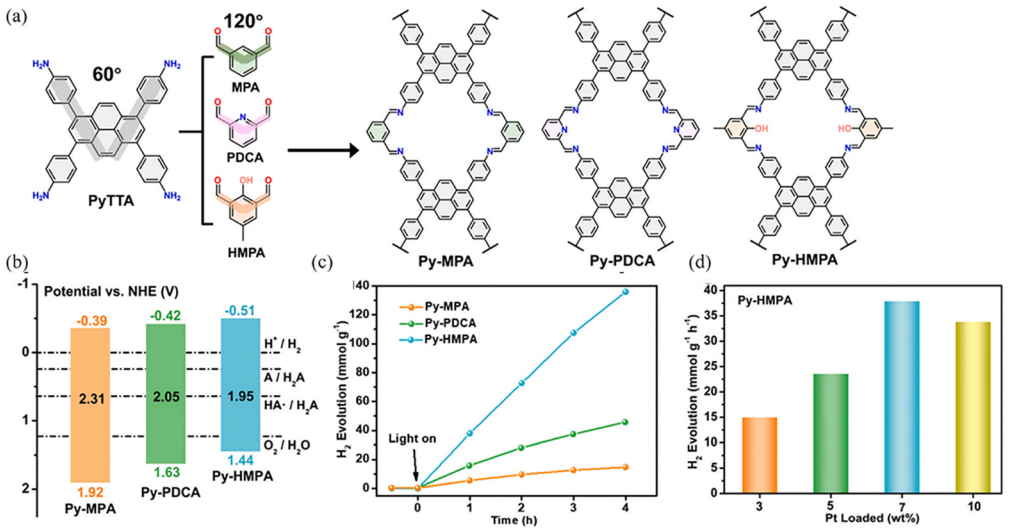


Fig. 22 (a) Synthesis and molecular structure of Py-MPA, Py-PDCA and Py-HMPA. (b) Electronic band structure. (c) Time dependent $H_2$ production in liquid water of three COFs. (d) The $H_2$ evolution in liquid water for Py-HMPA with different Pt loading amount. Reproduced with permission.[87] Copyright 2023, Elsevier.

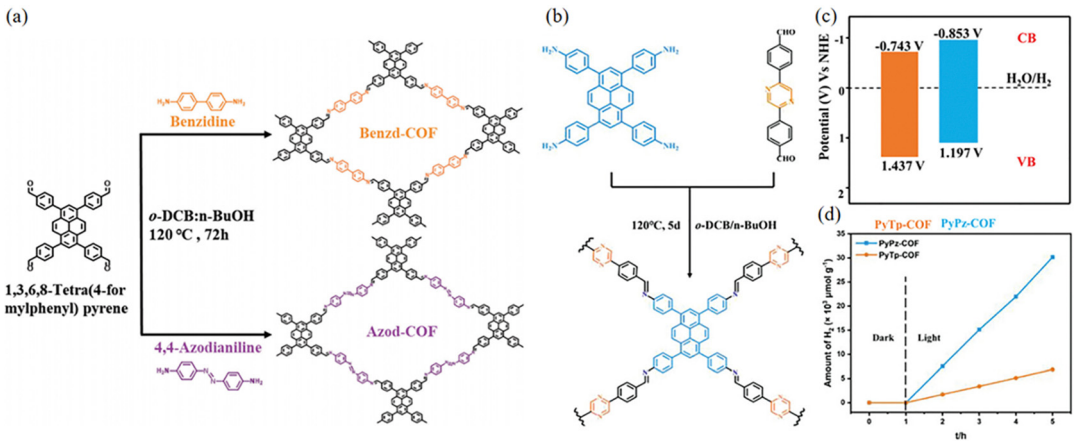


Fig. 23 (a) Synthetic routes to Benzd-COF and Azod-COF. Reproduced with permission.[88] Copyright 2023, Wiley-VCH GmbH. (b) Schematic diagram of the synthesis of PyPz-COF. (c) Band structure diagram of PyTp-COF and PyPz-COF. (d) The plots for time course photocatalytic $H_2$ evolution of PyPz-COF and PyTp-COF under visible light irradiation. Reproduced with permission.[89] Copyright 2023, Wiley-VCH GmbH.

and inhibits the complexation of photoexcited carriers, thus improving the photocatalytic performance.

Strong electron-withdrawing groups (*e.g.*, halogen, nitro, cyano) and electron-donating groups (*e.g.*, methyl, methoxy) are often introduced into the building blocks of COFs as functional groups to regulate the light absorption range and bandgap through the electron push–pull effect, facilitating the separation and transfer of photoinduced charge carriers.

Chen *et al.*[90] designed a strategy based on the well-established donor–acceptor (Py-XTP-BT-COF) integration to enhance charge separation efficiency and facilitate light absorption (Fig. 24a). The structure was finely tuned by introducing different halogen atoms to increase the rate of HER. Donor–acceptor (D–A) molecules are a family of functional compounds consisting of electron donors and acceptors. Integrating D–A moieties is a valid strategy to help electron–hole separation and charge transport of COFs (Fig. 24b and c).[91] Adopting this strategy, Sun *et al.*[92] reported two donor–acceptor COFs (TAPFy-PhI and TAPB-PhI) synthesized *via* a Schiff base reaction using phthalimide as the acceptor and TAPFy and TAPB as the donors (Fig. 24d). The D–A strategy can not only narrow the band gap and broaden photon absorption, but also enhance charge transport and separation, therefore, further improving the photocatalytic capacity for hydrogen evolution.

A longer π-conjugation can improve the light absorption capacity and narrow the π–π* energy. This not only increases the photogenerated electron cloud density, but also improves the proton reduction capability. Therefore, adjusting the π-conjugation degree of the building blocks is a valid method to influence the photocatalytic performance. Chen and co-

 

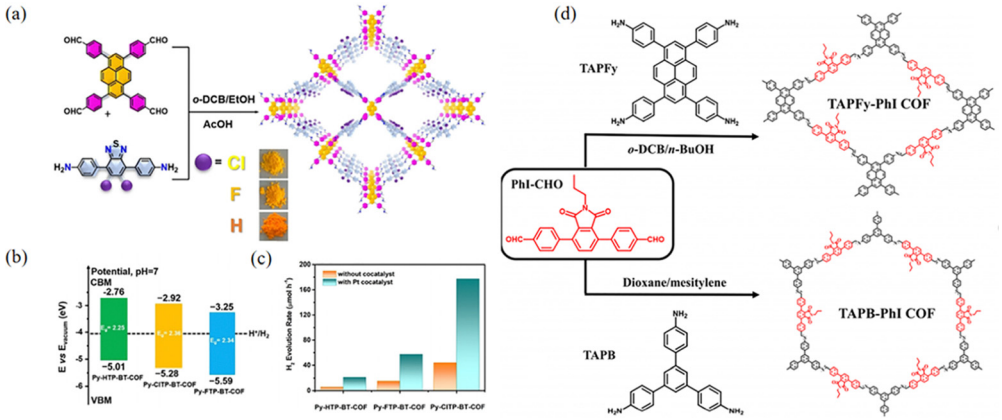


Fig. 24 (a) Synthetic routes to Py-XTP-BT-COFs under solvothermal conditions. (b) Band structure diagram for Py-XTP-BT-COFs as determined from SRPES and UV-DRS. (c) The photocatalytic performances of Py-XTP-BT-COFs (20 mg) with and without co-catalyst under visible ($\lambda > 420$ nm) light irradiation. Reproduced with permission.[90] Copyright 2020, Wiley-VCH GmbH. (d) Synthetic routes to the two COFs under solvothermal conditions. Reproduced with permission.[92] Copyright 2023, American Chemical Society.

workers[93] synthesized a series of donor–acceptor COFs (NKCOF-108, -109, -110, and -111) with V groups as donor groups. Benzothiadiazoles with different functional groups were introduced as an electron acceptor to tune the light-absorption ability of COFs (Fig. 25a). The bandgaps of NKCOF-108, -109, -110, and -111 were calculated by DFT to be 1.82, 1.89, 1.96, and 2.15 eV. With Pt as a cocatalyst, the trend of the HER was found to be NKCOF-108 > NKCOF-109 > NKCOF-110 > NKCOF-111. The HER of NKCOF-108 reached up to 120 μmol $g^{-1}$ $h^{-1}$, possibly attributed to the incorporation of fluorine groups. The larger conjugated system promotes the mobility and separation of photogenerated carriers.

Due to the incomplete delocalization of imine bonds, the stability of imine bonds is generally poor under acidic conditions. However, the hydrazone bond compensates for these disadvantages. Shen *et al.*[94] designed and synthesized a pyrene-based $S_4$-COF based on thioether group functionalization using the solvothermal method (Fig. 26a). It accelerates the separation of photogenerated carriers, enhances charge transfer, achieves long-term photostability, and uniformly distributes the ordered structure of the photocatalyst. The combination of COFs and NPs can adjust and modify the structure of COFs, and the surface of $S_4$-COF exhibits strong hydrophilic properties. Under light excitation, photogenerated electrons in $S_4$-COF can be transitioned to the conduction band. Then, these electrons are transferred and accumulated on the surface of Au NPs, effectively separating electrons and reducing water to $H_2$. Under visible light ($\lambda \geq 420$ nm) irradiation, the photocatalytic hydrogen production of pure $S_4$-COF is 302 μmol $g^{-1}$ $h^{-1}$. The photocatalytic hydrogen production of $S_4$-COF modified by Au NPs is 1377 μmol $g^{-1}$ $h^{-1}$, which is 4.5 times higher than that of pure $S_4$-COF (Fig. 26b).

COFs with rectangular pore structures were prepared by condensation reaction using building blocks with two-node ($C_2$) and four-node ($C_4$) symmetric structures. Meanwhile, due to the strong π-conjugated four-node ($C_4$) symmetric structures, the COFs with these building block nodes usually have high stability, thus broadening the application scope of this kind of COF. In 2024, Li *et al.*[95] reported the synthesis of PyAm-TpbAl-COF, where the pyrene molecule is electron-enriched and serves as the donor building block and benzene acts as the acceptor (Fig. 27). Although the structures of these COFs are similar, their performance in exciton dissociation and electron–hole pair separation differs significantly. The discrepancy may

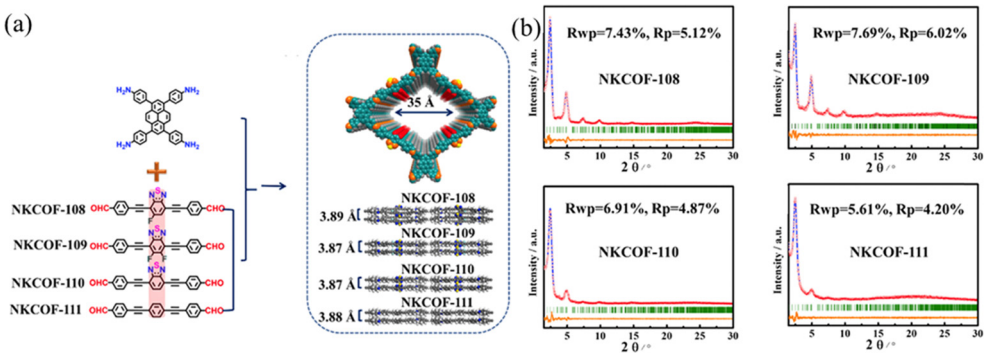


Fig. 25 (a) Synthesis of NKCOFs. (b) Experimentally observed PXRD of NKCOFs. Reproduced with permission.[93] Copyright 2021, American Chemical Society.

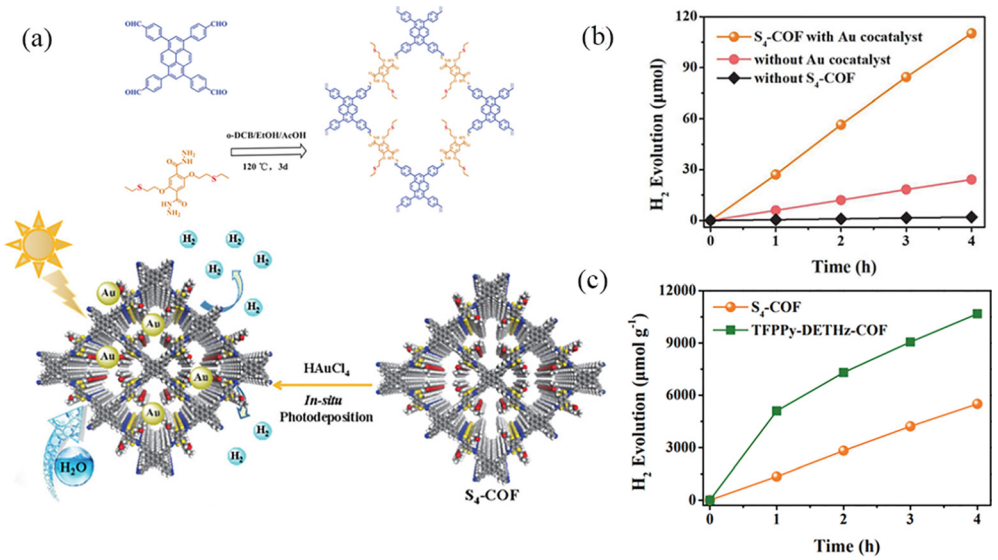


Fig. 26 (a) Schematic synthesis of $S_4$-COF and its application in photocatalytic $H_2$ generation. (b) Photocatalytic $H_2$ evolution of $S_4$-COF under different conditions. (c) Time courses of photocatalytic $H_2$ evolution of $S_4$-COF and TFPPy-DETHz-COF. Reproduced with permission.[94] Copyright 2024, Elsevier.

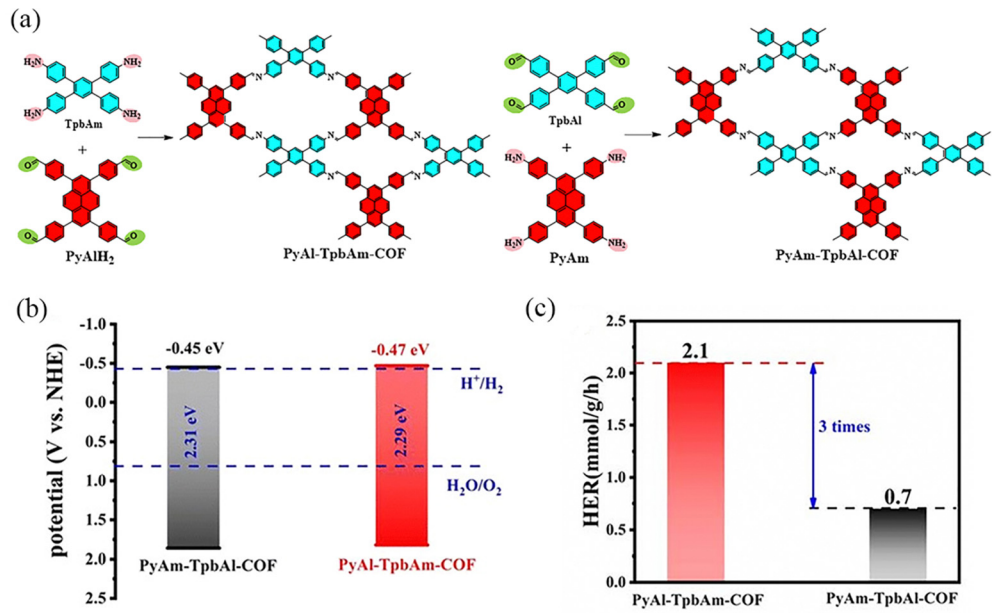


Fig. 27 (a) Synthesis route to PyAl-TpbAm-COF and PyAm-TpbAl-COF. (b) Band levels of PyAl-TpbAm-COF and PyAm-TpbAl-COF. (c) Average hydrogen evolution rate. Reproduced with permission.[95] Copyright 2023, Royal Society of Chemistry.

be attributed to the variation in the orientation of the imine bond. The photocatalytic hydrogen evolution performance of PyAl-TpbAm-COF is three times higher than that of PyAm-TpbAl-COF, with average hydrogen evolution rates of 2.1 mmol $g^{-1}$ $h^{-1}$ and 0.7 mmol $g^{-1}$ $h^{-1}$, respectively.

PyCOFs have attracted significant attention because of their π–π stacked structure, excellent response to visible light, tunable band gap and high stability. Kuo *et al.*[96] reported two tetraformyl carbazole species with different conjugation lengths as raw materials to prepare two ultrastable luminescent 2D COFs-PyTA-BC and PyTA-BC-Ph through the Schiff base reaction under solvothermal conditions (Fig. 28a). Increasing the conjugation length in the linker increased the degree of planarity and, thereby, increased the surface area and the $d_{100}$ value of the 2D COF. Therefore, in the absence of a noble metal cocatalyst, the system of COFs and ascorbic acid could provide a photocatalytic $H_2$ production of up to 1183 μmol $g^{-1}$ $h^{-1}$ ($\lambda \geq 420$ nm) (Fig. 28b). Dong *et al.*[97] employed [4+4] condensation methods to synthesize two ultrastable luminescent COFs, which designed and synthesized a novel imine-linked COF (DABT-Py-COF) by D–A–D type (Fig. 28c). Due to

 

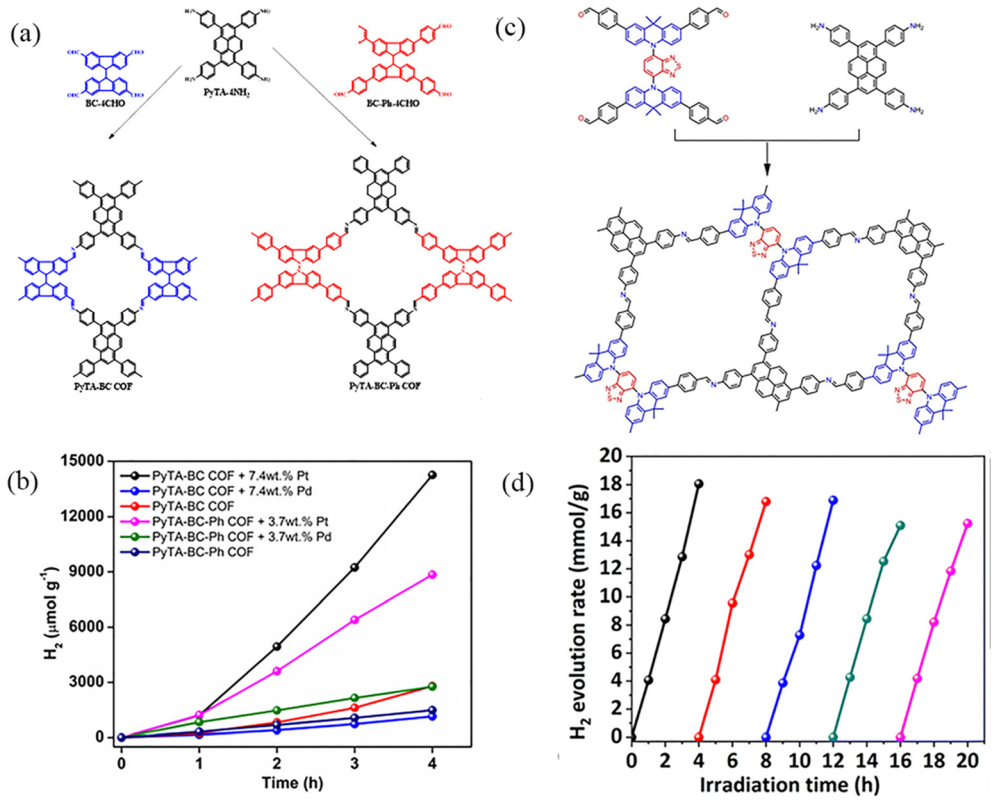


Fig. 28 (a) Synthetic routes to PyTPA-BC and PyTA-BC-Ph COFs. (b) Effect of different co-catalysts for photocatalytic $H_2$ production using visible light for PyTA-BC and PyTA-BC-Ph COFs. Reproduced with permission.[96] Copyright 2022, Wiley-VCH GmbH. (c) Schematic diagram of the synthesis of DABT-Py-COF. (d) Photostability test of DABT-Py-COF for cycling runs over 20 h under visible-light irradiation (AM 1.5). Reproduced with permission.[97] Copyright 2023, Royal Society of Chemistry.

the ordered arrangement of positive and negative charges in the framework, the D–A–D strategy is utilized to inhibit the recombination of photogenerated charges and regulate the structure to enhance the photocatalytic activity.

*3.1.1.2 Composite photocatalysis.* Due to the rapid recombination of photogenerated electron–hole pairs, the practical application of PyCOFs still faces great challenges: photogenerated carriers generated in the narrow bandgap of photocatalysts can easily recombine, while electron–hole pairs in wide bandgap photocatalysts are difficult to be generated, resulting in low quantum yields and low photocatalytic efficiencies. To address these issues, COF-based composite photocatalysts are considered to be the most promising materials on the verge of technological advancement, with significant improvements in charge separation and transfer. Excited electrons move from the higher CB to lower CB, and holes move from the higher VB in one semiconductor to the lower VB in the other. Thus, charge transfer between them effectively prevents photogenerated electron/hole complexation and improves the catalytic performance. Tight interfacial connections between metals and semiconductors or between different semiconductors can lead to efficient electron transfer, thus enhancing photocatalytic decomposition of water activity. The loading of suitable metal co-catalysts is an effective strategy to enhance the activity of semiconductor photocatalysts. For example, Chen *et al.*[98] constructed two new MCOFs (Ni-Py-COF and Ni-Bn-COF) from nickel ethoxime based building blocks (Fig. 29a). MCOFs not only inherit the advantages of COFs, such as high crystallinity, porosity, and specific surface area, but also have the advantages of multiple active sites of the metal, and the mutual synergistic effect promotes charge transfer, effective separation, and inhibition of photogenerated electron–hole pair recombination, reducing the band gap and increasing the photocatalytic efficiency.[99] Even without the addition of the Pt co-catalyst, the hydrogen evolution rates (HER) of Ni-Py-COF reached up to 626 μmol $g^{-1}$ $h^{-1}$ (Fig. 29b). Guo *et al.*[100] designed and constructed a class of $Cu_2O$/2D PyTTA-TPA COFs, which significantly improved the efficiency of photocatalytic hydrogen evolution (Fig. 29c). Driven by the electric field, the photogenerated electrons are transferred from the semiconductor with a more negative conduction-band potential to another semiconductor with a more positive conduction-band potential, and at the same time, the photogenerated holes are transferred from the semiconductor with a more positive valence-band potential to the other semiconductor with a more negative valence-band potential, which achieves the effective separation of photogenerated electrons and holes and improves the photocatalytic efficiency and hydrogen evolution and significantly inhibits the photocorrosion. Therefore, the as-made $Cu_2O$/PyTTA-TPA

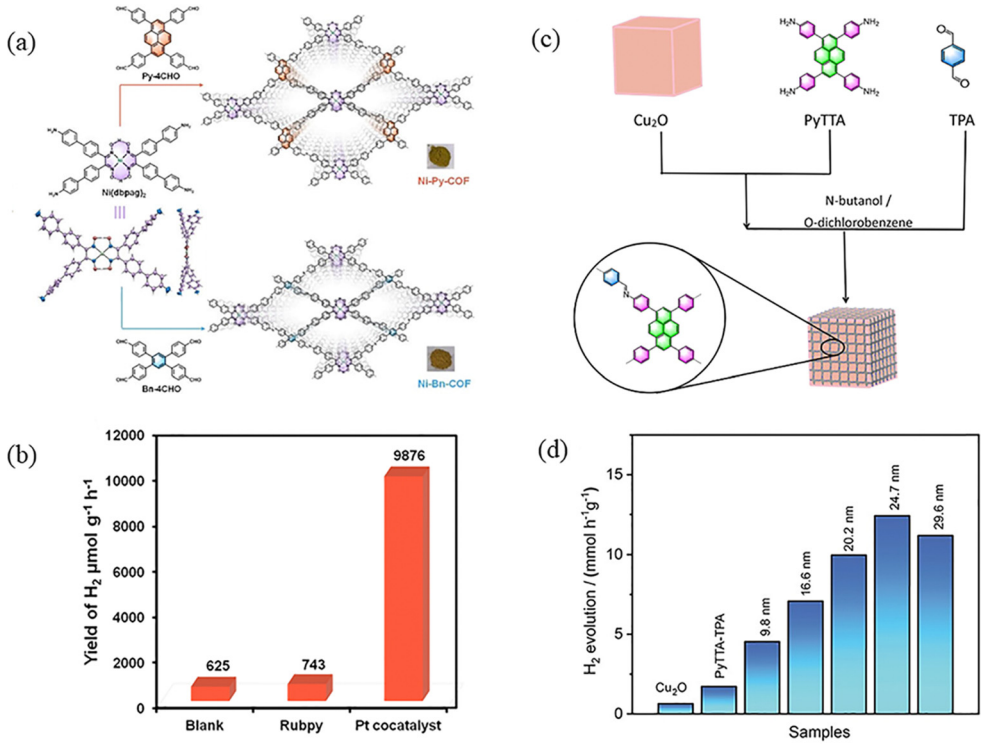


Fig. 29 (a) Synthetic route to Ni-glyoximate-COFs. (b) $H_2$ photogeneration control experiments of Ni-Py-COF. Reproduced with permission.[98] Copyright 2022, Wiley-VCH GmbH. (c) Schematic diagram of the synthesis of $Cu_2O$/PyTTA-TPA COFs core/shell nanocubes. (d) The photocatalytic $H_2$ evolution rate of different photocatalysts. Reproduced with permission.[100] Copyright 2023, American Chemical Society.

COF core/shell nanocubes with a shell thickness of 24.7 nm possess an exceptional photocatalytic $H_2$ evolution rate of 12.5 mmol $h^{-1}$ $g^{-1}$ (Fig. 29d).

Metals and semiconductors have different Fermi energy levels, and when a metal is coupled onto a semiconductor, electrons can be transferred from the semiconductor to the metal. The surface energy band of a semiconductor bends upwards, so the Schottky barrier formed at the metal–semiconductor interface can act as an effective electron trap to inhibit electron–hole complexation, thus prolonging the lifetime of the photogenerated electrons and improving the photocatalytic efficiency. Deng *et al.*[99] reported the heterogenization of a Salen metal-complex molecular catalyst into a rigid COF through covalent linkage with the light-harvesting unit of pyrene. The chemically conjugated bonds between two units contribute to the fast photogenerated electron transfer, thereby promoting the proton reduction reaction (Fig. 30a). Therefore, the Salen cobalt-based COF showed the best hydrogen evolution activity, which is 1378 μmol $h^{-1}$ $g^{-1}$ (Fig. 30b and c).

**3.1.2 Photocatalytic hydrogen peroxide production.** The photocatalytic generation of $H_2O_2$ from $H_2O$ and $O_2$ is an uphill reaction with a standard Gibbs free energy ($\Delta G_0$) of 117 kJ $mol^{-1}$. There are two routes for the synthesis of $H_2O_2$: the indirect two-step $2e^-$ reduction ($O_2 \rightarrow {}^{\bullet}OOH \rightarrow H_2O_2$) and the direct one-step $2e^-$ reduction ($O_2 \rightarrow H_2O_2$). The two-electron two-step process leads to the production of $H_2O_2$ through the coupling of superoxide radicals ($^{\bullet}OOH$) or hydroxyl radicals ($^{\bullet}OH$). In the direct one-step $2e^-$ process, $O_2$ can react directly with two $H^+$ ions in a two-electron oxygen reduction reaction or with $H_2O$ and two $H^+$ in a two-electron water oxidation reaction to form $H_2O_2$.[101]

Immobilizing functional groups on the backbones of building units enables the modulation of the electron push–pull effect and narrows the bandgap, thus facilitating the separation and transfer of photoinduced excitons. Hence, strong electron-absorbing groups (like halogen atoms, heteroatomic atoms) and electron-donating groups (like methyl, methoxy) are often adopted to modify COF structures to boost photocatalytic hydrogen peroxide generation.

Wang *et al.*[102] reported a series of D–A COFs (TZ-COF, OZ-COF, IZ-COF) with azoles as acceptors and pyrenes as donors to effectively enhance chemical stability and π-coupling, facilitating charge transfer and inhibiting photogenerated electron–hole recombination (Fig. 31a). Electronegativity follows the order O > N > S, and the difference in optical activity could be attributed to the distinct heteroatoms, the absorption of visible light, electron–hole separation, carrier migration, *etc.* At the optimal concentration, IZ-COF exhibited a $H_2O_2$ production rate of 102 μmol $g^{-1}$ $h^{-1}$, which was enhanced to 220 μmol $g^{-1}$ $h^{-1}$ for OZ-COF and 268 μmol $g^{-1}$ $h^{-1}$ for TZ-COF (Fig. 31b). According to DFT calculations, the linkage chemistry, which enhances the activities of neighboring benzene rings, promoted the formation of the necessary intermediates for the two-electron oxygen

 

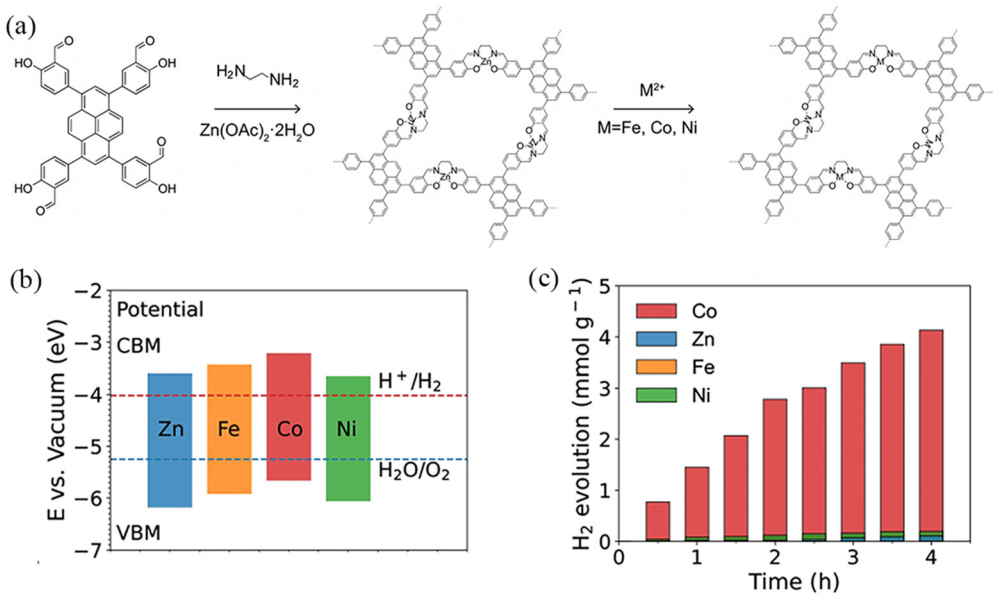


Fig. 30 (a) Synthesis and structure of Zn-Salen-COF and M/Zn-Salen-COF (M = Fe, Co, Ni). (b) Schematic energy band structures of Zn-Salen-COF and M/Zn-Salen-COF. (c) Photocatalytic $H_2$ production on Zn-Salen-COF and M/Zn-Salen-COF. Reproduced with permission.[99] Copyright 2023, Wiley-VCH GmbH.

reduction reaction ($2e^-$ ORR), leading to $H_2O_2$ production (Fig. 31c).

Pyrene units are the most active reduction centers over the other sites. Besides, the well distribution of active centers over a large surface area plays an important role in enhancing photocatalytic performance. Sun *et al.*[103] synthesized four imine PyCOFs *via* a Schiff-base condensation reaction of Py-CHO with Da-$NH_2$, 2,2-bipyridine-5,5′-diamine (Bpy-$NH_2$), TAPD and Py-$NH_2$ to obtain the corresponding Py-Da-COF, Py-Bpy-COF, Py-TAPD-COF, and Py-Py-COF. TAPD and Bpy are considered as electron-rich reduction centers for $O_2$ binding, which is a crucial step for $H_2O_2$ formation (Fig. 32a). The photocatalytic performance is positively correlated with COFs BET surface area. The large BET surface area ensures a high surface availability of the active pyrene sites for ORR and accelerates the mass transfer. The nature of the charge transfer resistance and the efficiency of electron and hole separation showed the trend of Py-Da-COF > Py-Bpy-COF > Py-TAPD-COF > Py-Py-COF, and the amount of $H_2O_2$ generated by Py-Da-COF (868 μmol $g^{-1}$) was much higher than that of the other three species in 3 h (Fig. 32c).

**3.1.3 Photocatalytic carbon dioxide reduction.** The photocatalytic conversion of $CO_2$ using semiconductors as catalysts is a very mild process, involving four main steps. The first step is the adsorption of the reactant ($CO_2/H_2O$), which is a prerequisite for the transfer of photogenerated electrons from the

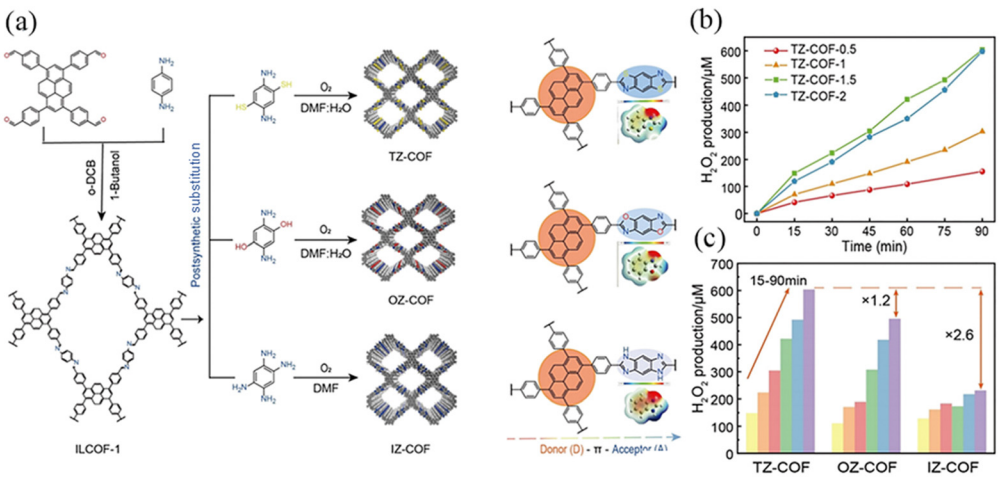


Fig. 31 (a) Synthetic routes to and the D–π–A model and differences of COFs with azoles linkages. (b) $H_2O_2$ yield rates of TZ-COF with different concentrations. (c) $H_2O_2$ yields of COFs dispersed in $H_2O$ at a concentration of 1.5 g $L^{-1}$. Reproduced with permission.[102] Copyright 2023, Wiley-VCH GmbH.

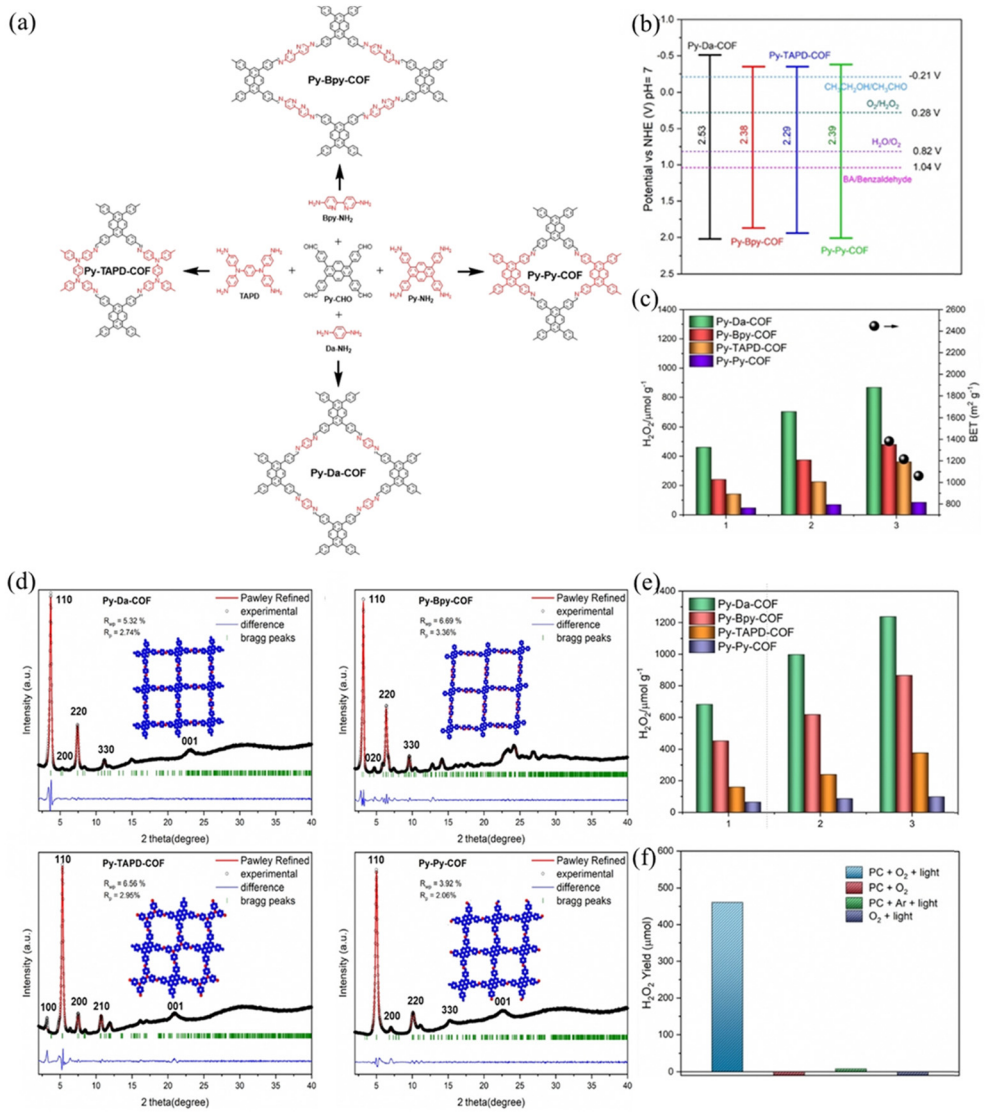


Fig. 32 (a) Schematic illustration of the PyCOFs. (b) Band gaps of the pyrene-based COFs. (c) Photoactivity of the COFs for $H_2O_2$ production in water. (e) Photoactivity of the COFs for $H_2O_2$ production in water–ethanol (9 : 1). (f) Photoactivity of the COFs for $H_2O_2$ production after three hours of irradiation in different systems. (d) The PXRD patterns and Pawley refinements of Py-Da-COF, Py-Bpy-COF, Py-TAPD-COF, and Py-Py-COF. Reproduced with permission.[103] Copyright 2023, Wiley-VCH GmbH.

photocatalyst to $CO_2$ molecules or intermediates to initiate subsequent reduction reactions. The second step is light absorption: when the photocatalyst is exposed to light, electrons and holes are generated in the conduction and valence bands; the photogenerated electrons are used for the reduction reaction and the photogenerated holes are used for the oxidation reaction. The third step involves the transfer of electrons and holes to the surface of the photocatalyst. The valence band of the photocatalyst should be positive compared to the oxidation potential of $H_2O$ and the conduction band should be negative compared to the reduction potential of $CO_2$, which will ensure the occurrence of the photocatalytic reaction and the effective separation of the photogenerated electron–hole pairs.[104] The fourth step is the redox reaction on the photocatalyst surface. After the unreconstituted $e^-$ and $h^+$ have migrated to the surface of the photocatalyst, $e^-$ binds to $h^+$ to reduce $CO_2$ while $h^+$ is consumed in the oxidation reaction. However, this is a surface redox reaction with multiple parallel pathways and side reactions, and it is also the most critical and complex step in photocatalytic $CO_2$ conversion. Different numbers of electrons and protons interact to produce different reduction products of $CO_2$, including carbon monoxide, formic acid, methane, methanol, *etc.*, while due to the oxidation capacity of holes, oxidation reactions occur in $H_2O$ or sacrificial materials to maintain the charge balance of the whole photocatalytic system. The regulation of product selectivity can be considered from the following aspects: $CO_2/H_2O$ adsorption, band structure, photoexcitation properties, carrier separation, active site, and intermediate adsorption/desorption.[105]

 

The absorbance range and intensity of COFs have very important effects on their photocatalytic performance. The π-conjugated unit in the framework structure of COFs plays an important role in their light absorption because the electron transition in the visible spectral range is π → π* transition. Chen *et al.*[106] synthesized $sp^2$c-COFs with excellent extended aromatic conjugation and potential embedding of redox active sites *via* simple base-catalyzed Knoevenagel polycondensation. Using TFPP and BPYDAN as the donor and acceptor, the fully π-conjugated system achieves intramolecular electron transfer (Fig. 33a) and the complete –C≡C– bridge in $sp^2$c-$COF_{dpy}$ creates and unblocks donor–acceptor channels to achieve intramolecular electron delocalization and cascade effects. Using embedded bipyridine, a range of base metals (Fe, Co, Ni and Cu) can be anchored by $sp^2$c-$COF_{dpy}$ to provide catalytic active sites for $CO_2$ photoreduction. The absorbance and band gap of $sp^2$c-$COF_{dpy}$ show significant changes, reaching up to 17.93 mmol $g^{-1}$ CO in the photocatalytic reaction with a selectivity of 81.4% (Fig. 33d). The structural advantage of electron cascade transfer in $sp^2$c-$COF_{dpy}$-Co is theoretically calculated to allow excitons to easily reach a single Co site, thus promoting proton–electron coupled $CO_2$ photoreduction.

Improving the separation and transfer efficiency of photogenerated electron–hole pairs by selecting suitable organic ligands is also conducive to enhancing the photocatalytic performance of COFs, and the orderly stacking of π units in COFs to form periodic columnar π arrays can provide an effective path for interlayer charge transfer. Mahdy *et al.*[107] reported a new ethene-based COF (EPPT-COF), through polycondensation between electron-rich (*E*)-1,2-diphenylethene and 1,3,6,8-tetraphenyl pyrene units *via* a Schiff-base reaction (Fig. 34a). The π–π conjugated interactions between the EPPT-COF layers provides high thermal and chemical stability, while the π-electron delocalization leads to easier charge separation and transport. EPPT-COF has a narrower bandgap (1.7 eV) compared to the CN, which has a larger wavelength absorption range and produces more photogenerated electrons (Fig. 34e). The higher electron concentration on the surface of EPPT-COF is favorable for the catalytic reduction reaction. EPPT-COF absorbed higher absorption performance at 298 K produced $CO_2$ (112 mg $g^{-1}$), and produced $CH_4$ (14.7 μmol $g^{-1}$ $h^{-1}$) consistently and constantly for 14 hours, and no other products were detected (Fig. 34b, c, e and f).

Gao *et al.*[108] prepared 1D PyTTA-COF and 2D PyTTA-COF by Schiff base condensation, which have good chemical and thermal stability (Fig. 35a). 1D PyTTA-COF exhibited considerable $CO_2$ reduction activity, with total CO release up to 1003 μmol $g^{-1}$ over 8 hours, and no liquid carbon production such as HCOOH was found in the reaction system (Fig. 35b). For 1D PyTTA-COF, the highest occupied molecular orbital (HOMO) is mainly distributed on the PyTTA and extends slightly to the imine moiety. The lowest unoccupied molecular orbital (LUMO) is assigned to the phenyl moiety. The HOMO of 2D PyTTA-COF is similar to that of 1D PyTTA-COF, while the LUMO of 2D PyTTA-COF is distributed throughout the fragment, which may play a key role in local electron modulation. 1D

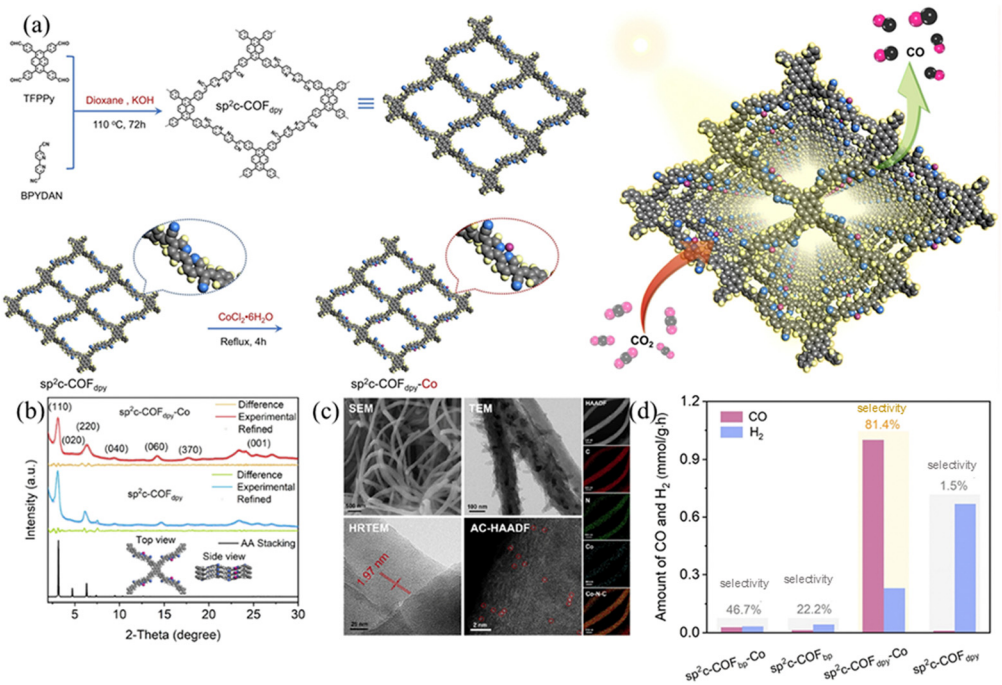


Fig. 33 (a) Synthesis of $sp^2$c-COFdpy and $sp^2$c-COFdpy-Co. Schematic of $CO_2$ photoreduction on the as-prepared $sp^2$c-COFdpy-Co. (b) The PXRD of $sp^2$c-COFdpy-Co and $sp^2$c-COFdpy and calculated patterns for AA stacking. (c) The SEM image, TEM image, HR-TEM image with lattice, aberration-corrected HAADF-STEM and EDX elemental mapping of $sp^2$c-COFdpy-Co. (d) Photocatalytic $CO_2$ reduction over $sp^2$c-$COF_{dpy}$-Co, $sp^2$c-$COF_{dpy}$, $sp^2$c-$COF_{bpy}$-Co and $sp^2$c-$COF_{bpy}$ under visible light in water using triethanolamine (TEOA) as the sacrificial agent. Reproduced with permission.[106] Copyright 2020, Elsevier.

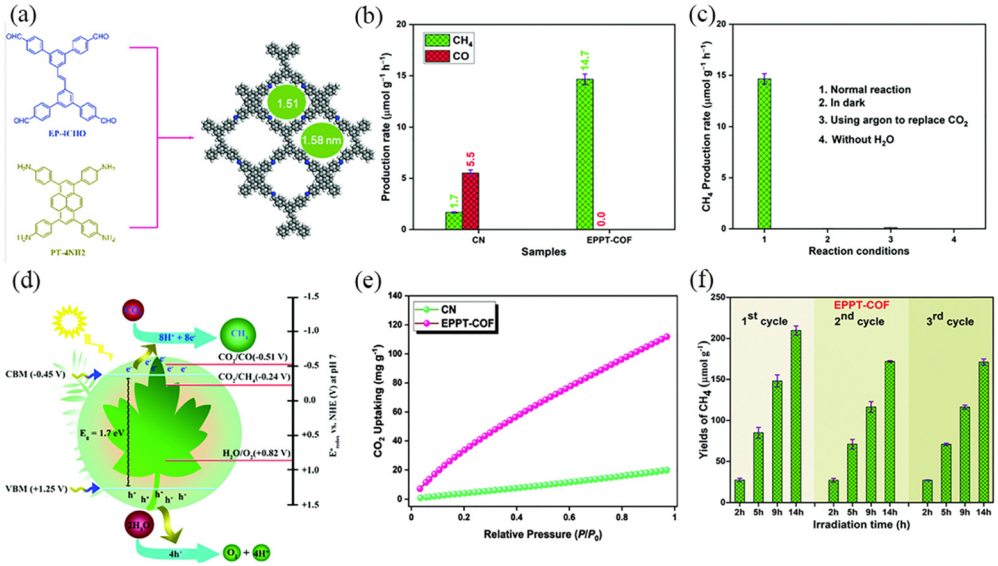


Fig. 34 (a) Synthetic route to and top view of the AA-eclipsed model of EPPT-COF. (b) Photocatalytic performance for $CO_2$ conversion over CN and EPPT-COF; each measurement was performed three times. (c) Control experiments of EPPT-COF were performed using various reaction conditions; each measurement was performed three times. (d) Proposed band structure diagram for EPPT-COF. (e) $CO_2$ uptake of CN and EPPT-COF. (f) Cyclic performance measurement of EPPT-COF; each measurement was performed three times. Reproduced with permission.[107] Copyright 2023, Elsevier.

PyTTA-COF has a narrower band gap, and this structural feature reduces the energy loss of excited photoelectrons, thus facilitating the transfer of photoelectrons to the catalytic active site *via* imine bonds (Fig. 35c).

**3.1.4 Photocatalytic organic transformations.** PyCOF materials are not only the stable non-homogeneous catalytic systems that can be reused, but they are also ideal platforms, where known homogeneous photocatalytic units can be immobilised. Almansaf *et al.*[109] synthesized a new COF based on imine bonds, which was assembled from 2-(4-formylphenyl)-5-formylpyridine and 1,3,6,8-tetrakis(4-aminophenyl)pyrene, showing an interesting dual-pore structure with high crystallinity (Fig. 36a). COF-UARK-49 is highly thermally and chemically stable and exhibits a homogeneous cubic morphology, and the bandgaps of COF-UARK-49 and COF-UARK-49-Pt are calculated to be 2.24 and 2.00 eV, respectively. The post-metallization of the COFs with Pt occurs selectively on the N-donors (imine and pyridine) in the larger pores. Under photo-excitation of COF-UARK49-Pt, the excited [COF-UARK-49-Pt]* produces RFI by single electron transfer (SET) reduction of an electron-oxidising substance [COF-UARK-49-Pt]$^{\bullet+}$ and a radical $^{\bullet}$RF, which reacts with deprotonated α,β-vinyl carboxylate to form I as a benzyl radical (Fig. 36b).

Liu *et al.*[110] synthesized imine COFs with electron donor and acceptor structures. COF-JLU22 was prepared through reacting 1,3,6,8-tetrakis(4-aminophenyl)pyrene with the highly electron-deficient longer linker 4,7-diphenylbenzo[*c*][1,2,5]thiadiazole. COF-JLU22 can be used as a metal-free and recyclable

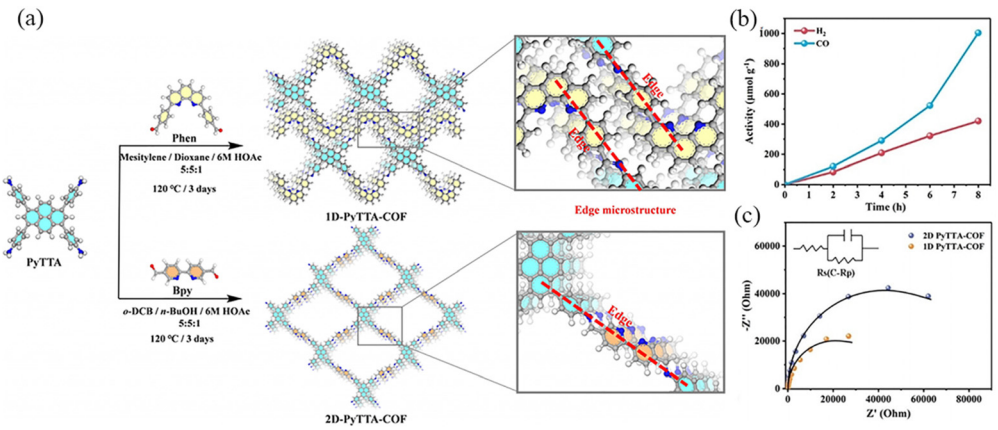


Fig. 35 (a) Synthesis route to and the microstructures (enlarged regions) of 1D PyTTA-COF and 2D PyTTA-COF. (b) Kinetic profile for the evolution of CO and $H_2$ over 1D PyTTA-COF-Co. (c) Nyquist plots of 1D PyTTA-COF and 2D PyTTA-COF. Reproduced with permission.[108] Copyright 2023, Wiley-VCH GmbH.

 

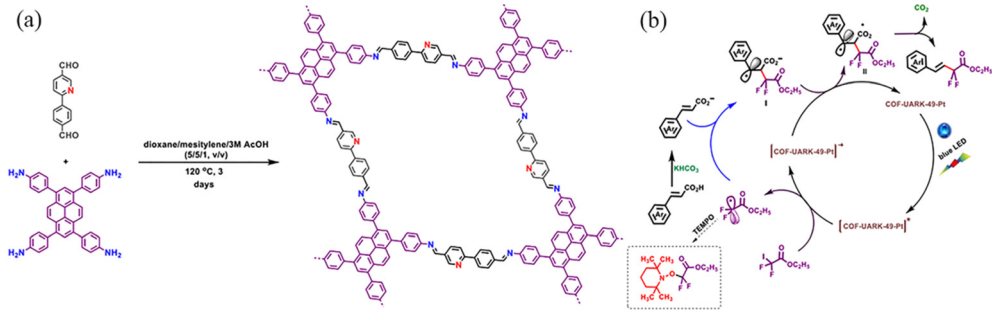


Fig. 36 (a) Synthesis of COF-UARK-49 *via* imine condensation. (b) Proposed mechanism for the decarboxylative difluoroalkylation reaction. Reproduced with permission.[109] Copyright 2021, American Chemical Society.

photocatalyst under visible light irradiation (Fig. 37a). Its red-shifted absorption can enhance the photocatalytic activity of the COF with high catalytic efficiency for reductive dehalogenation of benzoyl bromide derivatives and α-alkylation of aldehydes. The excited state of COF-JLU22 produces photogenerated holes and electrons through charge separation. The photogenerated holes extract electrons from the sacrificial agent *N*,*N*′-diisopropylethylamine (DIPEA). At the same time, the photogenerated electrons are transferred from the conduction band of COF-JLU22 ($E_{1/2}$ = −0.86 V) to benzoyl bromide ($E_{1/2}$ = −0.49 V), leading to the cleavage of C–Br and the formation of α-carbonyloxy radicals and bromine anions. The α-carbonyl radical can then take a proton and an electron from the Hantzsch ester to form the final product, acetophenone (Fig. 37b).

Wen *et al.*[53] reported COF-JLU25, where the D–A the electron-donor units in this overlapping stacked structure may be a source of abundant electrons to facilitate oxidation reactions (Fig. 38a). The COF-JLU25 sample exhibited two intense XRD peaks at 2.70° and 5.39°, and the BET surface area was measured to be 141.31 $m^{-1}$ $g^{-1}$ (Fig. 38c and d). COF-JLU25 was selected as a photocatalyst for the oxidative hydroxylation of arylboronic acids. The COF-JLU25-catalysed conversion is characterized by low catalyst loading, high efficiency, high reusability and compatibility with substrates bearing a wide range of functional groups.

Azine-linked COFs are constructed using two aldehyde derivatives to react with hydrazine monomers. Since hydrazine is the shortest diamino linker, azine-linked COFs have the smallest pore size among all COFs with the same building nodes. Lang *et al.*[111] reported that Py-Azine-COF as the photocatalyst could selectively realize aerobic conversion using 2,2,6,6-tetramethylpiperidine-1-oxyl (TEMPO) as an accelerator to facilitate hole transport and the formation of superoxide with oxygen for selective oxidation of organic sulfides (Fig. 39a). The partial charge density on pyrene was gradually transferred to the azine bond, and the interfacial transfer resistance of the charge carriers was decreased with the assistance of 2 mol% TEMPO, leading to a more efficient separation and migration of the charges on Py-Azine-COF. Under blue light irradiation, abundant photogenerated holes and electrons were generated on Py-Azine-COF, trapping the generated holes and converting TEMPO to $TEMPO^+$ (Fig. 39b). $TEMPO^+$ provides S-centred radical ions by acquiring electrons from methyl phenyl sulfide. The hole mediator TEMPO is capable of rapidly converting a variety of sulphides to sulphur oxides over the Py-Azine-COF photocatalyst in methanol.

**3.1.5 Application of PyCOFs in environmental remediation.** With the acceleration of industrialization and modernization, the problems of environmental pollution and energy shortage have become increasingly prominent, and there is an urgent need to develop efficient and environmentally friendly materials and technologies. PyCOFs have great application potential in the field of environmental remediation, such as wastewater treatment, air purification, soil remediation, *etc.*, because of their advantages of adjustable structures and diversified functions.

2D $sp^2c$ COFs are characterized by ordered π stacks, abundant active sites, adjustable open nanoporous

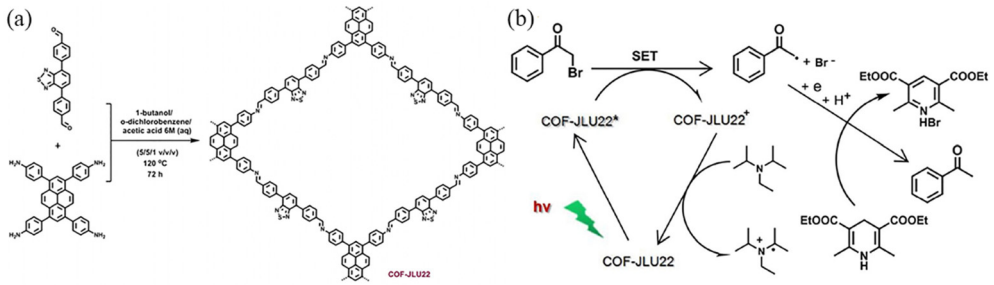


Fig. 37 (a) Synthesis of COF-JLU22 by imine condensation reaction. (b) Proposed reaction mechanism for the photoreductive dehalogenation reaction with COF-JLU22. Reproduced with permission.[110] Copyright 2018, Elsevier.

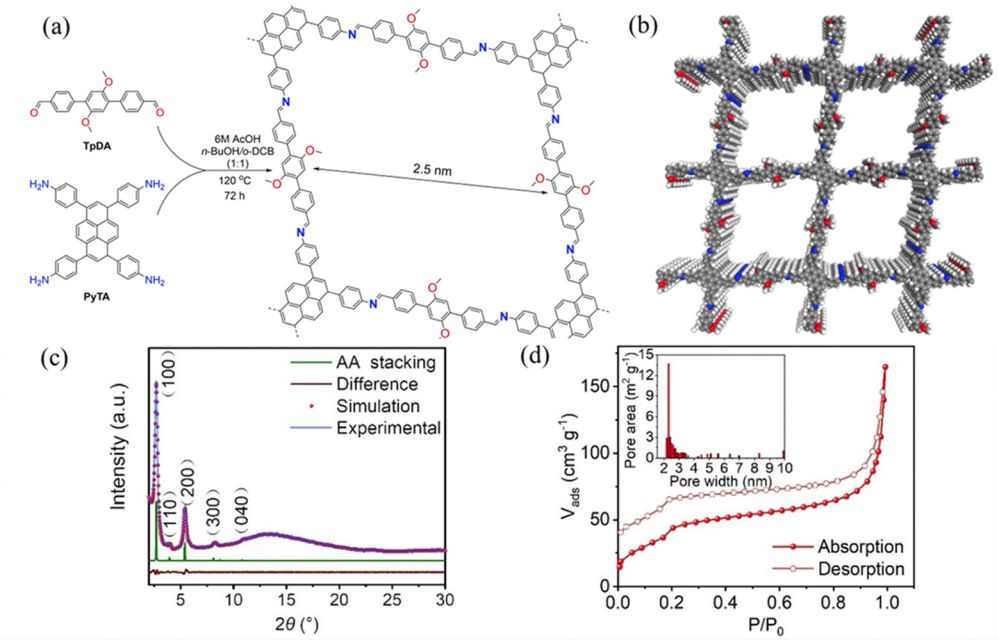


Fig. 38 (a) Synthesis of COF-JLU25. (b) The structural model of COF-JLU25. (c) PXRD patterns of COF-JLU25. (d) N2 adsorption isotherms of activated COF-JLU25 at 77 K. Reproduced with permission.[53] Copyright 2021, Wiley-VCH GmbH.

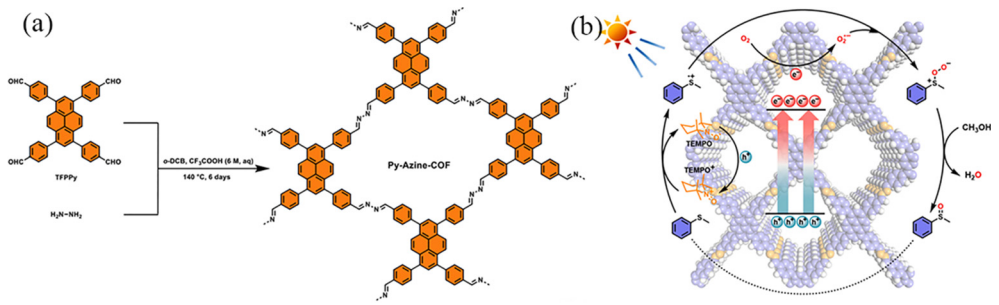


Fig. 39 (a) Schematic of the construction of Py-Azine-COF. (b) A proposed mechanism for selective oxidation of methyl phenyl sulfide with $O_2$ over the Py-Azine-COF photocatalyst with TEMPO. Reproduced with permission.[111] Copyright 2023, Elsevier.

structures, customizable molecular building blocks and strong covalent bonds. In 2024, using a solvothermal method, Hu *et al.*[34] prepared pyrene COF photocatalysts with different bond modes (C═C, N═C), and developed pyrene COFs (sp$^2$c-COF and py-NH$_2$-COF) to complete the photocatalytic degradation of tetracycline (TC) under visible light. The $E_g$ of sp$^2$c-COF is 1.98 eV. The sp$^2$c-COF catalyst absorbs energy to produce electron transition, forming photogenerated electron–hole pairs, and TC is effectively attacked by the formed holes, increasing the degradation rate. The universality of sp$^2$c-COF was analyzed by the degradation of tetracycline, chlortetracycline, oxytetracycline, and doxycycline under visible light irradiation. It was found that sp$^2$c-COF was a recyclable and universal catalyst for degradation of various organic pollutants.

### 3.2 Application of PyCOFs in battery based materials

COFs have recently attracted increasing attention in energy storage devices.[112] In 2018, Wang *et al.*[50] reported COF-based Li–S batteries by loading 70 wt% sulfur onto 2D PyCOF, which could be used as an electrode material to construct lithium–sulfur (Li–S) batteries with high multiplicative capacity and long-term stability (Fig. 40). The Py-COF/S electrode even outperforms some porous carbon-based sulfur body electrodes.[113] The uniform distribution of sulfur in the pore volume of Py-COF/S nanopores was dramatically reduced (from 1.25 cm$^3$ g$^{-1}$ to 0. 07 cm$^3$ g$^{-1}$) along with a reduction in BET surface area (from 2093 to 10 m$^2$ g$^{-1}$) after sulphur loading; the diffusion rate of $Li^+$ ions in the Py-COF/S electrode was faster than that of the BP2000/S electrode, and the difference in ion diffusion rate could be attributed to the pristine structure of Py-COF, which has a 1D ordered porous structure with a fast ion diffusion path.

2D COFs usually form thick laminated sheets due to strong interlayer π–π interactions between 2D nanosheets, which impede the access of electrolytic ions to their redox active sites. In addition, most 2D COFs have a bandgap of a few electron

 

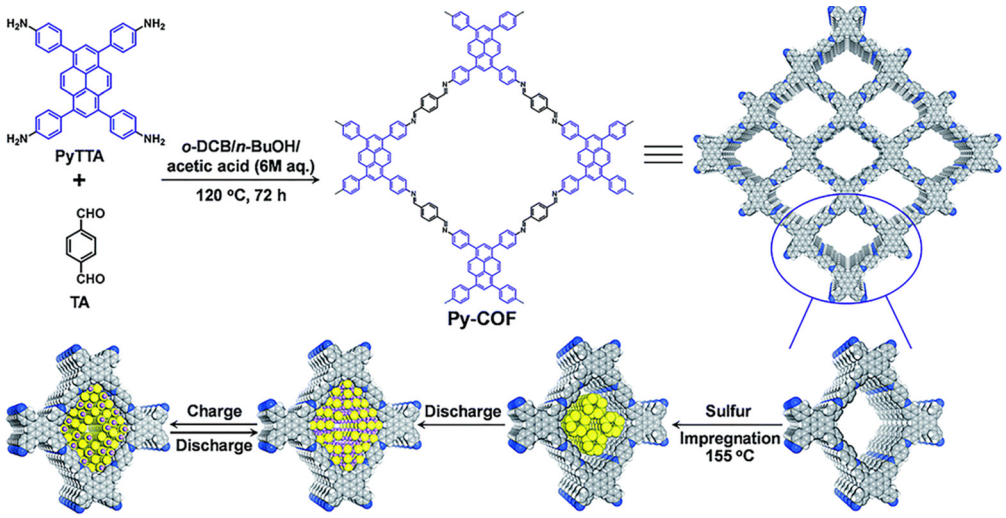


Fig. 40 Schematic illustration of the synthesis of Py-COF and Py-COF/S composite as well as the discharge/charge process. Reproduced with permission.[50] Copyright 2018, Royal Society of Chemistry.

volts and poor electrical conductivity, leading to poor rate capability at high charge/discharge current densities when tested as capacitive materials. Constructing heterostructures consisting of 2D and conductive materials can overcome the above challenges.[58]

In 2019, by tuning the mass ratio between COF precursors and CNTs (mprecursors: mCNTs$\frac{1}{4}x$), Xu *et al.*[114] prepared COF/CNT van der Waals heterostructures (vdWHs) with different COF mass loading (denoted as COF/CNT-$x$ ($x$ = 1, 0.5 and 0.2)) (Fig. 41a). The pyridine group in the TPP-Py COF undergoes two consecutive electron–proton transfer redox processes. All COF/CNT-$x$ exhibited larger CV area with improved capacitive energy storage capacity compared to the TPP-Py COF and CNT (Fig. 41b). Chen *et al.*[49] reported a thienothiophene-containing molecule TAPTt-COF. The carbon–sulfur region of the thiophene group in COFs is the active catalytic site for oxygen reduction and precipitation reactions, and coaxial 1D vdWHs are synthesized by π-electron interaction between 2D-COF and CNT. A strong π–π interaction occurs between CNT and pyrene groups in TTAP, and the interaction plays a key role in guiding the formation of 1D core–shell structure vdWHs.

The strong π–π interactions among the COF layers together with the extended structure can remarkably reduce the solubility of low molecular weight monomers in electrolytes. Zhang *et al.* (Fig. 42a) employed comprehensive characterization and theoretical calculations to confirm that pyrene-4,5,9,10-tetrone (PTO) was a carbonyl-rich compound, and the C═O group can provide a redox active site for $Zn^{2+}$. The 4KT-Tp-COF electrode is theoretically capable of holding 8 electrons, and considering the additional Tp fragment in 4KT-Tp-COF, 4KT-Tp-COF is believed to be capable of storing 6 electrons. For the Tp fragments, $Zn^{2+}$ tends to coordinate with the two adjacent carbonyls between the COF layers, whereas the two adjacent carbonyls in the PTO fragments can directly coordinate with the zinc ions, possibly because both Tp nodes near the PTO fragments have an effect on the PTO monomer (Fig. 42b). Imine-linked COFs have been extensively used for battery electrodes; however, the chemical instability of imine in acidic solutions has been widely known. For example, the β-ketoenamine-based COFs, prepared through irreversible keto–enol tautomerism, are the relatively stable type among the reported imine-based COFs.[115]

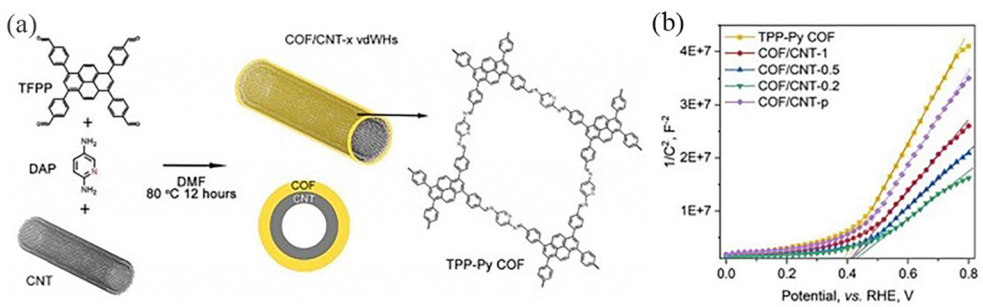


Fig. 41 (a) Schematic illustration of the synthesis of 1D core–shell COF/CNT vdWHs. (b) M–S plots of COF/CNT vdWHs and reference samples. Reproduced with permission.[114] Copyright 2021, AIP Publishing.

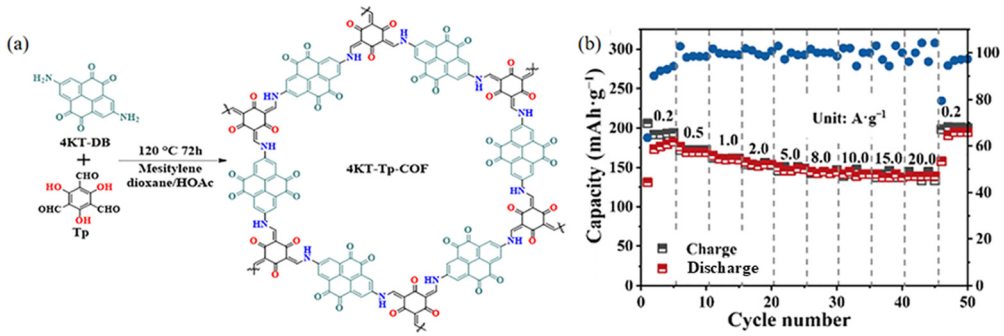


Fig. 42 (a) Schematic illustration of the synthesis of 4KT-Tp-COF. (b) Rate performance of 4KT-Tp-COF. Reproduced with permission.[116] Copyright 2024, Springer Nature.



### 3.3 Application of PyCOFs in fluorescence detection

Fluorescence detection is an important method for the detection of ions and certain contaminants.[117] COFs are a class of metal-free materials and therefore have superior biocompatibility and low biotoxicity.[24a,117c,118] PyCOFs have large conjugated structures with designable active sites. From the structural point of view, the regularly arranged channels of PyCOFs facilitate the interaction between the contact active site and the target substance. In addition, PyCOFs have excellent structural stability; therefore, chemically stable PyCOFs are ideal candidates for the fabrication of highly stable and ultrasensitive sensors.

Niu *et al.*[64] synthesized a fluorescent PyCOF (TFPPy-BDOH) through integrating a biphenyl diamine and a pyrene unit into the π-conjugated framework (Fig. 43a). TFPPy-BDOH has an excellent selectivity to uranium due to the synergistic effect of the nitrogen atom in the imine bond and hydroxyl groups in the conjugated framework. In 2021, the Lin group[48] designed photoactive donor–acceptor 2D COFs with enzyme-like catalytic properties as a robust colorimetric probe for inexpensive, highly sensitive and rapid colorimetric detection of GSH (Fig. 43b and c). Gu *et al.*[51] reported that the O–H···N=C chelating unit can form a bidentate ligand, which could selectively bind metal ions.

Imine-bonded COFs are capable of transmitting extended π-conjugation effects *via* C=N bonds. However, due to the highly polarized nature of C=N bonds, these bonds usually lead to relatively weak electronic delocalisation, which affects the conjugation of COF layers; however, the full $sp^2$-carbon linkage can increase the effectiveness of π-conjugation between the individual units in the 2D system. In 2021, Xiao *et al.*[32] synthesized $sp^2$-carbon-conjugated fluorescent COFs for detec-

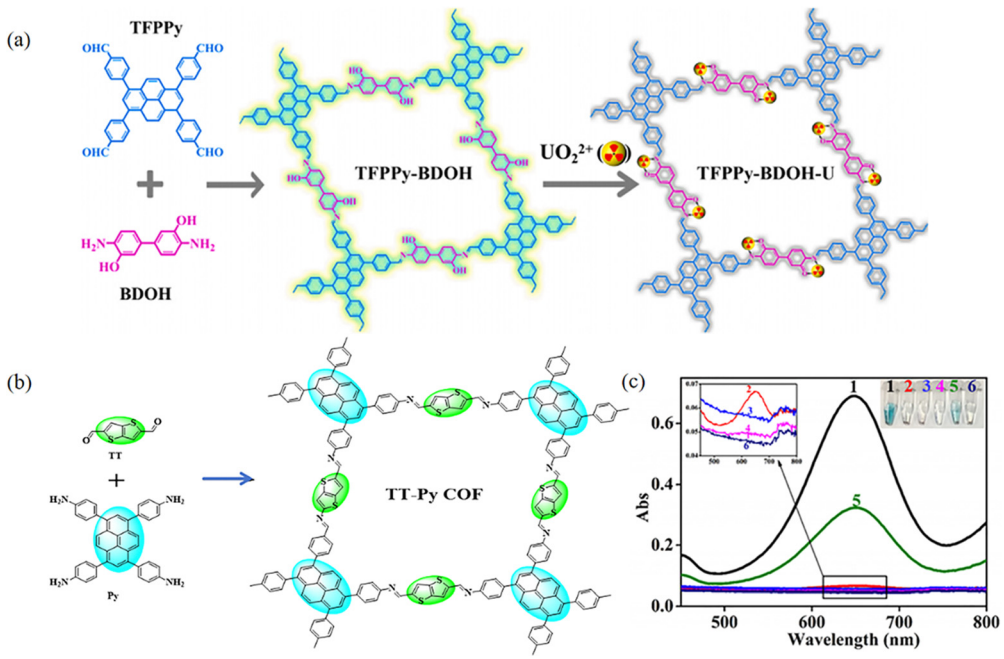


Fig. 43 (a) Synthesis of TFPPy-BDOH for detection. Reproduced with permission.[64] Copyright 2021, Elsevier. (b) Schematic synthesis of the Py-TT COF. (c) Typical absorption curves and color changes of TMB in different reaction systems. Reproduced with permission.[48] Copyright 2021, American Chemical Society.

 

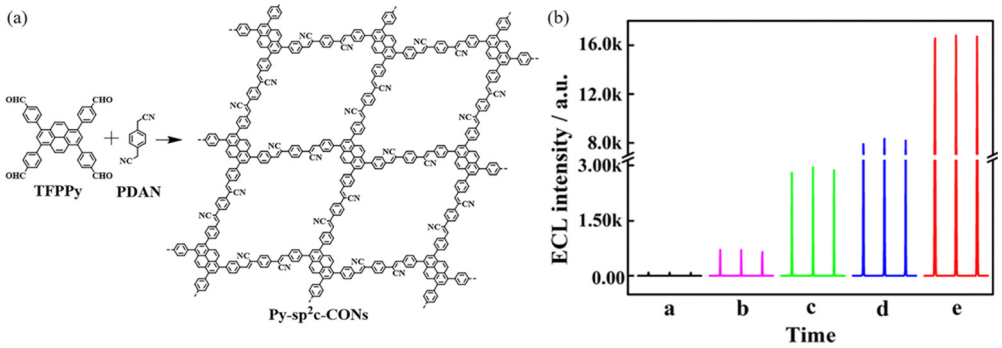


Fig. 44 (a) Synthesis of Py-sp$^2$c-CON. (b) ECL intensities of imine-linked pyrene COF/$S_2O_8^{2-}$. Reproduced with permission.[32] Copyright 2021, American Chemical Society.



tion of high-performance ECL emitters (Fig. 44a). Compared with imine-connected PyCOFs, Py-sp$^2$c-CONs exhibited higher ECL emission, where Py-sp$^2$c-CON was constructed with pyrene luminophores and sp$^2$c connecting bonds to effectively reduce

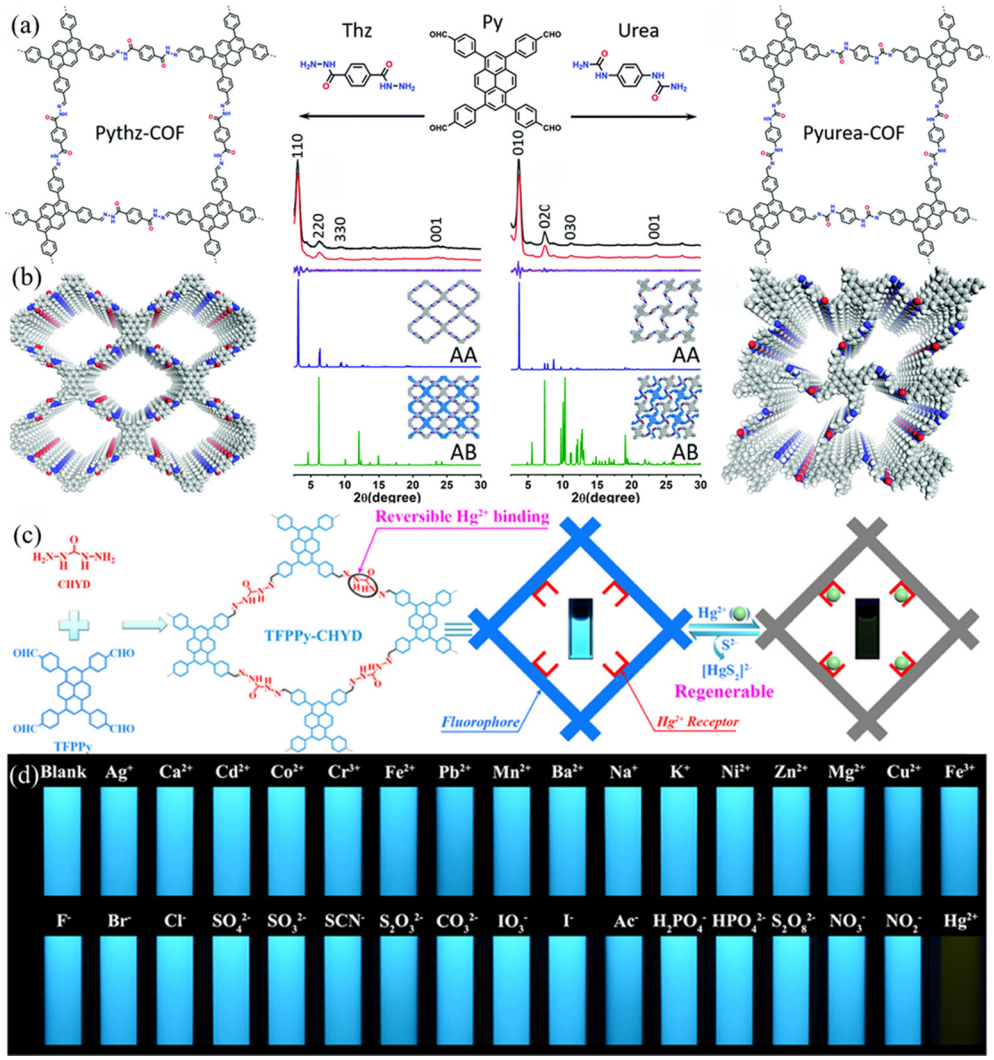


Fig. 45 (a) Schematic representation of the synthesis of Pythz-COF and Pyurea-COF. (b) PXRD patterns of Pythz-COF and Pyurea-COF. Reproduced with permission.[66] Copyright 2021, Royal Society of Chemistry. (c) Schematic diagram of preparation of the TFPPy-CHYD COF, its fluorescence detection and adsorption of $Hg^{2+}$, and easy regeneration by adding $Na_2S$. (d) Photographs showing the fluorescence emission change (under a portable 365 nm UV lamp) of TFPPy-CHYD with various ions. Fluorescence quenching of TFPPy-CHYD by $Cu^{2+}$ was masked by glycine solution (100 μM). Reproduced with permission.[65a] Copyright 2020, American Chemical Society.

the ACQ effect and increase the mobility of the luminophores. At the same time, ultrathin pores in Py-sp$^2$c-CONs could accelerate the migration of co-reactants, ions, and electrons to make more internal luminophores to be electrochemically activated, thus increasing the utilization of ECL luminophores and improving the ECL intensity (Fig. 44b).

The hydrazone bond is a type of flexible covalent bond that is easier to be constructed compared with the traditional Schiff base bond, thus allowing structural flexibility in the hydrazone-linked COF.[119] In 2021, the Tian group constructed hydrazine-conjugated Pythz-COFs and urea-conjugated polyurea-COFs (Fig. 45a).[66] These COFs have high specific surface area and good chemical stability, physical stability, and significant fluorescence-burst response to trace amounts of water in organic solvents. In 2022, Pythz-COFs were used for the detection and recovery of Au(III).[67] The Pythz-COFs were found to be sensitive to Au(III), with electron transfer induced to burst the fluorescence and change the visual colour from bright yellow to dark green. The possible reason is the synergistic effect of hydrogen bonding, coordination bonding and redox reaction between the amide functional group and Au(III), leading to the efficient selectivity of Pythz-COFs. Qiu *et al.*[65a] designed a novel fluorescent COF, TFPPy-CHYD, by combining a pyrene-based building block with a flexible carbocyclic hydrazide linker, in which the nitrogen-based ligand permits reversible and highly selective binding of $Hg^{2+}$, exhibiting excellent adsorption capacity (Fig. 45b).

## 4. Conclusion and outlook

Among various COFs, PyCOFs have high structural stability, strong designability, intrinsic charge-separation ability, and excellent visible-light-absorption ability. This review briefly summarizes the synthetic strategies of different PyCOF linkages, and the research progress of PyCOFs in photocatalysis (including hydrogen evolution, carbon dioxide reduction, hydrogen peroxide production, organic conversion, *etc.*), batteries, and fluorescence detection. These advances may provide insights into the design of new PyCOFs for future applications. However, to date, most PyCOFs have been constructed from PyTTA and TFFPy, and the remaining building units have been less reported. The practical application of PyCOFs is still in its infancy, and several issues are still required to be addressed.

Pyrene is a kind of polycyclic aromatic hydrocarbon, which actually has certain toxicity. In addition, some methods for the preparation of pyrene derivatives produce toxic by-products; thus, more efficient syntheses and purification methods are highly desirable to be developed to reduce the cost of materials and remove residual toxic substances. PyCOFs have been widely used in the field of photocatalysis because of their high efficiency of light energy absorption, good charge transport performance, and diversified photocatalytic reactions. However, the applications of PyCOFs in electrocatalysis are relatively rare due to some issues such as poor conductivity and poor stability. Therefore, optimizing the synthetic conditions to regulate the structures of PyCOFs and provide more efficient electron transport channels is a common method to improve electrical conductivity. In some cases, the synthesis of PyCOFs might involve toxic chemicals and solvents, which increases the environmental burden. Meanwhile, the synthesis of PyCOFs mainly relies on traditional solvothermal methods with mg-scale synthesis, and the realization of large-scale, efficient and green synthesis remains to be solved. Therefore, during the experiment, it is necessary to screen and study chemical substances with similar reactivity but lower toxicity or even non-toxicity to participate in the synthetic reactions of PyCOFs, and reduce the introduction of toxic substances from the source. At the same time, it is important to explore the green solvents to replace the traditional toxic organic solvents and reduce the harm to the environment. Furthermore, the relatively high price and toxicity for PyCOFs impel scientists to find more simple methods for the preparation of COFs as well as more alternative low toxic Py-based monomers. We hope that this review would give readers new insights into PyCOFs and inspire scientists to explore more appealing functions or applications for the future development of PyCOFs.

## Data availability

Data sharing is not applicable to this article as no new data were created or analyzed in this study.

## Conflicts of interest

There are no conflicts to declare.

## Acknowledgements

This work was supported by the Open Fund of Beijing National Laboratory for Molecular Sciences (No. BNLMS201842), and Postgraduate Innovation Foundation from Wuhan Institute of Technology. SH acknowledges the support from the collaborative Innovation Platform Project of Fu-Xia-Quan National Independent Innovation Demonstration Zone (No. 2022-P-021). Q. Z. acknowledges the funding support from the City University of Hong Kong (9380117 and 7020089) and the Innovation and Technology Fund (ITF, ITS/322/22), Hong Kong, P. R. China.

## References

1 (*a*) J. Li, X. Jing, Q. Li, S. Li, X. Gao, X. Feng and B. Wang, *Chem. Soc. Rev.*, 2020, **49**, 3565–3604; (*b*) Y. Yusran, H. Li, X. Guan, Q. Fang and S. Qiu, *Energy Chem.*, 2020, **2**, 100035; (*c*) J. Sun, Y. Xu, Y. Lv, Q. Zhang and X. Zhou, *CCS Chem.*, 2023, **5**, 1259–1276; (*d*) J. Sun, F. Kang, D. Yan, T. Ding, Y. Wang, X. Zhou and Q. Zhang, *Angew. Chem., Int. Ed.*, 2024, **63**, e202406511; (*e*) Y. Shi, J. Yang, F. Gao and Q. Zhang, *ACS Nano*, 2023, **17**, 1879–1905; (*f*) S. Xu and Q. Zhang, *Mater. Today Energy*, 2021, **20**, 100635.

 

2 (*a*) X. Chen, K. Geng, R. Liu, K. T. Tan, Y. Gong, Z. Li, S. Tao, Q. Jiang and D. Jiang, *Angew. Chem., Int. Ed.*, 2020, **59**, 5050–5091; (*b*) S. Y. Ding and W. Wang, *Chem. Soc. Rev.*, 2013, **42**, 548–568; (*c*) S. Xu, J. Wu, X. Wang and Q. Zhang, *Chem. Sci.*, 2023, **14**, 13601–13628; (*d*) Z. Chen, N. Li and Q. Zhang, *Small Struct.*, 2024, **5**, 2300495; (*e*) J. Yang, Z. Chen, L. Zhang and Q. Zhang, *ACS Nano*, 2024, **18**, 21804–21835.

3 A. P. Cote, A. I. Benin, N. W. Ockwig, M. O'Keeffe, A. J. Matzger and O. M. Yaghi, *Science*, 2005, **310**, 1166–1170.

4 (*a*) Y. Li, X. Song, G. Zhang, L. Wang, Y. Liu, W. Chen and L. Chen, *ChemSusChem*, 2022, **15**, e202200901; (*b*) Z. Lin and J. Guo, *Macromol. Rapid Commun.*, 2022, **44**, 2200719; (*c*) N. Romero, R. Bofill, L. Francàs, J. García-Antón and X. Sala, *Catalysts*, 2021, **11**, 754–771; (*d*) S. S. Zhu, Z. Zhang, Z. Li and X. Liu, *Mater. Chem. Front.*, 2024, **8**, 1513–1535; (*e*) Q. Gu, X. Lu, C. Chen, X. Wang, F. Kang, Y. Y. Li, Q. Xu, J. Lu, Y. Han, W. Qin and Q. Zhang, *Angew. Chem., Int. Ed.*, 2024, **63**, e202409708; (*f*) Q. Gu, J. Zha, C. Chen, X. Wang, W. Yao, J. Liu, F. Kang, J. Yang, Y. Y. Li, D. Lei, Z. Tang, Y. Han, C. Tan and Q. Zhang, *Adv. Mater.*, 2024, **36**, 2306414; (*g*) F. Kang, X. Wang, C. Chen, C.-S. Lee, Y. Han and Q. Zhang, *J. Am. Chem. Soc.*, 2023, **145**, 15465–15472; (*h*) Q. Gu, X. Lu, C. Chen, R. Hu, X. Wang, G. Sun, F. Kang, J. Yang, X. Wang, J. Wu, Y. Y. Li, Y.-K. Peng, W. Qin, Y. Han, X. Liu and Q. Zhang, *ACS Nano*, 2023, **17**, 23903–23912; (*i*) S. Zhang, X. Wang, F. Kang, Q. Gu, G. Sun, Y.-K. Peng and Q. Zhang, *SmartMat*, 2023, e1265.

5 (*a*) X. Feng, X. Ding and D. Jiang, *Chem. Soc. Rev.*, 2012, **41**, 6010–6022; (*b*) N. Huang, P. Wang and D. Jiang, *Nat. Rev. Mater.*, 2016, **1**, 1–19; (*c*) P. H. Kouwer, M. Koepf, V. A. L. Sage, M. Jaspers, A. M. V. Buul, Z. H. E. Akeroyd, T. Woltinge, E. Schwartz, H. J. Kitto, R. Hoogenboom, S. J. Picken, R. J. Nolte, E. Mendes and A. E. Rowan, *Nature*, 2013, **493**, 651–655; (*d*) D. Rodriguez-San-Miguel and F. Zamora, *Chem. Soc. Rev.*, 2019, **48**, 4375–4386; (*e*) J. L. Segura, M. J. Mancheno and F. Zamora, *Chem. Soc. Rev.*, 2016, **45**, 5635–5671.

6 (*a*) Y. Wang, W. Wang, Z. Zhang and P. Li, *Appl. Surf. Sci.*, 2022, **571**, 151355; (*b*) Y. X. Zhang, *React. Funct. Polym.*, 2023, **184**, 105516; (*c*) E. A. Gendy, J. Ifthikar, J. Ali, D. T. Oyekunle, Z. Elkhlifia, I. I. Shahib, A. I. Khodair and Z. Chen, *J. Environ. Chem. Eng.*, 2021, **9**, 105687.

7 (*a*) X. L. Hu, H. G. Li and B. E. Tan, *Chin. J. Polym. Sci.*, 2020, **38**, 673–684; (*b*) S. P. Qi, R. T. Guo, Z. X. Bi, Z. R. Zhang, C. F. Li and W. G. Pan, *Small*, 2023, **19**, e2303632; (*c*) Y. Zhang, H. Liu, F. Gao, X. Tan, Y. Cai, B. Hu, Q. Huang, M. Fang and X. Wang, *Energy Chem.*, 2022, **4**, 100078; (*d*) X. Chen, Y. Li, L. Jia, X. Yu, Q. Wang, Y. Zhang, Z. Zhang, E. Liang, B. Han and J. Li, *J. Solid State Chem.*, 2023, **328**, 124352; (*e*) F. Kang, X. Wang, C. Chen, C. S. Lee, Y. Han and Q. Zhang, *J. Am. Chem. Soc.*, 2023, **145**, 15465–15472; (*f*) Q. Wang, Y. Li, M. Zhou, J. Zhou, X. Liu, X. Yu, J. Gao, E. Liang, X. Chen, Y. Zhang, B. Han, J. Fan and J. Li, *Microporous Mesoporous Mater.*, 2024, **364**, 112872.

8 (*a*) P. H. Chang, M. C. Sil, K. S. K. Reddy, C. H. Lin and C. M. Chen, *ACS Appl. Mater.*, 2022, **14**, 25466–25477; (*b*) Y. Li, M. Liu, J. Wu, J. Li, X. Yu and Q. Zhang, *Front. Optoelectron.*, 2022, **15**, 38; (*c*) F. Yu, W. Liu, S. W. Ke, M. Kurmoo, J. L. Zuo and Q. Zhang, *Nat. Commun.*, 2020, **11**, 5534.

9 (*a*) S. Zhang, D. Liu and G. Wang, *Molecules*, 2022, **27**, 2586–2631; (*b*) Y. Xiang, X. Yu, Y. Li, J. Chen, J. Wu, L. Wang, D. Chen, J. Li and Q. Zhang, *Dyes Pigm.*, 2021, **195**, 109710; (*c*) Y. Zhang, J. Wu, J. Gao, X. Chen, Q. Wang, X. Yu, Z. Zhang, M. Liu and J. Li, *J. Solid State Chem.*, 2023, **318**, 123727.

10 (*a*) J. Lu, M. Wang, Y. Han, Y. Deng, Y. Zeng, C. Li, J. Yang and G. Li, *Anal. Chem.*, 2022, **94**, 5055–5061; (*b*) X. Tao, Z. Wang, Q. P. Zhang, N. Liu, Y. L. Sun, R. X. Niu, R. Sun, X. Wang, B. Tan and C. Zhang, *J. Am. Chem. Soc.*, 2023, **145**, 25471–25477.

11 (*a*) J. Li, S. Chen, Z. Wang and Q. Zhang, *Chem. Rec.*, 2016, **16**, 1518–1530; (*b*) S. E. A. M. Consuelo Cuquerella, M. A. Miranda and J. Pérez-Prieto, *J. Org. Chem.*, 2009, **74**, 3232–3235; (*c*) Z. Jiang, G. Huang, L. Sun, S. Wang and H. Chen, *Energy Fuels*, 2022, **36**, 12201–12211.

12 (*a*) X. He, S. Zhang, S. Qi, P. Xu, B. Dong and B. Song, *Dyes Pigm.*, 2023, **209**, 110933; (*b*) A. Kaplan, A. Erdem, C. Arslan, S. Savas, U. Tayfun and M. Dogan, *Silicon*, 2022, **15**, 3165–3180; (*c*) W. Chen, F. Yu, Q. Xu, G. Zhou and Q. Zhang, *Adv. Sci.*, 2020, **7**, 1903766; (*d*) W. Chen, X. Li, G. Long, Y. Li, R. Ganguly, M. Zhang, N. Aratani, H. Yamada, M. Liu and Q. Zhang, *Angew. Chem., Int. Ed.*, 2018, **57**, 13555–13559; (*e*) Z. Zhang, Z. Wang, N. Aratani, X. Zhu and Q. Zhang, *CCS Chem.*, 2022, **4**, 3491–3496; (*f*) Z. Zhang and Q. Zhang, *Mater. Chem. Front.*, 2020, **4**, 3419–3432; (*g*) Z. Wang, P. Gu, G. Liu, H. Yao, Y. Wu, Y. Li, G. Rakesh, J. Zhu, H. Fu and Q. Zhang, *Chem. Commun.*, 2017, **53**, 7772–7775; (*h*) P. Gu, Z. Wang, G. Liu, H. Yao, Z. Wang, Y. Li, J. Zhu, S. Li and Q. Zhang, *Chem. Mater.*, 2017, **29**, 4172–4175.

13 (*a*) T. Oyamada, H. Uchiuzou, S. Akiyama, Y. Oku, N. Shimoji, K. Matsushige, H. Sasabe and C. Adachi, *J. Appl. Phys.*, 2005, **98**, 074506; (*b*) P. Gu, Z. Wang and Q. Zhang, *J. Mater. Chem. B*, 2016, **4**, 7060–7074; (*c*) J. Li and Q. Zhang, *Synlett*, 2013, 686–696; (*d*) J. Li, S. Chen, Z. Wang and Q. Zhang, *Chem. Rec.*, 2016, **16**, 1518–1530; (*e*) J. Xiao, Y. Divayana, Q. Zhang, H. M. Doung, H. Zhang, F. Boey, X. W. Sun and F. Wudl, *J. Mater. Chem.*, 2010, **20**, 8167–8170; (*f*) Y. Wu, Z. Yin, J. Xiao, Y. Liu, F. Wei, K. J. Tan, C. Kloc, L. Huang, Q. Yan, F. Hu, H. Zhang and Q. Zhang, *ACS Appl. Mater. Interfaces*, 2012, **4**, 1883–1886; (*g*) Q. Zhang, Y. Divayana, J. Xiao, Z. Wang, E. R. T. Tiekink, H. M. Doung, H. Zhang, F. Boey, X. W. Sun and F. Wudl, *Chem. – Eur. J.*, 2010, **16**, 7422–7426.

14 (*a*) M. Sang, S. Cao, J. Yi, J. Huang, W. Y. Lai and W. Huang, *RSC Adv.*, 2016, **6**, 6266–6275; (*b*) Y. R. Shi, H. L. Wei, Y. T. Shi and Y. F. Liu, *Synth. Met.*, 2017, **223**, 218–225;

(*c*) R. Das, S. S. Manna, B. Pathak and C. M. Nagaraja, *ACS Appl. Mater.*, 2022, **14**, 33285.

15 (*a*) L. Ascherl, T. Sick, J. T. Margraf, S. H. Lapidus, M. Calik, C. Hettstedt, K. Karaghiosoff, M. Döblinger, T. Clark, K. W. Chapman, F. Auras and T. Bein, *Nat. Chem.*, 2016, **8**, 310–316; (*b*) T. M. Figueira-Duarte and K. Müllen, *Chem. Rev.*, 2011, **111**, 7260–7314.

16 X. Dong, H. Zhao, K. Zhang and X. Lang, *Coord. Chem. Rev.*, 2024, **513**, 215902.

17 (*a*) R. Das, R. Belgamwar, S. S. Manna, B. Pathak, V. Polshettiwar and C. M. Nagaraja, *J. Colloid Interface Sci.*, 2023, **652**, 480–489; (*b*) R. Das, P. Kumar Verma and C. M. Nagaraja, *Coord. Chem. Rev.*, 2024, **514**, 215944; (*c*) R. Das, S. Kamra and C. M. Nagaraja, *Inorg. Chem. Front.*, 2023, **10**, 2088–2099; (*d*) R. Das, T. Ezhil and C. M. Nagaraja, *Cryst. Growth Des.*, 2021, **22**, 598–607.

18 (*a*) F. P. Kinik, A. Ortega-Guerrero, D. Ongari, C. P. Ireland and B. Smit, *Chem. Soc. Rev.*, 2021, **50**, 3143–3177; (*b*) D. Guo, H. Li, Z. Xu and Y. Nie, *J. Alloys Compd.*, 2023, **968**, 172004; (*c*) J. Huang, Y. Ma, X. Jiang, J. Xian, Z. Fu and H. Ouyang, *Anal. Chem.*, 2024, **37**, 15042–15049; (*d*) Y. G. Li, J. J. Hu, J. L. Zhang, S. J. Liu, Y. Peng and H. R. Wen, *CrystEngComm*, 2022, **24**, 2464–2471; (*e*) Y. Zhang, J. Pang, J. Li, X. Yang, M. Feng, P. Cai and H. C. Zhou, *Chem. Sci.*, 2019, **10**, 8455–8460.

19 (*a*) J. Fang, L. Dai, X. Ren, D. Wu, W. Cao, Q. Wei and H. Ma, *Biosens. Bioelectron.*, 2024, **266**, 116726; (*b*) Q. Wang, P. Li, H. M. Wen, K. J. Hu, Z. Y. Huang and J. Chen, *Inorg. Chem. Commun.*, 2023, **156**, 111213; (*c*) R. Zhu, S. Yu, X. Yang, R. Zhu, H. Liu, K. Niu and L. Xing, *Chin. Chem. Lett.*, 2024, **35**, 109539.

20 (*a*) N. Baig, S. Shetty, S. Abdul Wahed, A. Hassan, N. Das and B. Alameddine, *ACS Appl. Mater.*, 2024, DOI: **10.1021/acsami.4c02948**; (*b*) M. G. Mohamed, W. C. Chang, S. V. Chaganti, S. U. Sharma, J. T. Lee and S. W. Kuo, *Polym. Chem.*, 2023, **14**, 4589–4601; (*c*) M. G. Mohamed, B. X. Su and S. W. Kuo, *ACS Appl. Mater.*, 2024, **16**, 40858–40872.

21 (*a*) J. Wang, X. X. Tian, L. Yu, D. J. Young, W. B. Wang, H. Y. Li and H. X. Li, *J. Mater. Chem. A*, 2021, **9**, 25474–25479; (*b*) X. Zhao, B. B. Qin, T. He, H. P. Wang and J. Liu, *Inorg. Chem.*, 2023, **62**, 18553–18562.

22 Y. N. Gong, X. Guan and H. L. Jiang, *Coord. Chem. Rev.*, 2023, **475**, 214889.

23 H. Yang, J. Wang, R. Zhao and L. Hou, *Small*, 2024, **20**, 202400688.

24 (*a*) W. Li, B. Gui and C. Wang, *Chin. Sci. Bull.*, 2023, **68**, 3969–3978; (*b*) Y. Zhang, Z. Qiao, R. Zhang, Z. Wang, H. J. Wang, J. Zhao, D. Cao and S. Wang, *Angew. Chem., Int. Ed.*, 2023, **62**, e202314539.

25 S. Wan, J. Guo, J. Kim, H. Ihee and D. Jiang, *Angew. Chem., Int. Ed.*, 2008, **47**, 8826–8830.

26 S. Wan, J. Guo, J. Kim, H. Ihee and D. Jiang, *Angew. Chem., Int. Ed.*, 2009, **48**, 5439–5442.

27 L. M. Salonen, D. D. Medina, E. Carbó-Argibay, M. G. Goesten, L. Mafra, N. Guldris, J. M. Rotter, D. G. Stroppa and C. Rodríguez-Abreu, *Chem. Commun.*, 2016, **52**, 7986–7989.

28 S. P. S. Fernandes, L. Frey, K. M. Cid-Seara, O. Oliveira, N. Guldris, E. Carbó-Argibay, C. Rodríguez-Abreu, Y. V. Kolen'ko, A. M. S. Silva, D. D. Medina and L. M. Salonen, *Microporous Mesoporous Mater.*, 2022, **343**, 112162.

29 L. Frey, O. Oliveira, A. Sharma, R. Guntermann, S. P. S. Fernandes, K. M. C. Seara, H. Abbay, H. Thornes, J. Rocha, M. Döblinger, T. Kowalczyk, A. Rao, L. M. Salonen and D. D. Medina, *Angew. Chem., Int. Ed.*, 2023, **62**, e202302872.

30 J. Zhen, S. Ding, W. Wang, J. Liu, J. Sun, Z. Huang and Q. Zheng, *Chin. J. Chem.*, 2016, **34**, 783–787.

31 J. W. Crowe, L. A. Baldwin and P. L. McGrier, *J. Am. Chem. Soc.*, 2016, **138**, 10120–10123.

32 J. L. Zhang, Y. Yang, W. B. Liang, L. Y. Yao, R. Yuan and D. R. Xiao, *Anal. Chem.*, 2021, **93**, 3258–3265.

33 E. Jin, J. Li, K. Geng, Q. H. Jiang, H. Xu, Q. Xu and D. L. Jiang, *Nat. Commun.*, 2018, **9**, 4143.

34 Z. Hu, Y. Luo, L. Wang, Y. Wang, Q. Wang, G. Jiang, Q. Zhang and F. Cui, *ACS Appl. Polym.*, 2023, **5**, 9263–9273.

35 M. Asada, E. Jin, Q. Xu, S. Dalapati, M. A. Addicoat, M. A. Brady, H. Xu, T. Nakamura, T. Heine, Q. H. Chen and D. L. Jiang, *Science*, 2017, **357**, 673–676.

36 A. Jati, S. Dam, S. Kumar, K. Kumar and B. Maji, *Chem. Sci.*, 2023, **14**, 8624–8634.

37 Y. Wang, Y. Z. Cheng, K. M. Wu, D. H. Yang, X. F. Liu, X. Ding and B. H. Han, *Angew. Chem., Int. Ed.*, 2023, **62**, e202310794.

38 (*a*) Y. Fan, D. W. Kang, S. Labalme, J. Li and W. Lin, *Angew. Chem., Int. Ed.*, 2023, **62**, e202218908; (*b*) B. Ma, X. Yang, J. Yuan, X. Yang, D. Han, K. Zhao, C. Lin, L. Wang, G. Liu and L. Mi, *Appl. Catal., A*, 2023, **666**, 119403.

39 E. Jin, K. Geng, S. Fu, M. A. Addicoat, W. Zheng, S. Xie, J. S. Hu, X. Hou, X. Wu, Q. Jiang, Q. H. Xu, H. I. Wang and D. Jiang, *Angew. Chem., Int. Ed.*, 2022, **61**, e202115020.

40 B. Gui, G. Lin, H. Ding, C. Gao, A. Mal and C. Wang, *Acc. Chem. Res.*, 2020, **53**, 2225–2234.

41 Y. Li, Q. Chen, T. Xu, Z. Xie, J. Liu, X. Yu, S. Ma, T. Qin and L. Chen, *J. Am. Chem. Soc.*, 2019, **141**, 13822–13828.

42 B. Zhang, X. Song, Y. Li, Y. Li, Z. Peng, L. Ye and L. Chen, *Chem. Commun.*, 2020, **56**, 3253–3256.

43 T. Wang, H. Xie, Y. Cao, Q. Xu and N. Gan, *J. Chromatogr. A*, 2022, **1685**, 463614.

44 Y. Zhang, C. Li, Z. Liu, Y. Yao, M. M. Hasan, Q. Liu, J. Wan, Z. Li, H. Li and Y. Nagao, *CrystEngComm*, 2021, **23**, 6234–6238.

45 (*a*) X. Yuan, N. Wu, Z. Guo and H. Zhan, *Microporous Mesoporous Mater.*, 2023, **355**, 112573; (*b*) B. Ma, F. Hu, X. Yang, Y. Huang, X. Yang, H. Qiao, Z. Wang, D. Yang, W. Ai and L. Mi, *Appl. Catal., A*, 2023, **662**, 119269; (*c*) H. Qiao, L. Yang, X. Yang, J. Wang, Y. Chen, L. Zhang, W. Sun, L. Zhai and L. Mi, *Chem. – Eur. J.*, 2022, **28**, e202200600.

46 X. Liu, H. Li, W. Zhang, Z. Yang, D. Li, M. Liu, K. Jin, L. Wang and G. Yu, *Angew. Chem., Int. Ed.*, 2023, **62**, e202308921.

 

47 Y. Meng, G. Lin, H. Ding, H. Liao and C. Wang, *J. Mater. Chem. A*, 2018, **6**, 17186–17191.
48 G. Li, W. Ma, Y. Yang, C. Zhong, H. Huang, D. Ouyang, Y. He, W. Tian, J. Lin and Z. Lin, *ACS Appl. Mater.*, 2021, **13**, 49482–49489.
49 C. Liu, F. Liu, H. Li, J. Chen, J. Fei, Z. Yu, Z. Yuan, C. Wang, H. Zheng, Z. Liu, M. Xu, G. Henkelman, L. Wei and Y. Chen, *ACS Nano*, 2021, **15**, 3309–3319.
50 Y. Meng, G. Lin, H. Ding, H. Liao and C. Wang, *J. Mater. Chem. A*, 2018, **6**, 17186–17191.
51 X. Fang, Y. Liu, W. K. Han, X. Yan, Y. X. Shi, L. H. Chen, Y. Jiang, J. Zhang and Z. G. Gu, *Dyes Pigm.*, 2022, **205**, 110507.
52 Y. Chai, Y. Li, H. Hu, C. Zeng, S. Wang, H. Xu and Y. Gao, *Catalysts*, 2021, **11**, 423–435.
53 G. Xiao, W. Li, T. Chen, W. B. Hu, H. Yang, Y. A. Liu and K. Wen, *Eur. J. Org. Chem.*, 2021, 3986–3991.
54 Z. Li, S. Han, C. Li, P. Shao, H. Xia, H. Li, X. Chen, X. Feng and X. Liu, *J. Mater. Chem. A*, 2020, **8**, 8706–8715.
55 Z. Wen, S. Wang, S. Fu, J. Qian, Q. Yan, H. Xu, K. Zuo, X. Su, C. Zeng and Y. Gao, *Chem. Res. Chin. Univ.*, 2022, **38**, 472–477.
56 (*a*) S. Bhunia, S. K. Das, R. Jana, S. C. Peter, S. Bhattacharya, M. Addicoat, A. Bhaumik and A. Pradhan, *ACS Appl. Mater.*, 2017, **9**, 23843–23851; (*b*) R. Chen, L. Kan, M. Xu, G. Zhang, M. Wang, J. Cui, N. Zhou and L. He, *Microchim. Acta*, 2022, **189**, 229–238; (*c*) Y. Chen, Y. Zhang and J. Huo, *J. Solid State Chem.*, 2022, **310**, 123047; (*d*) Z. Chen, K. Wang, X. Hu, P. Shi, Z. Guo and H. Zhan, *ACS Appl. Mater.*, 2020, **13**, 1145–1151; (*e*) C. Gao, X. Guan, M. Zhang, H. Hu, L. Chen, C. Sun, C. Zhang, Y. Du and B. Hu, *Macromol. Rapid Commun.*, 2023, **44**, 2300311; (*f*) A. Irfan, T. Wang, A. Wang, X. Jing, L. Yang and G. Zhu, *Anal. Chim. Acta*, 2022, **1209**, 339876.
57 M. G. Rabbani, A. K. Sekizkardes, Z. Kahveci, T. E. Reich, R. Ding and H. M. E. Kaderi, *Chem. – Eur. J.*, 2013, **19**, 3324–3328.
58 B. Sun, C. H. Zhu, Y. Liu, C. Wang, L. J. Wan and D. Wang, *Chem. Mater.*, 2017, **29**, 4367–4374.
59 Q. Guan, H. Guo, R. Xue, M. Wang, N. Wu, Y. Cao, X. Zhao and W. Yang, *Microchim. Acta*, 2021, **188**, 85–96.
60 T. Wang, I. Azhar, Y. Yang, Y. Lu, Y. Tian, N. Gao, F. Cui, L. Yang, X. Jing and G. Zhu, *Nano Res.*, 2022, **15**, 4569–4574.
61 L. Song, Q. Zhang, L. Min, X. Guo, W. Gao, L. Cui and C. Y. Zhang, *Talanta*, 2024, **266**, 124964.
62 (*a*) Z. Zhou, X. H. Xiong, L. Zhang, Y. Li, Y. Yang, X. Dong, D. Lou, Z. Wei, W. Liu, C. Y. Su, J. Sun and Z. Zheng, *J. Am. Chem. Soc.*, 2024, **146**, 3449–3457; (*b*) Z. H. He, S. D. Gong, S. L. Cai, Y. L. Yan, G. Chen, X. L. Li, S. R. Zheng, J. Fan and W. G. Zhang, *Cryst. Growth Des.*, 2019, **19**, 3543–3550; (*c*) J. Kang, J. Hang, B. Chen, L. Chen, P. Zhao, Y. Xu, Y. Luo and C. Xia, *ACS Appl. Mater.*, 2022, **14**, 57225–57234; (*d*) F. Yu, W. Liu, S.-W. Ke, M. Kurmoo, J.-L. Zuo and Q. Zhang, *Nat. Commun.*, 2020, **11**, 5534; (*e*) F. Yu, W. Liu, B. Li, D. Tian, J.-L. Zuo and Q. Zhang, *Angew. Chem., Int. Ed.*, 2019, **58**, 16101–16104; (*f*) J. Yang, F. Kang, X. Wang and Q. Zhang, *Mater. Horiz.*, 2022, **9**, 121–146; (*g*) M. Xue, J. Yang, F. Kang, X. Wang and Q. Zhang, *J. Mater. Chem. C*, 2022, **10**, 17027–17047.
63 C. S. Diercks and O. M. Yaghi, *Science*, 2017, **355**, 923–932.
64 C. P. Niu, C. R. Zhang, W. R. Cui, S. M. Yi, R. P. Liang and J. D. Qiu, *J. Hazard. Mater.*, 2022, **425**, 127951.
65 (*a*) W. R. Cui, W. Jiang, C. R. Zhang, R. P. Liang, J. Liu and J. D. Qiu, *ACS Sustainable Chem. Eng.*, 2019, **8**, 445–451; (*b*) Y. Zhang, X. Yuan, X. Zhu, D. Zhang, H. Liu and B. Sun, *Anal. Chim. Acta*, 2023, **1239**, 340671; (*c*) M. Zuo, L. Cui, S. Wang, W. Wei, W. Gao and C. Y. Zhang, *Analyst*, 2023, **148**, 1764–1769.
66 S. Jiang, L. Meng, W. Ma, G. Pan, W. Zhang, Y. Zou, L. Liu, B. Xu and W. Tian, *Mater. Chem. Front.*, 2021, **5**, 4193–4201.
67 L. Zhang, J. Q. Fan, Q. Q. Zheng, S. J. Xiao, C. R. Zhang, S. M. Yi, X. Liu, W. Jiang, Q. G. Tan, R. P. Liang and J. D. Qiu, *Chem. Eng. J.*, 2023, **454**, 140212.
68 V. A. Kuehl, J. Yin, P. H. H. Duong, B. Mastorovich, B. Newell, K. D. Li-Oakey, B. A. Parkinson and J. O. Hoberg, *J. Am. Chem. Soc.*, 2018, **140**, 18200–18207.
69 J. Guo, Y. Xu, S. Jin, L. Chen, T. Kaji, Y. Honsho, M. A. Addicoat, J. Kim, A. Saeki, H. Ihee, S. Seki, S. Irle, M. Hiramoto, J. Gao and D. Jiang, *Nat. Commun.*, 2013, **4**, 2736.
70 (*a*) N. Huang, K. H. Lee, Y. Yue, X. Xu, S. Irle, Q. Jiang and D. Jiang, *Angew. Chem., Int. Ed.*, 2020, **59**, 16587–16593; (*b*) M. Wang, M. Ballabio, M. Wang, H. H. Lin, B. P. Biswal, X. Han, S. Paasch, E. Brunner, P. Liu, M. Chen, M. Bonn, T. Heine, S. Zhou, E. Cánovas, R. Dong and X. Feng, *J. Am. Chem. Soc.*, 2019, **141**, 16810–16816; (*c*) M. Wang, M. Wang, H. H. Lin, M. Ballabio, H. Zhong, M. Bonn, S. Zhou, T. Heine, E. Cánovas, R. Dong and X. Feng, *J. Am. Chem. Soc.*, 2020, **142**, 21622–21627.
71 (*a*) D. S. García and J. L. Sessler, *Chem. Soc. Rev.*, 2008, **37**, 215–232; (*b*) M. Chen, H. Li, C. Liu, J. Liu, Y. Feng, A. G. H. Wee and B. Zhang, *Coord. Chem. Rev.*, 2021, **435**, 213778; (*c*) L. Zhang, T. Wang, J. Jiang and M. Liu, *Aggregate*, 2022, **4**, e198.
72 P. L. Wang, S. Y. Ding, Z. C. Zhang, Z. P. Wang and W. Wang, *J. Am. Chem. Soc.*, 2019, **141**, 18004–18008.
73 P. F. Wei, M. Z. Qi, Z. P. Wang, S. Y. Ding, W. Yu, Q. Liu, L. K. Wang, H. Z. Wang, W. K. An and W. Wang, *J. Am. Chem. Soc.*, 2018, **140**, 4623–4631.
74 K. Wang, Z. Jia, Y. Bai, X. Wang, S. E. Hodgkiss, L. Chen, S. Y. Chong, X. Wang, H. Yang, Y. Xu, F. Feng, J. W. Ward and A. I. Cooper, *J. Am. Chem. Soc.*, 2020, **142**, 11131–11138.
75 P. J. Waller, Y. S. AlFaraj, C. S. Diercks, N. N. Jarenwattananon and O. M. Yaghi, *J. Am. Chem. Soc.*, 2018, **140**, 9099–9103.
76 J. Li, S. Y. Gao, J. Liu, S. Ye, Y. Feng, D. H. Si and R. Cao, *Adv. Funct. Mater.*, 2023, **33**, 2305735.
77 A. Zadehnazari, A. Khosropour, A. A. Altaf, S. Amirjalayer and A. Abbaspourrad, *Adv. Opt. Mater.*, 2023, **11**, 2300412.
78 T. He and Y. Zhao, *Angew. Chem., Int. Ed.*, 2023, **62**, 2005256.

79 (*a*) L. Qin, C. Ma, J. Zhang and T. Zhou, *Adv. Funct. Mater.*, 2024, 2401562; (*b*) Q. Niu, L. Mi, W. Chen, Q. Li, S. Zhong, Y. Yu and L. Li, *Chin. J. Catal.*, 2023, **50**, 45–82.
80 (*a*) N. Khan, C. Azad, M. Luo, J. Chen, T. Kesharwani, A. Badshah and D. Wang, *Energies*, 2023, **16**, 5888–5927; (*b*) Y. I. A. Reyes, L. Y. Ting, X. Tu, H. Y. T. Chen, H. H. Chou and C. Coluccini, *Appl. Sci.*, 2020, **10**, 7017–7031; (*c*) Q. Wang and K. Domen, *Chem. Rev.*, 2019, **120**, 919–985.
81 (*a*) J. Zhang and X. Wang, *Angew. Chem., Int. Ed.*, 2015, **54**, 7230–7232; (*b*) S. J. A. Moniz, S. A. Shevlin, D. J. Martin, Z. X. Guo and J. Tang, *Energy Environ. Sci.*, 2015, **8**, 731–759.
82 (*a*) Y. Cao, P. Wang, J. Fan and H. Yu, *Ceram. Int.*, 2021, **47**, 654–661; (*b*) D. E. Lee, M. Danish, U. Alam and W. K. Jo, *J. Energy Chem.*, 2024, **92**, 322–356; (*c*) J. Sheng, C. Wang, F. Duan, S. Yan, S. Lu, H. Zhu, M. Du, X. Chen and M. Chen, *Catal. Sci. Technol.*, 2021, **11**, 7683–7693; (*d*) H. Yang, K. Dai, J. Zhang and G. Dawson, *Chin. J. Catal.*, 2022, **43**, 2111–2140.
83 (*a*) T. He, W. Zhen, Y. Chen, Y. Guo, Z. Li, N. Huang, Z. Li, R. Liu, Y. Liu, X. Lian, C. Xue, T. C. Sum, W. Chen and D. Jiang, *Nat. Commun.*, 2023, **14**, 329–330; (*b*) M. Wang, Z. Wang, M. Shan, J. Wang, Z. Qiu, J. Song and Z. Li, *Chem. Mater.*, 2023, **35**, 5368–5377; (*c*) L. J. Wang, P. Y. Dong, G. Zhang and F. M. Zhang, *Energy Fuel.*, 2023, **37**, 6323–6347.
84 (*a*) C. C. Gu, F. H. Xu, W. K. Zhu, R. J. Wu, L. Deng, J. Zou, B. C. Weng and R. L. Zhu, *Chem. Commun.*, 2023, **59**, 7302–7320; (*b*) S. Liu and J. Guo, *Chem. Res. Chin. Univ.*, 2022, **38**, 373–381.
85 E. Jin, Z. Lan, Q. Jiang, K. Geng, G. Li, X. Wang and D. Jiang, *Chem.*, 2019, **5**, 1632–1647.
86 X. Deng, N. Gao and L. Bai, *Small*, 2024, 2311927.
87 Y. Liu, W. K. Han, W. Chi, J. X. Fu, Y. Mao, X. Yan, J. X. Shao, Y. Jiang and Z. G. Gu, *Appl. Catal., B*, 2023, **338**, 123074.
88 H. Wu, X. He, X. Du, D. Wang, W. Li, H. Chen, W. Fang and L. Zhao, *Small*, 2023, **19**, 2304367.
89 F. D. Wang, L. J. Yang, X. X. Wang, Y. Rong, L. B. Yang, C. X. Zhang, F. Y. Yan and Q. L. Wang, *Small*, 2023, **19**, 2207421.
90 W. Chen, L. Wang, D. Mo, F. He, Z. Wen, X. Wu, H. Xu and L. Chen, *Angew. Chem., Int. Ed.*, 2020, **59**, 16902–16909.
91 W. Li, X. Huang, T. Zeng, Y. A. Liu, W. Hu, H. Yang, Y. B. Zhang and K. Wen, *Angew. Chem., Int. Ed.*, 2020, **60**, 1869–1874.
92 G. Zhang, M. Zhao, L. Su, H. Yu, C. Wang, D. Sun and Y. Ding, *ACS Appl. Mater.*, 2023, **15**, 20310–20316.
93 Z. Zhao, Y. Zheng, C. Wang, S. Zhang, J. Song, Y. Li, S. Ma, P. Cheng, Z. Zhang and Y. Chen, *ACS Catal.*, 2021, **11**, 2098–2107.
94 Z. Zhou, C. Bie, P. Li, B. Tan and Y. Shen, *Chin. J. Catal.*, 2022, **43**, 2699–2707.
95 H. He, R. Shen, P. Zhang, G. Liang and X. Li, *J. Mater. Chem. A*, 2024, **12**, 227–232.
96 A. F. M. Mahdy, A. M. Elewa, S. W. Huang, H. H. Chou and S. W. Kuo, *Adv. Opt. Mater.*, 2020, **8**, 2000641.
97 G. B. Wang, H. P. Xu, K. H. Xie, J. L. Kan, J. Fan, Y. J. Wang, Y. Geng and Y. B. Dong, *J. Mater. Chem. A*, 2023, **11**, 4007–4012.
98 L. Sun, M. Lu, Z. Yang, Z. Yu, X. Su, Y. Q. Lan and L. Chen, *Angew. Chem., Int. Ed.*, 2022, **61**, e202204326.
99 Q. Wang, D. W. Zhou, H. J. He, L. Yang, T. Y. Liu, X. Wang, D. Y. Zheng, Z. B. Dai, L. Sun, C. C. Liu, H. Wu, Z. Li and W. Q. Deng, *Angew. Chem., Int. Ed.*, 2023, **62**, e202214143.
100 Y. X. Liu, Y. N. Wei, M. H. Liu, J. X. Hong, W. Q. Gao, S. Q. Zhao, S. P. Zhang and S. J. Guo, *ACS Nano*, 2023, **17**, 5994–6001.
101 (*a*) F. Chen, T. Ma, T. Zhang, Y. Zhang and H. Huang, *Adv. Mater.*, 2021, **33**, 2005256; (*b*) H. Hou, X. Zeng and X. Zhang, *Angew. Chem., Int. Ed.*, 2020, **59**, 17356–17376; (*c*) D. Tan, R. Zhuang, R. Chen, M. Ban, W. Feng, F. Xu, X. Chen and Q. Wang, *Adv. Funct. Mater.*, 2023, **34**, 2311655.
102 Y. Mou, X. Wu, C. Qin, J. Chen, Y. Zhao, L. Jiang, C. Zhang, X. Yuan, E. Huixiang Ang and H. Wang, *Angew. Chem., Int. Ed.*, 2023, **62**, e202309480.
103 J. Sun, H. S. Jena, C. Krishnaraj, K. S. Rawat, S. Abednatanzi, J. Chakraborty, A. Laemont, W. Liu, H. Chen, Y. Y. Liu, K. Leus, H. Vrielinck, V. V. Speybroeck and P. V. D. Voort, *Angew. Chem., Int. Ed.*, 2023, **62**, e202216719.
104 (*a*) P. D. Tran, L. H. Wong, J. Barber and J. S. C. Loo, *Energy Environ. Sci.*, 2012, **5**, 5902–5918; (*b*) Y. Amao, *ChemCatChem*, 2011, **3**, 458–474.
105 (*a*) J. Albero, Y. Peng and H. García, *ACS Catal.*, 2020, **10**, 5734–5749; (*b*) J. L. White, M. F. Baruch, J. E. Pander, Y. Hu, I. C. Fortmeyer, J. E. Park, T. Zhang, K. Liao, J. Gu, Y. Yan, T. W. Shaw, E. Abelev and A. B. Bocarsly, *Chem. Rev.*, 2015, **115**, 12888–12935.
106 (*a*) Y. Xiang, W. Dong, P. Wang, S. Wang, X. Ding, F. Ichihara, Z. Wang, Y. Wada, S. Jin, Y. Weng, H. Chen and J. Ye, *Appl. Catal., B*, 2020, **274**, 119096; (*b*) Z. Fu, X. Wang, A. M. Gardner, X. Wang, S. Y. Chong, G. Neri, A. J. Cowan, L. Liu, X. Li, A. Vogel, R. Clowes, M. Bilton, L. Chen, R. S. Sprick and A. I. Cooper, *Chem. Sci.*, 2020, **11**, 543–550.
107 A. F. M. E. Mahdy, H. A. E. Omr, Z. A. Alothman and H. Lee, *J. Colloid Interface Sci.*, 2023, **633**, 775–785.
108 L. Zou, Z. A. Chen, D. H. Si, S. L. Yang, W. Q. Gao, K. Wang, Y. B. Huang and R. Cao, *Angew. Chem., Int. Ed.*, 2023, **62**, e202309820.
109 Z. Almansaf, J. Hu, F. Zanca, H. R. Shahsavari, B. Kampmeyer, M. Tsuji, K. Maity, V. Lomonte, Y. Ha, P. Mastrorilli, S. Todisco, M. Benamara, R. Oktavian, A. Mirjafari, P. Z. Moghadam, A. R. Khosropour and H. Beyzavi, *ACS Appl. Mater.*, 2021, **13**, 6349–6358.
110 Z. Li, Y. Zhi, P. Shao, H. Xia, G. Li, X. Feng, X. Chen, Z. Shi and X. Liu, *Appl. Catal., B*, 2019, **245**, 334–342.
111 X. Dong, F. Zhang, Y. Wang, F. Huang and X. Lang, *Appl. Catal., B*, 2024, **345**, 123660.

 

112 (*a*) D. Guo, D. B. Shinde, W. Shin, E. A. Hamad, A. H. Emwas, Z. Lai and A. Manthiram, *Adv. Mater.*, 2022, **34**, 2201410; (*b*) L. Liu, Y. Gong, Y. Tong, H. Tian, X. Wang, Y. Hu, S. Huang, W. Huang, S. Sharma, J. Cui, Y. Jin, W. Gong and W. Zhang, *CCS Chem.*, 2024, **6**, 1255–1263; (*c*) X. Wu, S. Zhang, X. Xu, F. Wen, H. Wang, H. Chen, X. Fan and N. Huang, *Angew. Chem., Int. Ed.*, 2024, **63**, e202319355; (*d*) J. Sun, Y. Fei, H. Tang, J. Bao, Q. Zhang and X. Zhou, *ACS Appl. Energy Mater.*, 2023, 7592–7602; (*e*) M. Zhang, Y. Tong, Z. Sun, J. Wang, Y. Lin, F. Kang, Q. Zhang and W. Huang, *Chem. Mater.*, 2023, **35**, 4873–4881; (*f*) Y. Tong, Z. Sun, J. Wang, W. Huang and Q. Zhang, *SmartMat*, 2022, **3**, 685–694; (*g*) S. Xu, J. Wu, X. Wang and Q. Zhang, *Chem. Sci.*, 2023, **14**, 13601–13628; (*h*) S. Xu, C. Wang, T. Song, H. Yao, J. Yang, X. Wang, J. Zhu, C.-S. Lee and Q. Zhang, *Adv. Sci.*, 2023, **10**, 2304497.

113 (*a*) Y. Song, X. Li and C. He, *Chin. Chem. Lett.*, 2021, **32**, 1106–1110; (*b*) Y. Xiang, L. Lu, A. G. P. Kottapalli and Y. Pei, *Carbon Energy*, 2022, **4**, 346–398.

114 F. Liu, C. Wang, C. Liu, Z. Yu, M. Xu, Y. Chen and L. Wei, *Appl. Phys. Lett.*, 2021, **119**, 211905.

115 M. K. Shehab, K. S. Weeraratne, O. M. E. Kadri, V. K. Yadavalli and H. M. E. Kaderi, *Macromol. Rapid Commun.*, 2022, **44**, 2200782.

116 M. Cheng, S. Zheng, T. Sun, D. Li, W. Zhang, Z. Zha, Q. Sun, J. Tian, K. Zhang and Z. Tao, *Nano Res.*, 2024, **17**, 5095–5103.

117 (*a*) Z. Yan, Y. Cai, J. Zhang and Y. Zhao, *Measurement*, 2022, **187**, 110355; (*b*) Z. Wang, B. Yao, Y. Xiao, X. Tian and Y. Wang, *Chemosensors*, 2023, **11**, 405; (*c*) D. Zhen, C. Liu, Q. Deng, S. Zhang, N. Yuan, L. Li and Y. Liu, *Chin. Chem. Lett.*, 2024, **35**, 109249.

118 (*a*) L. L. Wang, C. X. Yang and X. P. Yan, *Sci. China: Chem.*, 2018, **61**, 1470–1474; (*b*) L. Li, X. Bi, M. Zhen, Y. Ren, L. Zhang and T. You, *TrAC, Trends Anal. Chem.*, 2024, **171**, 117488.

119 H. Zhuang, C. Guo, J. Huang, L. Wang, Z. Zheng, H. N. Wang, Y. Chen and Y. Q. Lan, *Angew. Chem., Int. Ed.*, 2024, e202404941.